AD-A086 127 MCDONNELL AIRCRAFT CO ST LOUIS MO F/G 20/4
THE EFFECTS OF GROUND WALL-JET CHARACTERISTICS ON FOUNTAIN UPWA--ETC(U)
JUN 80 D R KOTANSKY, L W GLAZE N00014-79-C-0130
UNCLASSIFIED ONR-CR218-261-1F NL

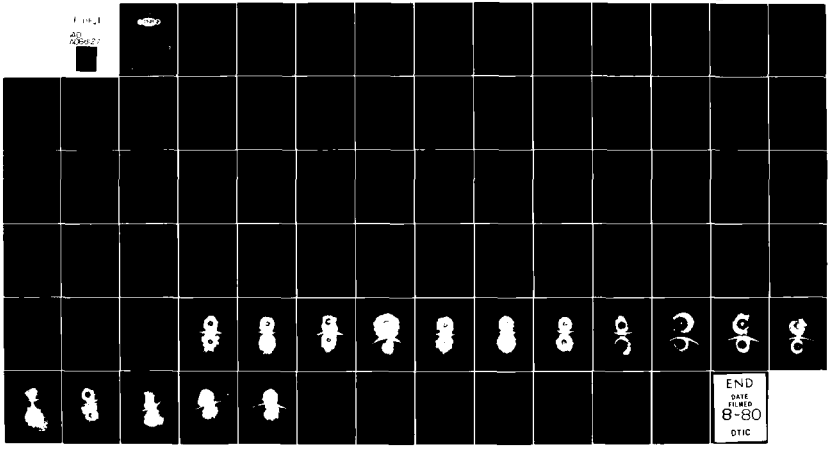

END
DATE FILMED
8-80
DTIC

REPORT ONR-CR212-261-1F

LEVEL II

11

THE EFFECTS OF GROUND WALL-JET CHARACTERISTICS ON FOUNTAIN UPWASH FLOW FORMATION AND DEVELOPMENT

D.R. Kotansky and L.W. Glaze

McDonnell Aircraft Company
St. Louis, Missouri 63166

CONTRACT N00014-79-C-0130

15 June 1980

Final Technical Report for period 15 February 1979 - 15 June 1980

PREPARED FOR THE

OFFICE OF NAVAL RESEARCH · 800 N. QUINCY ST · ARLINGTON · VIRGINIA · 22217

Change of Address

Organizations receiving reports on the initial distribution list should confirm correct address. This list is located at the end of the report. Any change of address or distribution should be conveyed to the Office of Naval Research, Code 438, Arlington, VA 22217.

Disposition

When this report is no longer needed, it may be transmitted to other organizations. Do not return it to the originator or the monitoring office.

Disclaimer

The findings and conclusions contained in this report are not to be construed as an official Department of Defense or Military Department position unless so designated by other official documents.

Reproduction

Reproduction in whole or in part is permitted for any purpose of the United States Government.

Unclassified
SECURITY CLASSIFICATION OF THIS PAGE (When Data Entered)

REPORT DOCUMENTATION PAGE

READ INSTRUCTIONS BEFORE COMPLETING FORM

1. REPORT NUMBER: ONR-CR212-261-1F	2. GOVT ACCESSION NO.: AD-A086 127
3. RECIPIENT'S CATALOG NUMBER:	
4. TITLE (and Subtitle): The Effects of Ground Wall-Jet Characteristics on Fountain Upwash Flow Formation and Development	5. TYPE OF REPORT & PERIOD COVERED: Final Technical Report for Period 15 Feb 79 - 15 June 80
	6. PERFORMING ORG. REPORT NUMBER: ONR-CR212-261-1F
7. AUTHOR(s): D. R. Kotansky and L. W. Glaze	8. CONTRACT OR GRANT NUMBER(s): N00014-79-C-0130
9. PERFORMING ORGANIZATION NAME AND ADDRESS: McDonnell Douglas Corporation, McDonnell Aircraft Company, P.O. Box 516, St. Louis, MO 63166	10. PROGRAM ELEMENT, PROJECT, TASK AREA & WORK UNIT NUMBERS:
11. CONTROLLING OFFICE NAME AND ADDRESS: Office of Naval Research, 800 N. Quincy Street, Arlington, VA 22217	12. REPORT DATE: 15 June 1980
	13. NUMBER OF PAGES: 70
14. MONITORING AGENCY NAME & ADDRESS (if different from Controlling Office):	15. SECURITY CLASS. (of this report): Unclassified
	15a. DECLASSIFICATION/DOWNGRADING SCHEDULE:

16. DISTRIBUTION STATEMENT (of this Report)

Approved for Public Release; Distribution Unlimited

17. DISTRIBUTION STATEMENT (of the abstract entered in Block 20, if different from Report)

18. SUPPLEMENTARY NOTES

19. KEY WORDS (Continue on reverse side if necessary and identify by block number)

V/STOL
WALL JETS
FOUNTAIN UPWASH

20. ABSTRACT (Continue on reverse side if necessary and identify by block number)

An experimental program was conducted to investigate the effects of ground wall jet characteristics on two-jet fountain upwash flow formation and development. Variations in wall jet properties were generated through parametric variations in nozzle pressure ratio and jet impingement angle. Hot film anemometer measurements of the wall jet and fountain upwash flow fields resulted in the determination of fountain upwash formation momentum recovery coefficients, fountain upwash inclination and spreading characteristics, and fountain upwash mass entrainment characteristics. → next page

DD FORM 1 JAN 73 1473

Unclassified
SECURITY CLASSIFICATION OF THIS PAGE (When Data Entered)

The data obtained in this investigation provides empirical information required for an analytical model of fountain inclination developed during this study. This analytical model is compatible with a methodology and software for the prediction of multiple jet V/STOL aircraft ground surface flow fields previously developed for the Naval Air Development Center and later modified for the NASA Ames Research Center.

FOREWORD

This study was conducted for the Office of Naval Research, Arlington, Virginia, by the Aerodynamics Department of the McDonnell Aircraft Company (MCAIR) St. Louis, Missouri. The objectives of this study were to experimentally investigate, by hot film anemometer measurements, the effects of ground wall jet characteristics on two-jet fountain upwash flow formation and development.

The data obtained in this investigation will be used to complement an existing V/STOL aircraft ground flow field prediction methodology, originally developed for axisymmetric jets by MCAIR under contract to the Naval Air Development Center. This methodology (later modified under contracts to the NASA Ames Research Center to include rectangular jets) calculates free jet and wall jet properties, including jet entrainment velocities, and predicts the ground wall jet stagnation line location for multiple lift jet V/STOL aircraft hovering in ground effect. Three primary elements missing from this methodology required for the prediction of the complete forces and moments induced on a V/STOL aircraft in hover, are the fountain upwash formation momentum recovery, the fountain upwash trajectory and the fountain impingement momentum transfer coefficient which is dependent on the geometry of the aircraft undersurface. The results of this study supply the first two of the above missing elements providing for the prediction of fountain upwash strength and inclination.

The principal investigator of this study was Dr. Donald R. Kotansky of the McDonnell Aircraft Company Aerodynamics Department. The experimental test program was conducted by Mr. Lloyd W. Glaze, also of the McDonnell Aircraft Company Aerodynamics Department. The Office of Naval Research Scientific Officer was Dr. Robert E. Whitehead.

TABLE OF CONTENTS

LIST OF ILLUSTRATIONS

LIST OF TABLES

NOMENCLATURE

A	Area
AR	Aspect ratio
D	Jet exit diameter
$f(\phi)$	Momentum distribution about jet impingement point
H	Nozzle exit height above ground plane measured perpendicular to ground plane
$\dot{m}$	Mass flow
$\dot{M}$	Momentum flux
N	Normal distance above ground plane
NPR	Nozzle pressure ratio
N_1	Derived limit of integration
R	Radial distance
S	Nozzle exit centerline spacing
$s_{V/2}$	Velocity profile width at point in profile where $V = \frac{V_{max}}{2}$
U	Wall jet velocity
V	Velocity
X,Y,Z	Cartesian coordinates
α	Jet impingement angle
γ	Direction in ground plane of projection of negative free jet mean velocity at impingement point
θ	Stagnation line slope
$\lambda_{\dot{M}}$	Momentum flux magnitude recovery (conservation) factor
ρ	Density
ϕ	Azimuthal angle in ground plane; $\phi = 0°$ in direction of the horizontal component of free jet mean velocity

ϕ'	Computational polar angle measured in the ground plane about the jet impingement point
ψ	Fountain upwash flow field angularity
ω	Fountain upwash inclination measured from the ground plane

Subscripts

A, B	Jet designation (see Figure 2)
f	Fountain, final
j	Jet
je	Jet exit
max	Maximum
min	Minimum
N	Normal
o	Initial
R	Radial
TH	Theoretical

SECTION I

INTRODUCTION

Recent interest in the development of V/STOL fighter and attack aircraft utilizing powered lift jet or powered lift augmentation systems has revealed the need for a better understanding of the complex flow fields produced by these multiple lift jet systems in the hover mode both in and out of ground effect. The major flow field elements of a typical multiple lift jet system in hover in ground effect are shown in Figure 1. Many research studies have recently been conducted and are currently in progress relating to various aspects of this VTOL flow field prediction problem. Some of these studies have been directed at the development of overall approaches and methodologies for the prediction of VTOL vehicle aerodynamic characteristics (for example, References 1 and 2) and others have addressed specific elemental problem areas encountered in these complex three-dimensional, turbulent flow fields (for example, References 3 and 4). This study is of the latter type; specifically, an experimental investigation of fountain formation and fountain upwash flow development and its dependence on the physical characteristics of the interacting radial wall jets from which it (the upwash) is formed.

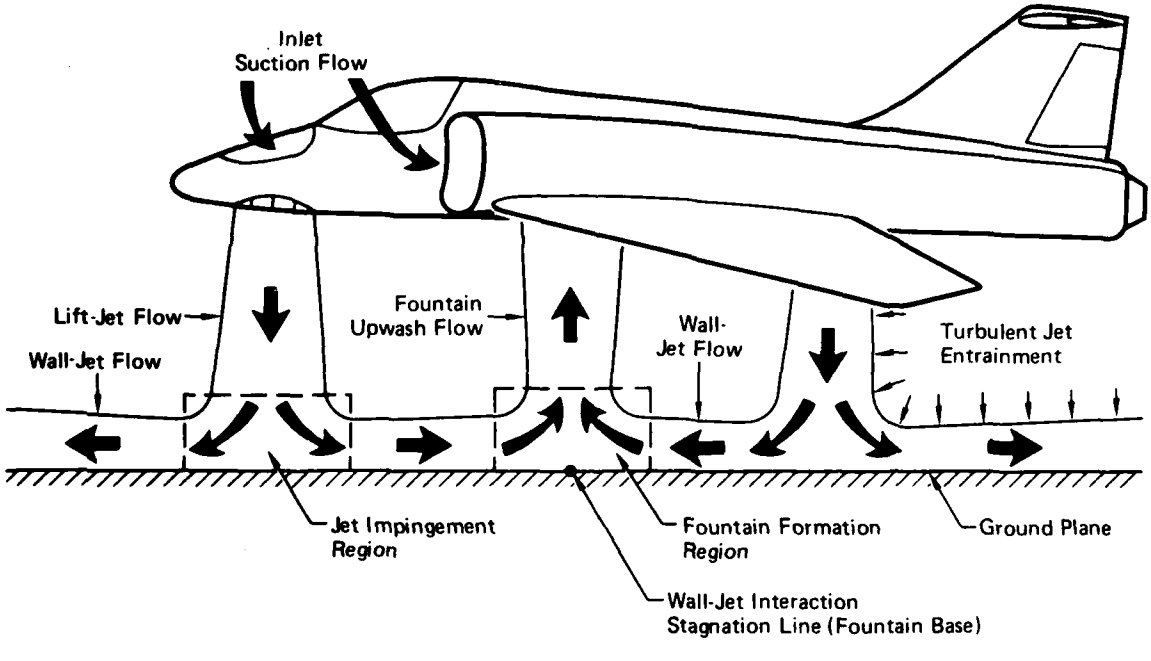

Figure 1. Flow Field about a VTOL Aircraft Hovering in Ground Effect

Fundamental understanding of fountain upwash formation and development is a key element in the improvement of methods for the prediction of VTOL vehicle forces and moments in ground effect. Fountain flows can contribute significantly to the net normal force and pitch and rolling moments imposed on the vehicle in ground effect, and can cause and contribute significantly to lift system engine exhaust gas ingestion levels. Inaccurate or incomplete prediction of vehicle forces and moments in ground effect in the early stages of the vehicle design process can lead to serious propulsion system sizing, vehicle performance and stability and control problems in the vehicle development phase. Similarly, engine exhaust gas ingestion must be minimized to avoid engine thrust loss due to temperature rise.

An analytical program conducted by the McDonnell Aircraft Company (MCAIR) in 1976 for the Naval Air Development Center, has resulted in a methodology (Reference 1) for the prediction of multiple jet induced forces and moments on VTOL aircraft hovering in and out of ground effect. The approach in the prediction methodology was to separate jet entrainment induced suck-down forces from fountain upwash impingement forces. The former are then computed from the jet entrainment induced potential flow-field, and the latter are computed from jet efflux momentum conservation considerations with the superposition of an empirically determined fountain upwash impingement momentum transfer coefficient. However, it was found that this method overpredicted the magnitude of the fountain force, and as a result, flow field regions in which large momentum losses might occur were identified. Subsequently, the need for a detailed investigation of the fountain formation and upwash flow development regions was identified to establish a quantitative link between the wall jet flows on the ground plane and the resulting fountain upwash prior to airframe undersurface impingement.

Specifically, the improvement of existing prediction methodologies and the future development of more accurate approaches required the following detailed information on fountain upwash flow formation and development:

1. Quantification of the influence of the physical characteristics of the interacting radial wall jets on:

    a. The magnitude of wall jet radial momentum converted to fountain upwash momentum in the fountain formation process, and

b. The local direction of the fountain upwash flow at the exit of the fountain formation region and beyond.*

2. Quantification of the development of fountain upwash flow in the free fountain jet development region (above the fountain formation region) in terms of:

   a. The upwash mean flow velocity decay and velocity profile spreading characteristics, and

   b. The mass entrainment characteristics of the fountain upwash.

This information was obtained during this experimental program by hot film anemometer surveys of wall jets and fountain upwash flows created by the impingement, on a ground board, of parametric combinations of axisymmetric turbulent jets (in two-jet pairs). Jet nozzle exit diameters, nozzle pressure ratios and ground impingement angles were varied to produce the desired variations in interacting wall jet properties on the ground plane. Fountain upwash momentum (magnitude and direction) and upwash flow development were then correlated with the measured interacting wall jets through the use of the parametric set of nozzle exit flow conditions.

*The fountain formation region is nominally defined as the volume at the base of the fountain adjacent to and above the ground surface within which mean flow pressure gradients exist (see Figure 1).

SECTION II

EXPERIMENTAL TEST PROGRAM

The experimental test program was designed to investigate thoroughly the two-jet fountain formation process and to establish a reliable data base for current and future prediction techniques. Specifically, the quantification of the influence of the physical characteristics of interacting wall jets on the magnitude of wall jet radial momentum converted to fountain upwash momentum in the fountain formation process and the local direction of the fountain upwash flow were sought. In addition, quantification of fountain upwash flow properties in terms of the upwash mean flow velocity profile spreading characteristics and the fountain upwash mass entrainment characteristics were sought.

The desired information was obtained for the two-jet configuration by hot film anemometer surveys of the wall jet and fountain upwash flows resulting from the impingement of turbulent, axisymmetric, ambient temperature jets upon a ground plane. Nozzle exit area, nozzle pressure ratio and jet impingement angle were varied to produce the desired range of interacting wall jet properties on the ground plane. Fountain upwash momentum and upwash flow development data were then correlated with the parametric jet exit test conditions. Free jet surveys were performed for each of the basic nozzles prior to the fountain test program to ensure that the flow exiting the nozzles was uniform and symmetrical.

Table 1 provides a summary of the test conditions and parametric variations for the experimental test program. A schematic depicting the pertinent test nomenclature is presented in Figure 2. A constant nozzle-to-ground board height (H) of 5.0 baseline nozzle exit diameters (D_A) and a constant nozzle exit centerline spacing (S) of 12.8 baseline nozzle exit diameters were used throughout the investigation. Case 1 represents the baseline configuration using two 6.45 cm^2 (1.00 $in.^2$) exit area nozzles oriented for vertical jet impingement. The effect of nozzle exit area variations on wall jet development and fountain formation was investigated in Case 2, while Cases 3 and 4 examined the effects of nozzle pressure ratio. Jet impingement angle (α_j) effects were investigated in Case 5 in which one jet impinged vertically while the second jet impinged at an oblique angle of 60° to the ground plane. The effects of a non-uniform (in the azimuthal direction) wall jet momentum flux distribution on fountain development were then examined as the oblique nozzle was rotated through five angles between $\phi' = 0°$ and $\phi' = 180°$ (see Figure 2). In addition, the effect of a nozzle exit plane plate on fountain upwash development was investigated in Cases 1 and 3 for two rectangular plates with length-to-width ratios of 1.5 and 3.0, located in the nozzle exit plane. Two wall jet surveys just upstream of the fountain formation region and up to four fountain upwash flow surveys were

TABLE 1. TEST CONDITIONS

D_A = 2.865 cm (1.128 in.) A_{jeA} = 6.45 cm^2
S/D_A = 12.80 NPR_A = 1.89
H/D_A = 5.0 α_{j_A} = 90°

	Case	$\frac{D_B}{D_A}$	A_{jeB} (cm^2)	$\frac{NPR_B}{NPR_A}$	NPR_B	α_{jB} (deg)	AR Exit Plane Plate	$\Delta\phi'_B$	
Symmetrical Fountain with Blocking Plate	1a	1.0	6.45	1.0	1.89	90	–	–	
	1b	1.0	6.45	1.0	1.89	90	1.5	–	
	1c	1.0	6.45	1.0	1.89	90	3.0	–	
Mass and Momentum Flux Change Due to Increased Mass Flow	2a	0.707	3.23	1.0	1.89	90	–	–	
	2b	1.414	12.90	1.0	1.89	90	–	–	
	2c	2.000	25.81	1.0	1.89	90	–	–	
Nozzle Pressure Ratio Effect with Blocking Plate	3a1	1.0	6.45	0.95	1.80	90	–	–	
	3a2	1.0	6.45	0.95	1.80	90	1.5	–	
	3a3	1.0	6.45	0.95	1.80	90	3.0	–	
	3b1	1.0	6.45	0.87	1.64	90	–	–	
	3b2	1.0	6.45	0.87	1.64	90	1.5	–	
	3b3	1.0	6.45	0.87	1.64	90	3.0	–	
	3c1	1.0	6.45	0.74	1.40	90	–	–	
	3c2	1.0	6.45	0.74	1.40	90	1.5	–	
	3c3	1.0	6.45	0.74	1.40	90	3.0	–	
	3d1	1.0	6.45	0.67	1.26	90	–	–	
	3d2	1.0	6.45	0.67	1.26	90	1.5	–	
	3d3	1.0	6.45	0.67	1.26	90	3.0	–	
Nozzle Pressure Ratio Effects with Mass Flow Change	4a	2.0	25.81	0.95	1.80	90	–	–	
	4b	2.0	25.81	0.87	1.64	90	–	–	
	4c	2.0	25.81	0.74	1.40	90	–	–	
Impingement Angle Effects	5a	1.0	6.45	1.0	1.89	60	–	0°	
	5b	1.0	6.45	1.0	1.89	60	–	45°	
	5c	1.0	6.45	1.0	1.89	60	–	90°	
	5d	1.0	6.45	1.0	1.89	60	–	135°	
	5e	1.0	6.45	1.0	1.89	60	–	180°	
Symmetrical Fountain with Blocking Plate	1e	1.0	6.45	1.0	1.89	90	–	–	ϕ' = 90°
	1f	1.0	6.45	1.0	1.89	90	–	–	180°
	1h	1.0	6.45	1.0	1.89	90	3.0	–	ϕ' = 90°
	1j	1.0	6.45	1.0	1.89	90	3.0	–	180°
Oblique Jet Impingement	6a	–	12.90	–	1.89	90	–	–	ϕ' = 0° - 180°
	6b	–	12.90	–	1.89	75	–	–	0° - 180°
	6c	–	12.90	–	1.89	60	–	–	0° - 180°

GP03-0366-51

made for each case shown in Table 1. Fountain base locations were determined for each case utilizing ground plane static pressure distributions as well as flow visualization techniques employing a mixture of lampblack and oil.

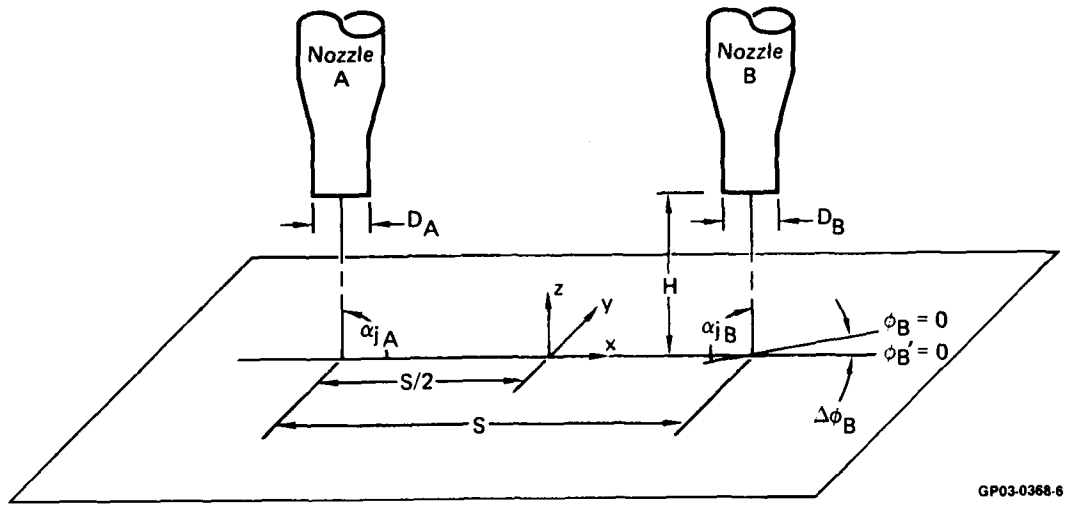

Figure 2. Test Nomenclature

SECTION III

TEST FACILITIES, HARDWARE AND INSTRUMENTATION

1. TEST FACILITIES - Test operations were conducted utilizing the multiple jet interaction test apparatus of the Inlet Simulator (IS) test cell, which is a part of the McDonnell Aircraft Company (MCAIR) Propulsion Subsystem Test Facility (PSTF). The PSTF was designed and developed specifically to allow a wide range of exploratory static testing to be accomplished rapidly and economically. The facility utilizes high pressure (4137 kPa) air, sharing the air storage system of the MCAIR Polysonic Wind Tunnel and vacuum sources of low pressure facilities.

The jet interaction test apparatus utilizes the pressure control system of an adjacent PSTF test cell to set, and automatically hold, nozzle pressure ratio. Two 48.3 cm. ID settling chambers are supplied with high pressure air to provide uniform flow to the two nozzle plenums. The settling chambers have conical and normal screens. The nozzle plenums are "D" shaped and mounted one above the other with the flat side toward the test model. The plenums are provided with two internal screens and removable nozzle mounting plates that are compatible with various nozzle configurations. Three nozzle mounting plates were utilized during the test program. Two of the nozzle mounting plates contain eight possible 5.08 cm (2.00 in.) orifice locations with cover plates provided for the unused orifices. The third plate contains a single 10.16 cm (4.0 in.) orifice.

2. NOZZLES - A total of four axisymmetric, converging nozzle pipes were used in the test program. Two of these nozzles were the baseline nozzles and are designated N1. The N1 nozzles are 70.485 cm (27.75 in.) long with a 2.865 cm (1.128 in.) exit internal diameter and have a 7.117 cm (2.802 in.) offset of the nozzle exit centerline from the nozzle flange centerline. A N1 nozzle was used for the reference nozzle (Nozzle A in Table 1 and Figure 1) in all of the cases shown in Table 1. The third nozzle pipe, designated N2, is also 70.485 cm in length and is a straight, converging nozzle with a 5.730 cm (2.256 in.) exit internal diameter. The N2 nozzle was used in conjunction with a N1 baseline nozzle for the investigation of nozzle exit area effects in Cases 2 and 4. The fourth nozzle pipe, designated N3 and shown schematically in Figure 3, was used for the oblique impingement investigation of Case 5. A 3.81 cm thick nozzle adapter plate was utilized to adapt the 5.08 cm diameter inlet section of the N3 nozzle to the 10.16 cm diameter orifice of the required nozzle mounting plate. Like nozzle N1, the N3 nozzle with adapter plate is 70.485 cm long and has a 2.865 cm exit internal diameter. However, nozzle N3 was designed such that the exit flow issues from the nozzle at a 30° angle to the centerline of the nozzle mounting plate orifice and such that the center of the nozzle exit coincides with the nozzle mounting plate orifice centerline. Consequently, a rotation of the N3 nozzle about the

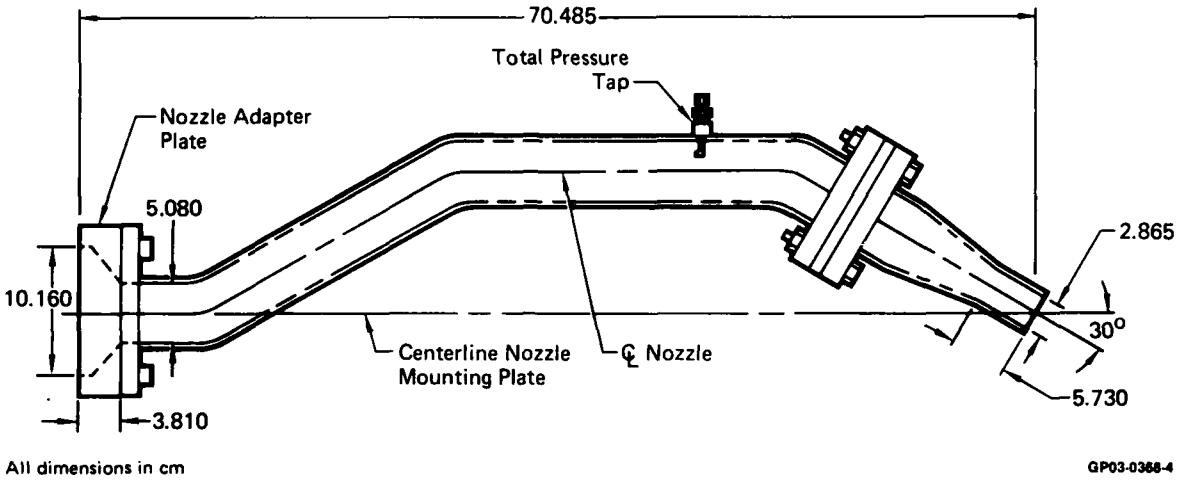

Figure 3. N3 Nozzle Pipe

nozzle mounting plate orifice centerline results in a change in the direction of the N3 nozzle exit mean flow without altering the nozzle exit location. All four nozzles were instrumented for total pressure utilizing a Kiel probe located upstream of the final converging section.

Further variations in nozzle exit geometry were effected with the use of appropriate nozzle adapter sleeves (designated A1, A2 and A3) as shown in Figure 4. The nozzle adapter sleeves were fabricated from aluminum and were secured to the N1 or N2 nozzle with shear pins. Nozzle adapter sleeves A1 and A3 are convergent area nozzle sections that were used for Cases 2A and 2B, respectively. Nozzle adapter sleeve A2 is a constant area nozzle extension that was used in conjunction with adapter sleeve A1 in Case 2a to ensure a consistent nozzle exit-to-ground board height, H, for each nozzle of the nozzle pair. In Case 2b, however, three 2.54 cm (1.00 in.) thick spacer plates (located between the N1 nozzle flange and the plenum) were required in addition to the A2 nozzle adapter sleeve to ensure nozzle exit-to-ground board height consistency for the nozzle pair.

3. NOZZLE EXIT PLANE PLATES - Two flat, rectangular, nozzle exit plane plates having aspect ratios (AR) of 1.5 and 3.0 were used in Cases 1 and 3 to provide a fountain upwash blocking surface between the nozzle exits. The plates were fabricated from .635 cm (.25 in.) plexiglas with a length of 54.52 cm (21.46 in.), extending two nozzle exit diameters in length beyond the nozzle exit outer edges. A small cut-out in the lower corner of each plate was required to accommodate the hot film anemometer probe traversing device during the fountain flow field surveys.

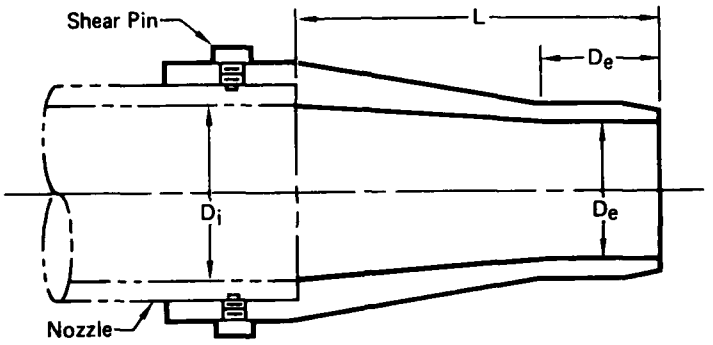

Adapter	Case	Nozzle	D_i (cm)	D_e (cm)	A_e (cm^2)	L (cm)
A1	2a	N1	2.865	2.026	3.224	4.567
A2	2a, 2b	N1	2.865	2.865	6.447	4.567
A3	2b	N2	5.730	4.052	12.894	12.243

GP03-0368-5

All dimensions in cm

Figure 4. Nozzle Adapter Sleeves

4. GROUND BOARD - A 121.9 cm (48.0 in.) square ground board, fabricated from aluminum, was used to simulate the ground plane. One hundred forty-five (145) static pressure taps are located in a cruciform pattern in the center of the ground board. Several static pressure taps were utilized in conjunction with a bank of water manometers to aid in the determination of the fountain base location for each of the cases cited in Table 1.

The ground board is mounted vertically on a rotational bearing which allows for 360° rotation in the plane of the ground board. The rotational bearing is mounted to a slide mechanism which was attached to a remotely controlled, movable cart located in the IS test cell. The slide mechanism provides ±30.5 cm (±12.0 in.) of lateral movement to aid in positioning the ground board relative to the fixed nozzle/plenum assembly.

The wall jet and fountain flow field surveys were performed utilizing a remotely controlled, one degree-of-freedom probe traverse device attached to the ground board. For the wall jet surveys, the probe traverse device was attached to the back of the ground board such that the probe traversed through a 0.5 cm (0.2 in.) diameter hole in the ground board in a direction normal to the ground board surface. For the fountain upwash flow surveys, the probe traverse device was mounted to the front (upper) surface of the ground board such that the probe traversed along a line parallel to and directly above the line connecting the two jet impingement points at a height of one baseline nozzle exit internal diameter (D_A = 1.0). In addition, three 2.865 cm (1.128 in.) spacer blocks were available to enable probe-to-ground board

survey heights of 2, 3 and 4 baseline nozzle exit internal diameters (Z/D_A = 2, 3, 4). The traverse device was mounted to the ground board at a location beyond the projection of the lower nozzle location on the ground board to prevent interaction with the wall jet or fountain flow fields.

5. HOT FILM ANEMOMETER - A dual channel Thermo Systems, Inc. (TSI) Model 1050-2C anemometer was used in conjunction with a two-component, directionally sensitive TSI Model 1240-20 "Cross Flow" hot film anemometer probe to measure wall jet and fountain upwash flow velocity profiles. The anemometer was operated in the constant temperature mode at an overheat ratio of 1.5. The hot film probes were supported by a 45.7 cm (18.0 in.) dual channel TSI Model 1155-18 probe support which was, in turn, mounted to the remotely controlled one degree-of-freedom probe traverse device.

The "Cross Flow" probes were calibrated for mean velocity and flow angularity (in the plane of the sensors) utilizing a TSI Model 1125 Calibrator. Flow angularity data were obtained by rotating the probe about its support axis while holding the calibrator velocity constant. Calibrations were performed for mean velocities in the range of 0 to approximately 90 m/sec and for angularity, ψ, of $\pm 25°$ at four selected mean velocity magnitudes. The mean velocity and angularity calibration data were curve-fit with polynomial expressions for inclusion in the data reduction program. A total of five hot film probes were consumed during the experimental test program. Three probes were lost due to excessive vibrations resulting from flow field turbulence, one probe was lost during an accidental surge in the compressed air supply system, and the fifth probe was lost due to handling.

SECTION IV

DATA ACQUISITION AND DATA REDUCTION

1. DATA ACQUISITION - Hot film anemometer voltage outputs, probe position potentiometer output, pressure transducer outputs and other pertinent test information were recorded for each survey on magnetic tape utilizing the PSTF data acquisition system. The data acquisition system was a 40 channel Datum Model 120 Digital Data Acquisition System (DDAS). The DDAS scanned all data channels continuously at a scan rate of ten scans per second. The anemometer output signals were filtered with a low pass filter to 2 Hz. Probe position and sensor outputs were recorded continuously for two second intervals at a rate of twelve data intervals per minute as the probe traversed through the wall jet or fountain upwash flow field. The traverse rate was remotely controlled and varied from approximately 3 to 8 cm per minute depending on the wall jet or fountain upwash thickness. For the wall jet, the traverses were begun slightly below the ground board surface and continued through the wall jet until a minimum velocity was observed. In addition to recording the hot film anemometer output and probe position on the PSTF DDAS, an on-line X-Y-Y mechanical plotter was wired into the test instrumentation system to provide graphical displays of both channels of anemometer output as a function of probe position. Both types of data recording were used for all of the velocity profile surveys in the test program. The X-Y-Y plotter output allowed on-line monitoring of the quality and repeatability of the data as well as providing a back-up to the magnetic tape data acquisition system.

In order to properly align the anemometer probe with the wall jet flow, the probe calibration chamber was used to establish a reference direction. The probe calibration chamber was mounted to the ground board such that the chamber centerline coincided with a radial line connecting the jet impingement point and the probe support center. With the anemometer probe extended through the ground board and aligned with the calibration chamber nozzle flow, conditions corresponding to a point on the mean velocity calibration curve were reproduced, and the probe was rotated until the two channel outputs matched those determined during the calibration procedure. This procedure was repeated each time the probe was moved to a new ground board hole position or each time a new probe was installed.

2. DATA REDUCTION - The wind tunnel data reduction program, executed on a CDC Cyber 175 computer, summed and averaged each two second interval of data scans to produce single point hot film anemometer and probe position data. The averaged hot film data were then input into the calibration curves with the resulting output being mean velocity and flow angularity. The program also integrated the normal components of the mean velocity and velocity squared profiles using the trapezoidal rule with the limits of

integration, N_1 (or X_1), predetermined for each run as the value of N (or X) corresponding to the largest velocity ratio, U_{min}/U_{max} (or V_{min}/V_{max}), of each run of a wall jet pair or series of fountain upwash surveys. These integrated values were then used to calculate the wall jet radial mass flow, $\dot{m}_R$, and radial momentum flux, M_R; as well as the fountain mass flow, $\dot{m}_N$, and normal momentum flux M_N, as follows:

wall jet

$$\dot{m}_R = \rho R_{wj} \int_0^{N_1} U_R \, dN \tag{1}$$

$$\dot{M}_R = \rho R_{wj} \int_0^{N_1} U_R^2 \, dN \tag{2}$$

fountain

$$\dot{m}_N = \rho R_f \int_{-X_1}^{X_1} V_N \, dX \tag{3}$$

$$\dot{M}_N = \rho R_f \int_{-X_1}^{X_1} V_N^2 \, dX \tag{4}$$

The values $\dot{m}_R$ and $\dot{M}_R$ represent the mass flow and momentum flux, respectively, in the wall jet available for conversion to fountain upwash mass flow ($\dot{m}_N$) and momentum flux ($\dot{M}_N$). The factor R_{wj} is defined as the radial distance on the ground plane from the jet impingement point to the point of measurement in the wall jet. As shown in Reference 1, the symmetrical two-jet fountain upwash approximates a radial jet with the virtual orgin located at S/2 below the ground plane; consequently, the factor R_f is defined as the radial distance from the virtual origin of the fountain upwash to the point of measurement in the fountain flow field. However, since by the method of Reference 1, the virtual origin is undefined for the case of asymmetric jet impingement conditions, the virtual origin was assumed to be at S/2 below the ground plane for all of the cases investigated. Thus, for this investigation, the radial distance in the fountain is defined as:

$$R_f = S/2 + Z/\sin \omega \tag{5}$$

where ω is the fountain inclination angle. The radial factors, Rwj and R_f are required to account for the increase in area of the radial wall jet and fountain flows with increased "radial" distance.

SECTION V

EXPERIMENTAL RESULTS

The wall jet and fountain upwash velocity profiles obtained for each of the two-jet cases defined in Table 1 were correlated to provide fountain upwash momentum flux recovery factors ($\lambda_{\dot{M}}$) and fountain upwash inclinations (ω) as a function of the jet exit momentum flux ratio ($M_{je_{LOW}}/M_{je_{HIGH}}$), as well as to define fountain upwash spreading and mass entrainment characteristics. The following sections describe the experimental data obtained and the procedures used in the correlation and analysis of the experimental results.

1. VELOCITY PROFILES - Wall jet mean velocity profiles were obtained for both jet A and jet B for each of the cases defined in Table 1. The hot film anemometer probe was positioned along the X axis, for each wall jet survey, at two baseline nozzle exit diameters ($2D_A$) upstream of the stagnation line position determined from ground plane static pressure taps and ground plane flow visualization techniques which employed a mixture of lampblack and oil. This $2D_A$ distance (later reduced to $1.5D_A$) was assumed to ensure a probe position upstream of, but as close as possible to, the fountain formation region. The position of each wall jet survey is then represented by the distance (R_{wj}) from the jet impingement point to the point of measurement normalized by the baseline nozzle exit diameter (D_A).

Fountain upwash mean velocity profiles were obtained at up to four probe-to-ground board heights (Z/D_A = 1.0, 2.0, 3.0, 4.0) for each of the cases in Table 1. The velocity profile surveys were obtained by traversing the hot film anemometer probe along a line parallel to the X axis. The probe was oriented such that the flow angularity, ψ, was measured in the X-Z plane with $\psi = 0°$ corresponding to vertical flow.

Figures 5, 6, 7 and 8 present the wall jet and fountain upwash velocity profiles for Cases 1a, 1c, 2b and 3c3, respectively. The velocity profiles shown represent the magnitude of the total velocity vector. As seen from Figures 5 and 6 (Cases 1a and 1c), the wall jets appear thicker and more energetic with the nozzle exit plate present. A comparison of the fountain upwash velocity profiles of Figures 5 and 6 indicates the effect of the nozzle exit plane plate on the fountain flow formed between the two baseline nozzles operating under otherwise identical conditions. Other than a reduction of the flow angularity in the fountain, the presence of the plate is seen to have little effect on the fountain flow up to a height of $4D_A$, at which point there is a severe flattening of the fountain velocity profile as the upwash reaches the region of influence of the exit plane plate. Case 2b (Figure 7) indicates the effect of a nozzle exit area bias (A_{je_B}/A_{je_A} = 2.0) on the wall jet and fountain upwash flow fields.

A comparison of the wall jet velocity profiles in Figure 7 indicates a broadening of the velocity profile due to the larger jet at 1.5 D_A from the stagnation line. The effect of the nozzle exit area bias on the fountain flow is distinguished by a shift in the lateral location of the fountain peak velocity (increasing with increasing Z/D_A) toward the smaller jet (jet A) indicating an inclined fountain upwash. The effect of a nozzle pressure ratio bias (NPR_B/NPR_A = .74) between the two baseline nozzles in the presence of an aspect ratio three (AR = 3.0) nozzle exit plane plate is shown in Figure 8. From this figure, the wall jet velocity profile corresponding to the stronger jet (jet A) is seen to be thicker than that produced by the weaker jet (jet B) at two baseline nozzle exit diameters ($2D_A$) from the stagnation line. The fountain upwash velocity profiles again indicate an inclination of the fountain, in this case toward the weaker jet, with the characteristic flattening of the velocity profile at Z/D_A = 4.0 due to the presence of the nozzle exit plane plate.

The fountain upwash flow surveys shown in Figures 5 through 8 indicate a random variation of flow angularity in the X,Z plane as denoted by the recorded values of the angle ψ shown in these figures. Figure 7, Case 2b, yielded ψ distributions most closely representing the expected distribution of ψ, i.e. slightly positive on the "right hand" side of the fountain, changing sign near the center of the fountain, and slightly negative on the "left hand" side. Deviations from this expected or ideal distribution are unexplained. The largest deviations occurred in the low velocity edges of the fountain upwash flow, as shown for example in Figure 5. To what extent the unsteadiness or large scale turbulent structures may have influenced these data was not quantified. Further explanation would require, at a minimum, angularity measurements in the Y,Z plane and numerous unsteady measurements.

2. AZIMUTHAL DISTRIBUTION OF WALL JET RADIAL MASS FLOW AND MOMENTUM FLUX (CASE 1) - The azimuthal distribution of wall jet radial mass flow ($\dot{m}_R$) and radial momentum flux (M_R) were determined for one jet (jet A) of Case 1 by applying equations (1) and (2) to the velocity profiles recorded at a constant radius of 4.38 D_A about the periphery of the jet impingement point. Velocity profile data were recorded at azimuthal stations, ϕ, of 0°, 90° and 180°; where ϕ = 0° in the direction of the second jet (jet B). Figure 9 presents the azimuthal distributions of the radial wall jet mass flow and radial momentum flux, normalized by the value at ϕ = 0°. The radial mass flow in the absence of a nozzle exit plane plate is shown to be fairly symmetrical. When the AR = 3.0 nozzle exit plane plate was installed, however, some asymmetry in the mass flow is indicated with a decrease in $\dot{m}_N$ with ϕ. The radial momentum flux distribution indicates some asymmetry both with and without the AR = 3.0 nozzle exit plane plate.

3. FOUNTAIN UPWASH MOMENTUM FLUX RECOVERY - An important parameter in the modeling of fountain induced forces and moments on V/STOL aircraft hovering in ground effect is the amount of wall jet momentum flux converted to vertical fountain momentum flux. A fountain upwash momentum flux recovery factor, $\lambda_{\dot{M}}$, was determined for Cases 1-5. The fountain upwash momentum flux recovery factor ($\lambda_{\dot{M}}$) is defined as the ratio of the fountain normal momentum flux exiting the fountain formation region to the total wall jet radial momentum flux entering the fountain formation region. For this investigation, the flow through the fountain formation region was incompressible (ρ = constant), and the fountain formation region was assumed to be small so that radial area change effects were negligible ($dR \approx 0$), thus

$$\lambda_{\dot{M}} = \frac{\left(\int_{X_o}^{X_f} V_N^2 \, dX\right)_f}{\left(\int_0^{N_1} U_R^2 \, dN\right)_{wj(A+B)}} \tag{6}$$

where $\left(\int_{X_o}^{X_f} V_N^2 dX\right)_f$ is representative of the fountain normal momentum flux at $Z/D_A = 1.0$ and $\left(\int_0^{N_1} U_R^2 dN\right)_{wj(A+B)}$ is representative of the sum of the wall jet radial momentum flux produced by each jet in the system. Since the velocity ratios, V_{min}/V_{max}, for the fountain velocity profiles were considerably higher than those determined for the wall jet velocity profiles, the following procedure was established to define the limits of integration and to lend consistency to the calculation process.

As discussed in the Data Reduction section, the upper limits of integration of the wall jet velocity profiles were established for each case by the normal distance, N_1, corresponding to the larger velocity ratio, U_{min}/U_{max}, of the two wall jet velocity profiles. The wall jet velocity and velocity squared profiles for jet A and jet B were then integrated and summed to yield $\left(\int_0^{N_1} U_R \, dN\right)_{wj}$ and $\left(\int_0^{N_1} U_R^2 dN\right)_{wj}$. Now, since the fountain formation region is assumed to be small, with little exposed jet area available for mass entrainment, conservation of mass was assumed throughout the fountain formation region to yield

$$\left(\int_{X_o}^{X_f} V_N \, dX\right)_{f_{Z/D_A=1}} = \left(\int_0^{N_1} U_R \, dN\right)_{wj(A+B)} \tag{7}$$

Thus, the initial and final limits ot integration (X_o, X_f) for the fountain velocity and velocity squared profiles were determined such that equation (7) was satisfied.

a. Cases 1-4 - Figure 10 presents the fountain momentum flux recovery factor, $\lambda_{\dot{M}}$, as a function of the jet exit momentum flux ratio, $\dot{M}_{je_{LOW}}/\dot{M}_{je_{HIGH}}$, for Cases 1-4. The data indicate a general decrease in the fountain momentum flux recovery with a decrease in the nozzle thrust bias (increased $\dot{M}_{je_{LOW}}/\dot{M}_{je_{HIGH}}$). In addition, an increase in $\lambda_{\dot{M}}$ is shown in the presence of a nozzle exit plane plate over that found without the plate. A polynomial curve-fit (also shown in Figure 10) was determined for the data and is given by the following expression:

$$\lambda_{\dot{M}} = 1.0373 - 1.4758 \left(\frac{\dot{M}_{je_{LOW}}}{\dot{M}_{je_{HIGH}}}\right) + 1.5117 \left(\frac{\dot{M}_{je_{LOW}}}{\dot{M}_{je_{HIGH}}}\right)^2 - .5215 \left(\frac{\dot{M}_{je_{LOW}}}{\dot{M}_{je_{HIGH}}}\right)^3 \quad (8)$$

The behavior of the momentum flux recovery factor with jet exit momentum flux ratio is not surprising. The strongest wall jet interaction and associated loss of mean flow energy or momentum occur with two equal strength impinging jets. As one of the impinging jets becomes weaker (increased thrust bias), the wall jet interaction becomes weaker. For a high thrust bias, the weaker wall jet simply tends to deflect the stronger jet with an attendant reduction in mixing and loss of mean flow energy.

b. Case 5 - The fountain momentum flux recovery for Case 5, in which jet A impinges vertically while jet B impinges at 60° to the ground plane, is shown in Figure 11 as a function of ϕ'_B. The angle ϕ'_B is defined as the direction of the horizontal component of the jet B free jet mean flow, with $\phi'_B = 0°$ in the direction opposite that of jet A. The data, shown for a jet exit momentum ratio of 1.0, indicate an increase in $\lambda_{\dot{M}}$ with ϕ'_B up to approximately $\phi'_B = 45°$ followed by a decrease in $\lambda_{\dot{M}}$ as ϕ'_B approaches 180°. This trend is opposite of that which would be expected based on the data of Figure 10 and the azimuthal wall jet radial momentum flux distributions for impingement angles, α_j, of 60° and 90° discussed in Section V.7. The wall jet radial momentum flux distributions indicate an initial increase in the momentum flux ratio, $\dot{M}_{je_{LOW}}/\dot{M}_{je_{HIGH}}$, with ϕ'_B up to approximately $\phi'_B = 75°$ followed by a decrease in $\dot{M}_{je_{LOW}}/\dot{M}_{je_{HIGH}}$ as ϕ'_B approaches 180°. Applying this information to Figure 10 yields a curve for Case 5 which initially decreases, then increases as ϕ'_B varies from 0° to 180°, contrary to that shown in Figure 11. No explanation, however, has been determined for this discrepancy.

4. FOUNTAIN UPWASH MASS FLOW - The mass flow in the fountain upwash was determined as a function of vertical height (Z) utilizing three different methods of computation. The first two methods employed the standard mass flow equation:

$$\dot{m}_N = \rho R_f \int_{X'_o}^{X'_f} V_N \, dX \tag{9}$$

with the limits of integration (X'_o, X'_f) established differently for each method. The third method assumed similar fountain upwash velocity profiles so that

$$\dot{m} = \text{constant} \times \rho R_f \, s_{V/2} \, V_{max} \tag{10}$$

where $s_{V/2}$ represents the width of the fountain velocity profile at the point in the profile where the velocity is equal to one half of its maximum velocity. Figure 12 presents the variation of $s_{V/2}$, normalized by the jet exit spacing (S), with Z/D_A for Cases 1-5. The three methods are discussed in more detail below.

a. Method 1 - The first method determines the fountain mass flow ($\dot{m}_N$) with the assumption of conservation of vertical momentum flux throughout the fountain upwash flow region, external to the fountain formation region. Thus, the fountain vertical momentum flux determined at $Z/D_A = 1.0$ for the determination of the fountain upwash momentum flux recovery factors in Section V.3 was held constant throughout the fountain upwash flow field so that:

$$(\dot{M}_N)_{Z/D_A} = (\dot{M}_N)_{Z/D_A=1} \tag{11}$$

or

$$(\rho R_f \int_{X'_o}^{X'_f} V_N^2 \, dX)_{Z/D_A} = (\rho R_f \int_{X'_o}^{X'_f} V_N^2 \, dX)_{Z/D_A=1} \tag{12}$$

Consequently, the limits of integration (X'_o, X'_f) required to satisfy equation (12) were applied to equation (9) to calculate the fountain upwash mass flow. Figure 13 presents the fountain mass flow (normalized by the value at $Z/D_A = 1$) as a function of height (Z/D_A) for Cases 1-5. Cases 1, 2, 3a and 3b exhibit an initial decrease in mass flow, $\dot{m}_N$, from $Z/D_A = 1$ to $Z/D_A = 2$ followed by an increase in mass flow with increasing Z/D_A. The cause of this initial indicated decrease in fountain upwash mass flow is not known. The remaining cases, however, display an increase of $\dot{m}_N$ with increasing Z/D_A from $Z/D_A = 1$ to $Z/D_A = 4$.

b. Method 2 - The second method calculated the mass flow ($\dot{m}_N$) in the fountain by applying equation (9) with the limits of integration, X'_o and X'_f, established for each case by the largest velocity ratio, V_{min}/V_{max}, determined for the series of fountain surveys (Z/D_A = 1, 2, 3, 4). This computation was performed only for those cases in which the fountain minimum velocity satisfied

the condition that $V_{min}/V_{max} \leq 0.5$ on both sides of the fountain velocity profile peak for at least three values of Z/D_A (Cases 1 and 3). Figure 14 presents the fountain mass flow, normalized by the value at $Z/D_A = 1$, as a function of Z/D_A for Cases 1 and 3. Figure 14 indicates an increase in fountain mass flow with Z/D_A up to a height of four jet exit diameters in the fountain for both Case 1 and Case 3.

c. Method 3 - The third method of computation calculated the fountain mass flow ($\dot{m}$) using equation (10) with the assumption of similarity of the fountain velocity profiles. The computation was again performed only for those cases for which the fountain minimum velocity satisfied the condition that $V_{min}/V_{max} \leq 0.5$ on both sides of the fountain velocity profile peak. The fountain mass flows, calculated using Method 3 and normalized by the value at $Z/D_A = 1$, are presented for Cases 1 and 3 in Figure 15. The fountain mass flow is shown to increase with increasing Z/D_A throughout the fountain upwash flow field.

5. FOUNTAIN UPWASH INCLINATION - A key element in the analytical modeling of multiple jet flow fields in ground effect is the determination of fountain upwash inclination, (ω), with respect to the ground plane. An analytical model, based on the ground flow field modeling techniques presented in References 1 and 5, has been developed and was correlated with the experimentally derived values of ω for Cases 1-5.

a. Analytical Model of Fountain Upwash Inclination - In Reference 1, a methodology was developed which included a model of wall jet interaction on a ground plane which will be denoted as the "Momentum Flux Method". This model establishes the location of the stagnation line between two jet impingement points by balancing the total momentum flux in the wall jets in a direction normal to the stagnation line in the ground plane. As a result of the requirement of a total momentum flux balance (normal to the stagnation line), the direction of the fountain in a vertical plane normal to stagnation line must itself be vertical, although a non-vertical sidewash component is allowed. A model for the prediction of this sidewash component was presented in Reference 1.

Green, Reference 5, has modified the criterion for determination of the location of the stagnation line by requiring a balance of wall jet momentum flux per unit area of the wall jet at the stagnation line. The balance of momentum flux per unit area is imposed in a direction normal to the stagnation line in the ground plane. Imposition of this criterion results in an imbalance of total wall jet momentum flux at the stagnation line in a direction normal to the stagnation line in the ground plane and, also, results in a non-vertical trajectory of the fountain upwash flow in a vertical plane normal to the stagnation line. This model for the determination of the stagnation line is denoted as the "Momentum Flux Density Method". The "Momentum Flux Method" (MFM) and the "Momentum Flux Density Method" (MFDM) models are compared in Table 2.

TABLE 2.
TWO METHODS FOR THE COMPUTATION OF STAGNATION LINE LOCATION

MOMENTUM FLUX METHOD (MFM)	MOMENTUM FLUX DENSITY METHOD (MFDM)
Stagnation Line Slope:	
$\tan\theta = \dfrac{\beta \sin\phi'_2}{1+\beta\cos\phi'_2}$	$\tan\theta = \dfrac{\beta \sin\phi'_2}{1+\beta\cos\phi'_2}$
where $\beta = \dfrac{R_1}{S}\sqrt{\dfrac{\gamma_2 f_2(\phi_2)\dot{M}_{je2}/\gamma_1 f_1(\phi_1)\dot{M}_{je1}}{R_2/R_1}} + \dfrac{R_2}{S}$	where $\beta = \dfrac{R_1}{S}\left[\dfrac{\gamma_2 f_2(\phi_2)\dot{M}_{je2}/\gamma_1 f_1(\phi_1)\dot{M}_{je1}}{R_2^2/R_1^2}\right] + \dfrac{R_2}{S}$
On the Line Joining the Jet Impingement Points:	
$\dfrac{R_2}{R_1} = \dfrac{\dot{M}_{je2} f_2(\phi_2)\gamma_2}{\dot{M}_{je1} f_1(\phi_1)\gamma_1}$	$\dfrac{R_2}{R_1} = \sqrt{\dfrac{\dot{M}_{je2} f_2(\phi_2)\gamma_2}{\dot{M}_{je1} f_1(\phi_1)\gamma_1}}$

GP03-0368-54

Computation of wall jet stagnation lines using the "Momentum Flux Method" and the "Momentum Flux Density Method" were recently compared with actual stagnation line locations obtained experimentally through flow visualization techniques, and the results were presented in Reference 6. Based on these and other comparisons, the "Momentum Flux Density Method" was found to give a more accurate prediction of wall jet stagnation line location. Utilizing the nomenclature of Reference 1 as shown in Figure 16, the equations for the slope of the stagnation line in the ground plane for the MFDM is the following:

$$\tan\theta = \frac{\beta \sin \phi'_2}{1+\beta\cos\phi'_2} \tag{13}$$

where

$$\beta = \frac{R_1}{S}\left[\frac{\gamma_2 f_2(\phi_2)\dot{M}_{je_2}/\gamma_1 f_1(\phi_1)\dot{M}_{je_1}}{R_2^2/R_1^2}\right] + \frac{R_2}{S} \tag{14}$$

and, at the line joining the jet impingement points in the ground plane,

$$\frac{R_2}{R_1} = \sqrt{\frac{\dot{M}_{je_2} f_2 (\phi_2) \gamma_2}{\dot{M}_{je_1} f_1 (\phi_1) \gamma_1}} \tag{15}$$

Through the use of a control volume located on the stagnation line and a total momentum flux balance in a direction normal to the stagnation line, a relation between the momentum flux quantities in the two interacting wall jets and the momentum flux exiting the control volume in the fountain is obtained (for negligible side-wash):

$$\frac{\gamma_1 f_1 \dot{M}_{je_1}}{2\pi} \sin(\theta - \phi'_1)\, \partial\phi'_1 - \frac{\gamma_2 f_2 \dot{M}_{je_2}}{2\pi} \sin(\phi'_2 - \theta)\, \partial\phi'_2 \tag{16}$$

$$+ \rho V_f \cos\omega \left[U_{R_1} R_1 \partial\phi'_1 + U_{R_2} R_2 \partial\phi'_2\right] h = 0$$

where V_f is the fountain upwash velocity, ω is the fountain inclination angle and h is the wall jet height. Assuming a total momentum flux magnitude conservation factor $\lambda_{\dot{M}}$ in the fountain formation region:

$$\rho V_f \left[U_{R_1} R_1 \partial\phi'_1 + U_{R_2} R_2 \partial\phi'_2\right] h =$$

$$\lambda_{\dot{M}} \left[\gamma_1 f_1 \dot{M}_{je_1} \frac{\partial\phi'_1}{2\pi} + \gamma_2 f_2 \dot{M}_{je_2} \frac{\partial\phi'_2}{2\pi}\right. \tag{17}$$

Substituting equation (17) in equation (16) and solving for $\lambda_{\dot{M}} \cos\omega$ the following result is obtained:

$$\lambda_{\dot{M}} \cos\omega = \frac{\frac{\gamma_2 f_2 \dot{M}_{je_2}}{R_2} \sin^2(\phi'_2 - \theta) - \frac{\gamma_1 f_1 \dot{M}_{je_1}}{R_1} \sin^2(\theta - \phi'_1)}{\frac{\gamma_2 f_2 \dot{M}_{je_2}}{R_2} \sin(\phi'_2 - \theta) + \frac{\gamma_1 f_1 \dot{M}_{je_1}}{R_1} \sin(\theta - \phi'_1)} \tag{18}$$

For the special case of two round jets impinging vertically, on the line joining the jet impingement points,

$$\lambda_{\dot{M}} \cos\omega = \frac{1 - \sqrt{\dot{M}_{je_1}/\dot{M}_{je_2}}}{1 + \sqrt{\dot{M}_{je_1}/\dot{M}_{je_2}}} \tag{19}$$

Figure 17 demonstrates the relation between ω and the impinging jet pair momentum flux ratio as obtained from equation (19) with $\lambda_{\dot{M}}$ as a parameter. The validity of this model of fountain upwash flow inclination was investigated with experimental data from the test program conducted during this study and is presented below.

b. Experimental Investigation of Fountain Upwash Inclination

The experimentally determined fountain upwash trajectories are presented in Figure 18 for Cases 1-5. The trajectories shown in the figure represent the loci of maximum velocity points as determined from the fountain velocity profiles. The dashed symbols represent points for which V_{max} was not clearly distinguishable while the dashed lines represent extrapolations of the fountain trajectories. The fountain base (stagnation line) locations were established from ground plane static pressure measurements. The fountain upwash inclination, ω, was determined twice for each case based on: (1) the angle between the ground plane and a straight line connecting the fountain base and the fountain trajectory at $Z/D_A = 3$, and (2) the angle between the ground plane and a straight line connecting the fountain base and the fountain trajectory at $Z/D_A = 4$. These angles are also indicated in Figure 18.

The fountain inclination, ω, for Cases 1-4, is plotted as a function of the jet exit momentum flux ratio ($\dot{M}_{je_{LOW}}/\dot{M}_{je_{HIGH}}$) for a fountain inclination at $Z/D_A = 3$ in Figure 19. Also shown in the figure are the theoretical values of the fountain inclination, ω_{TH}, based on equation (18). Figure 19 indicates that for a fountain inclination determined at $Z/D_A = 3$, a momentum flux recovery factor, $\lambda_{\dot{M}}$, of approximately 0.65 results in a reasonable fit to the experimental data.

6. STAGNATION LINE PREDICTIONS - In 1976, MCAIR developed, under contract to the Naval Air Development Center, a semi-empirical methodology for the computation and prediction of jet impingement points; free and wall jet flow properties including local jet entrainment velocities; and stagnation line coordinates in a ground plane based coordinate system. This program accounts for arbitrary nozzle locations (up to six jets) in the aircraft coordinate system, aircraft pitch and roll, independently variable nozzle exit flow conditions, jet vector and splay angles, and aircraft height above ground. Originally developed for axisymmetric jets (Reference 1) using the "Momentum Flux Method", this program was subsequently modified under contracts to the NASA Ames Research Center (References 6 and 7) to include rectangular nozzles with exit area aspect ratios between one and eight. In addition, an option has been added to the program to allow for the computation of the stagnation line coordinates based on the "Momentum Flux Density Method".

This ground flow field computer program was utilized in the prediction of the stagnation line locations for those cases described in Table 1 for which no nozzle exit plane plate was present. Figures 20-35 compare the predicted stagnation line locations (dashed line) based on the MFDM, with the stagnation

lines determined experimentally using flow visualization techniques employing a mixture of lampblack and oil. As seen in the figures, the agreement between the predicted and actual stagnation line positions varies from good to excellent for all cases, with the predicted stagnation line diverging slightly from the actual position as the jet exit momentum flux ratio ($M_{je_{LOW}}/M_{je_{HIGH}}$) decreases.

7. AZIMUTHAL DISTRIBUTION OF WALL JET RADIAL MOMENTUM FLUX - A significant element in the prediction of the ground wall jet stagnation line location is the azimuthal distribution of the wall jet radial momentum flux about the periphery of the jet impingement points. The ground flow field prediction program described above uses the experimental data of Donaldson and Snedeker (Reference 8) for the vertical ($\alpha_j = 90°$) and oblique ($\alpha_j = 75°$, 60°) impingement of axisymmetric jets. Reference 8 presents jet impingement data for nozzle-to-ground plane heights (H/D) of 1.95 and 23.5. This data was interpolated for use in the MCAIR ground flow field program to represent H/D ≃ 7.

As a check of the Donaldson and Snedeker data, an investigation was performed following the basic test program, to determine the impingement characteristics associated with one of the baseline nozzles (N1) for NPR = 1.89 and H/D = 5.0. The azimuthal distribution of wall jet radial momentum flux determined for the N1 nozzle is shown in Figure 36 for jet impingement angles, α_j, of 90°, 75° and 60°. The independent variable in the figure is the azimuthal angle, ϕ. For oblique impingement ($\alpha_j \neq 90°$), $\phi = 0°$ is defined as the direction of the horizontal component of the free jet mean flow. In order to be consistent with the experimental data of Donaldson and Snedeker (which is also shown in Figure 36 for comparison), the momentum flux data was normalized by the average value of the momentum flux recorded for an impingement angle of 90° ($M_{avg_{\alpha_{j=90°}}}$). A comparison of the two sets of data reveals that the current data indicate a lesser flux of momentum in the range of azimuth of $0 \leq \phi \leq \pi/4$ than that shown by Donaldson and Snedeker with general agreement between the two sets of data for $\phi > \pi/4$.

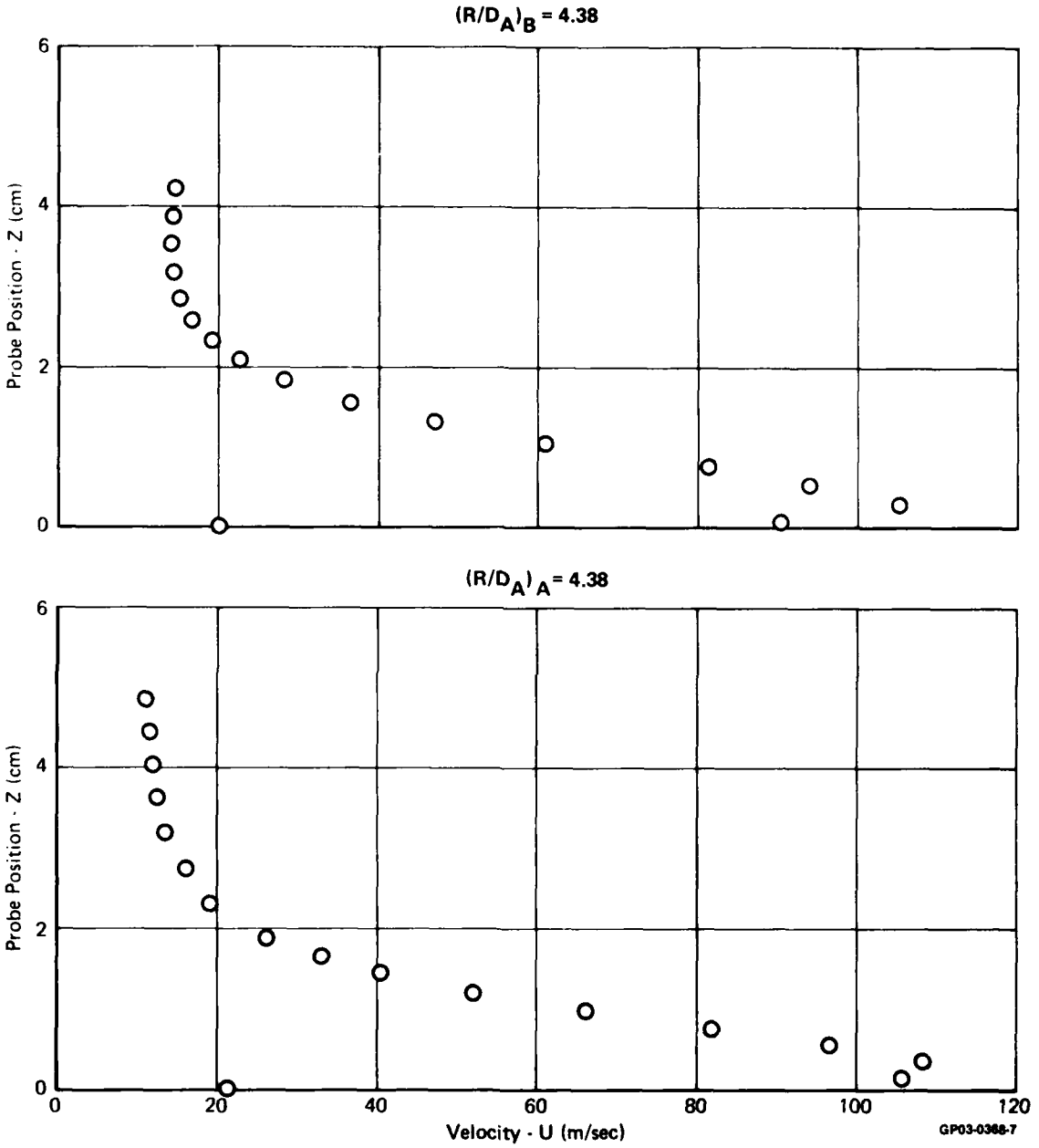

Figure 5. Wall Jet Velocity Profiles
Case 1a
$NPR_B/NPR_A = 1.00$ $D_B/D_A = 1.00$

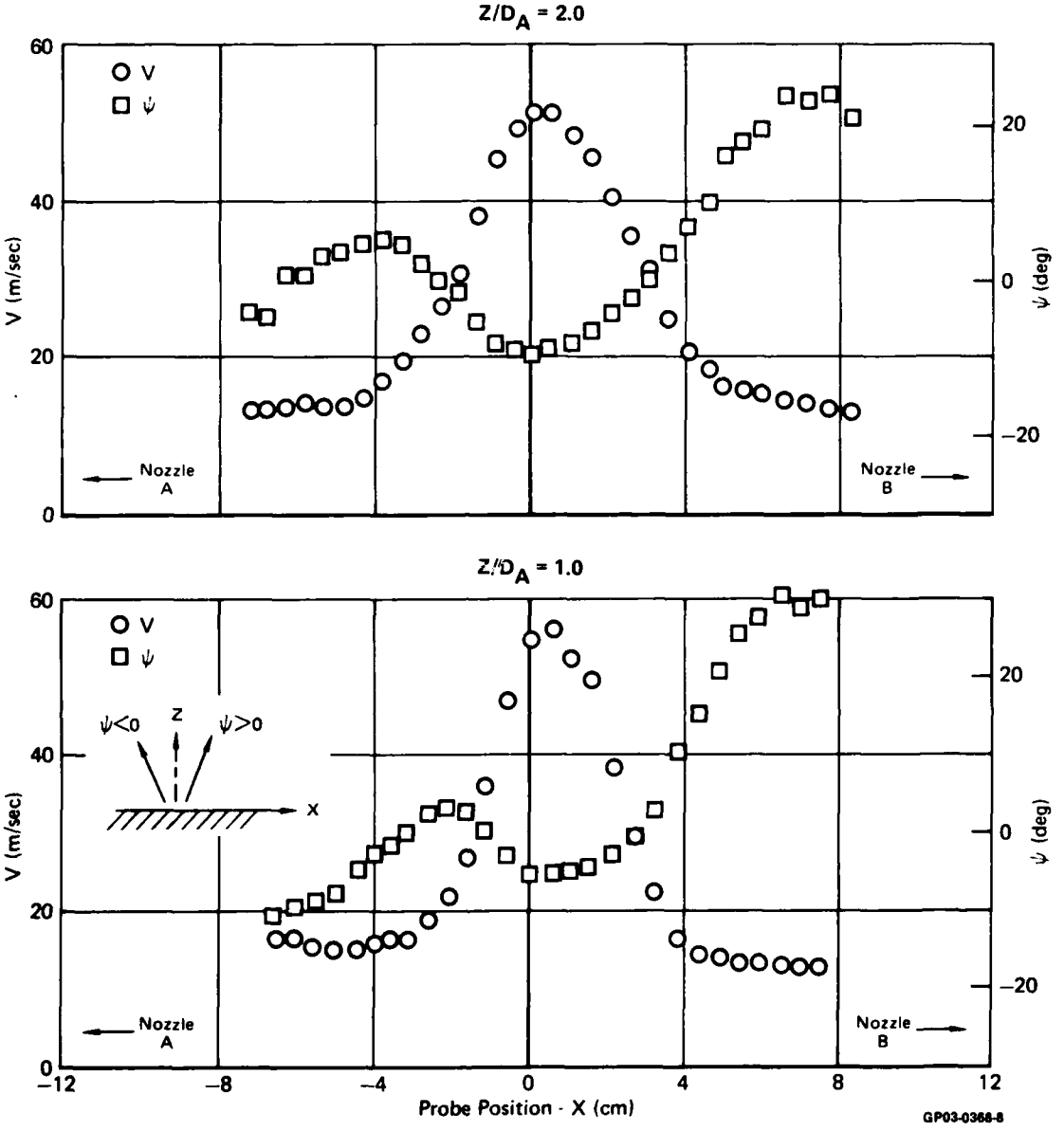

Figure 5. (Continued) Fountain Velocity Profiles
Case 1a
$NPR_B/NPR_A = 1.00 \quad D_B/D_A = 1.00$

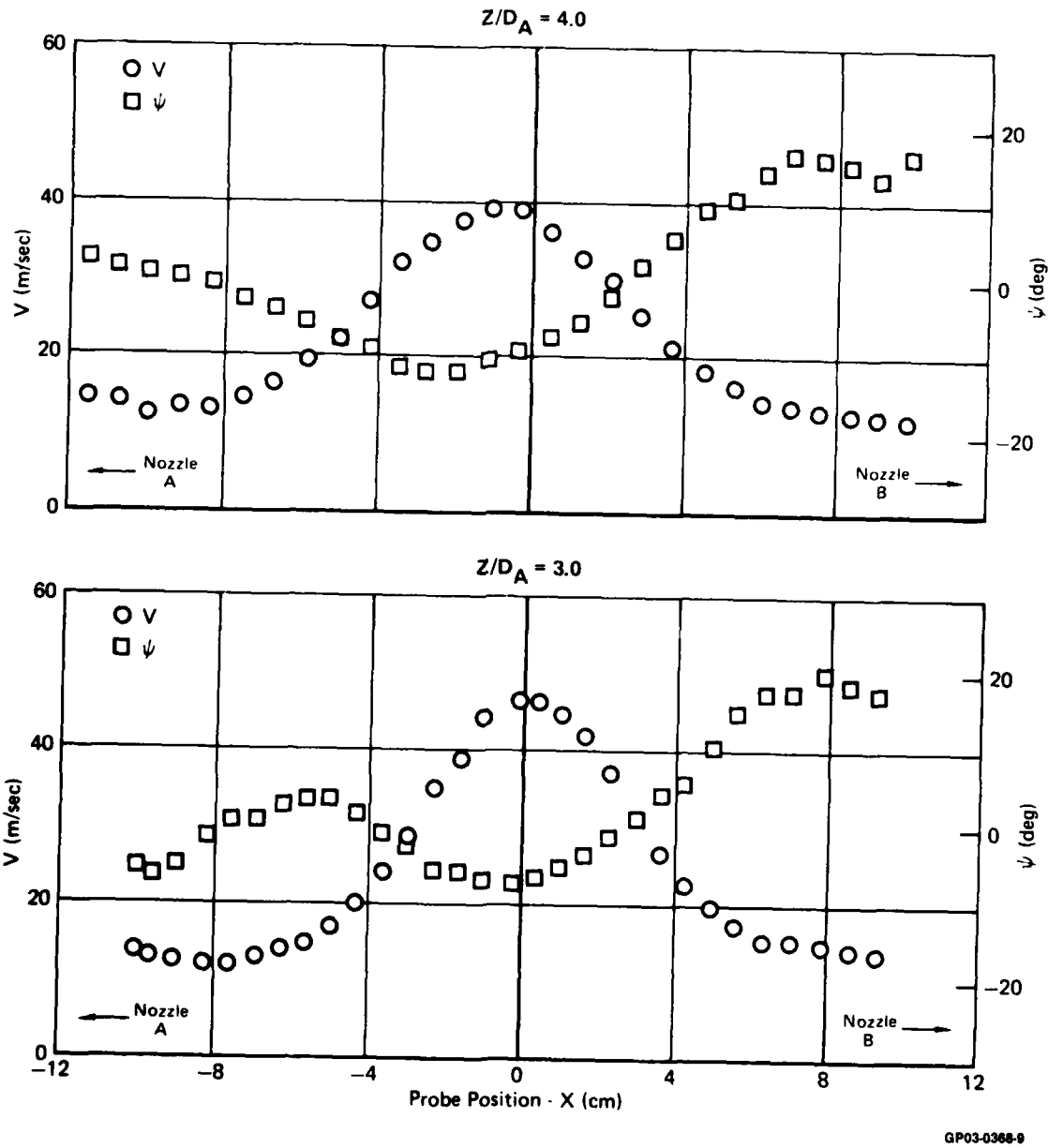

Figure 5. (Concluded) Fountain Velocity Profiles

Case 1a

$NPR_B/NPR_A = 1.00 \quad D_B/D_A = 1.00$

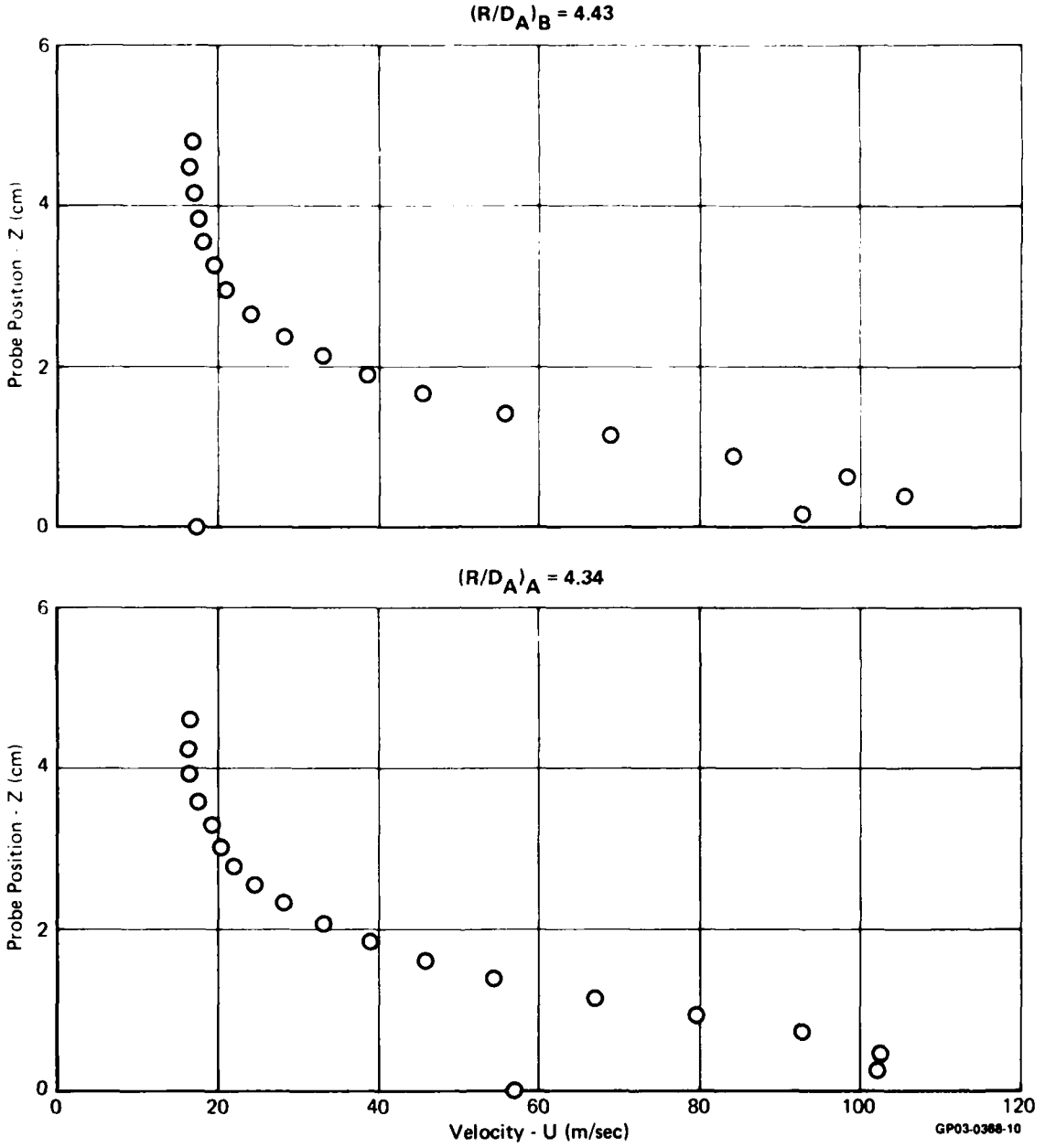

Figure 6. Wall Jet Velocity Profiles
Case 1c
NPR_B/NPR_A = 1.00 D_B/D_A = 1.00 AR_{Plate} = 3.0

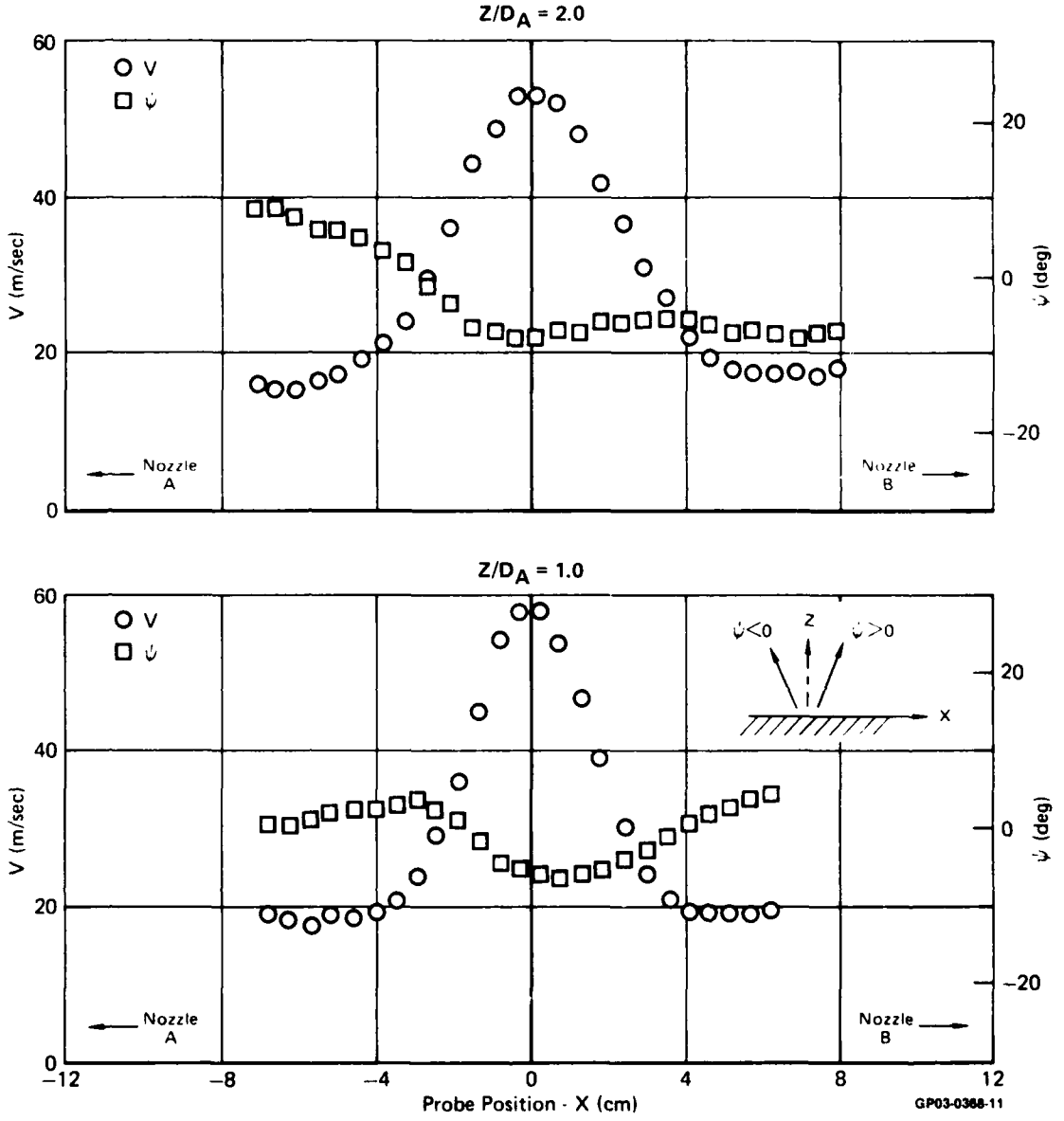

Figure 6.(Continued) Fountain Velocity Profiles
Case 1c
NPR_B/NPR_A = 1.00 D_B/D_A = 1.00 AR_{Plate} = 3.0

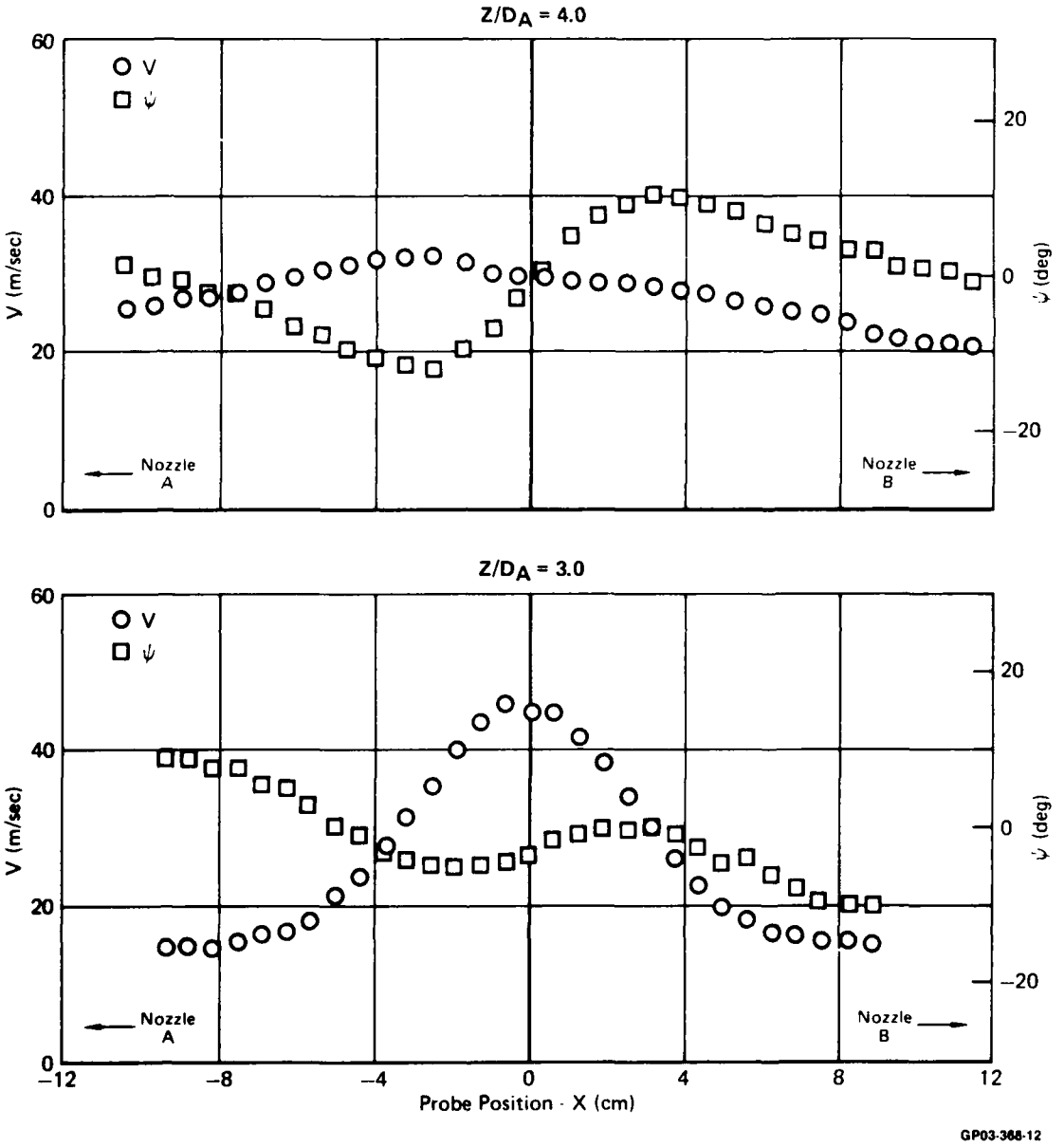

Figure 6. (Concluded) Fountain Velocity Profiles

Case 1c

$NPR_B/NPR_A = 1.00$ $D_B/D_A = 1.00$ $AR_{Plate} = 3.0$

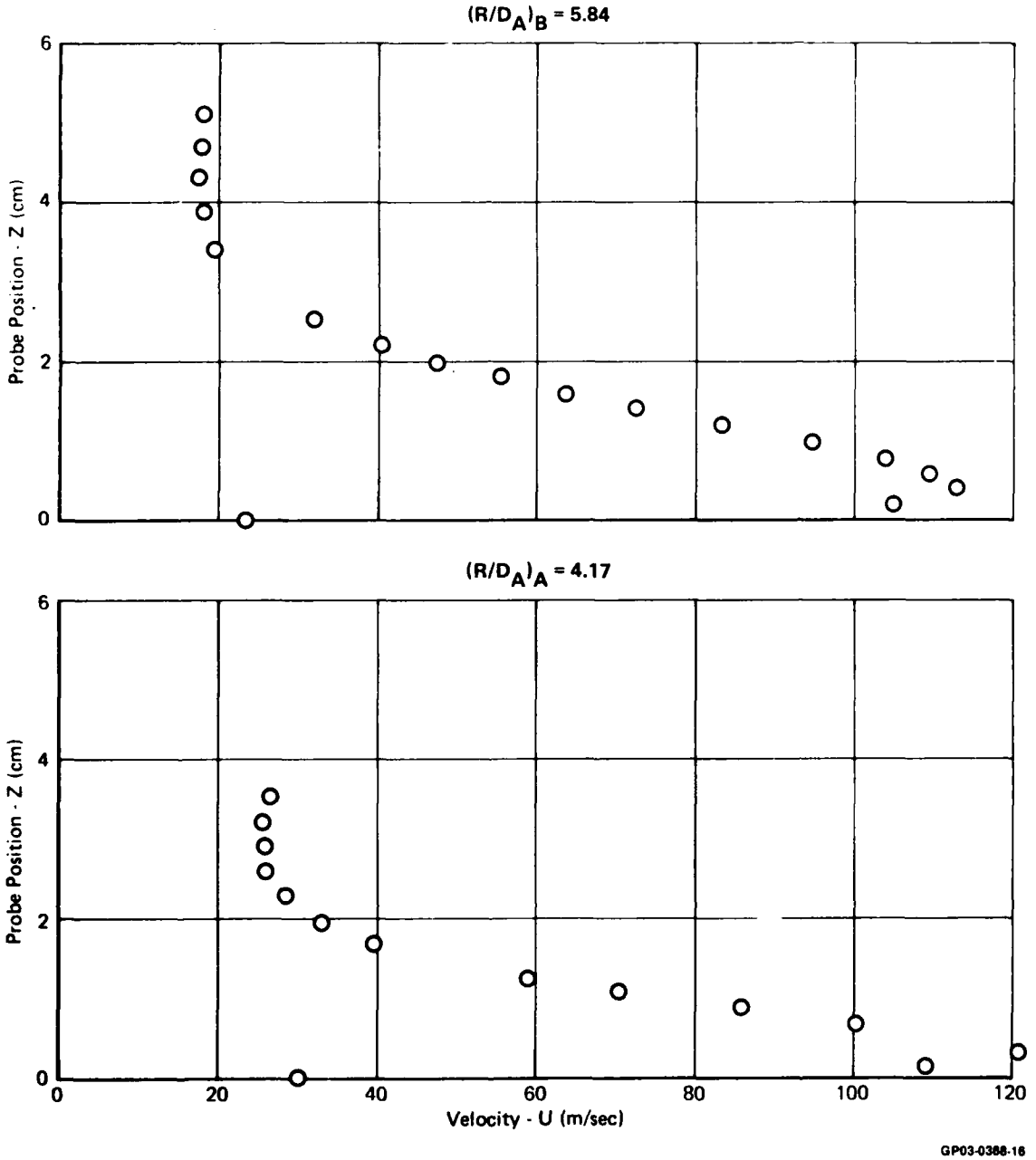

Figure 7. Wall Jet Velocity Profiles
Case 2b
$NPR_B/NPR_A = 1.00$ $D_B/D_A = 1.414$

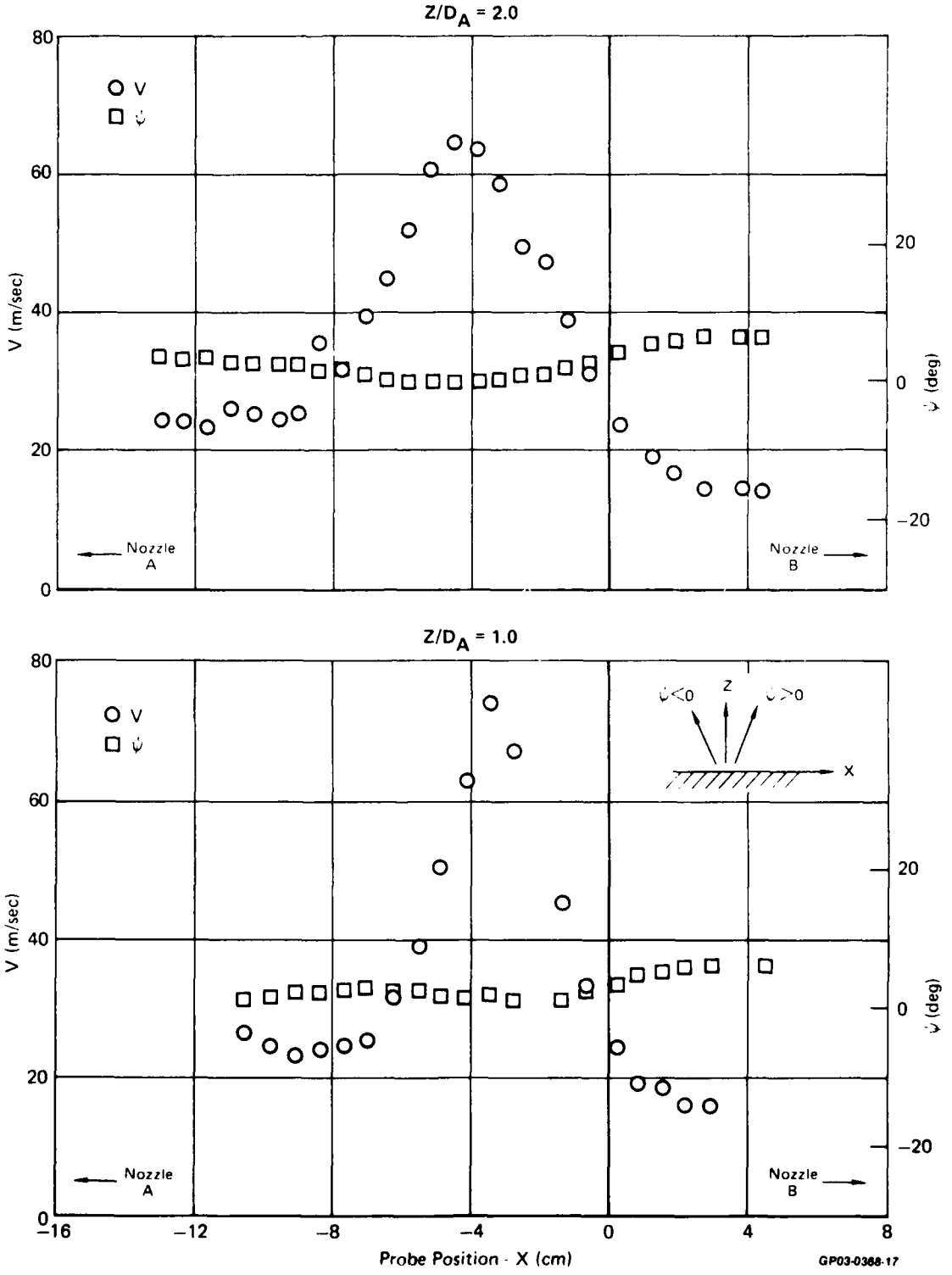

Figure 7. (Continued) Fountain Velocity Profiles
Case 2b
$NPR_B/NPR_A = 1.00 \quad D_B/D_A = 1.414$

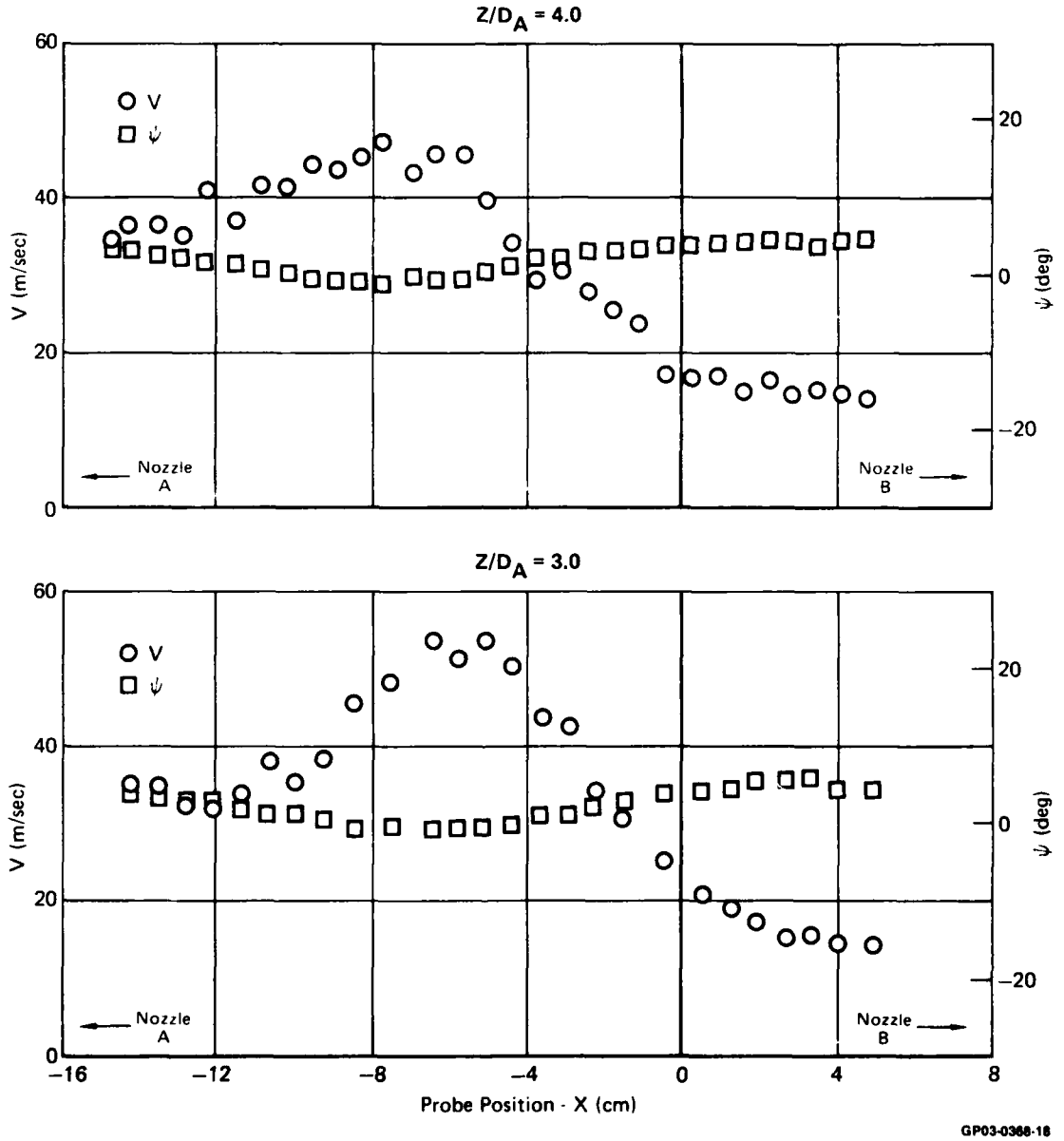

Figure 7. (Concluded) Fountain Velocity Profiles
Case 2b
$NPR_B/NPR_A = 1.00 \quad D_B/D_A = 1.414$

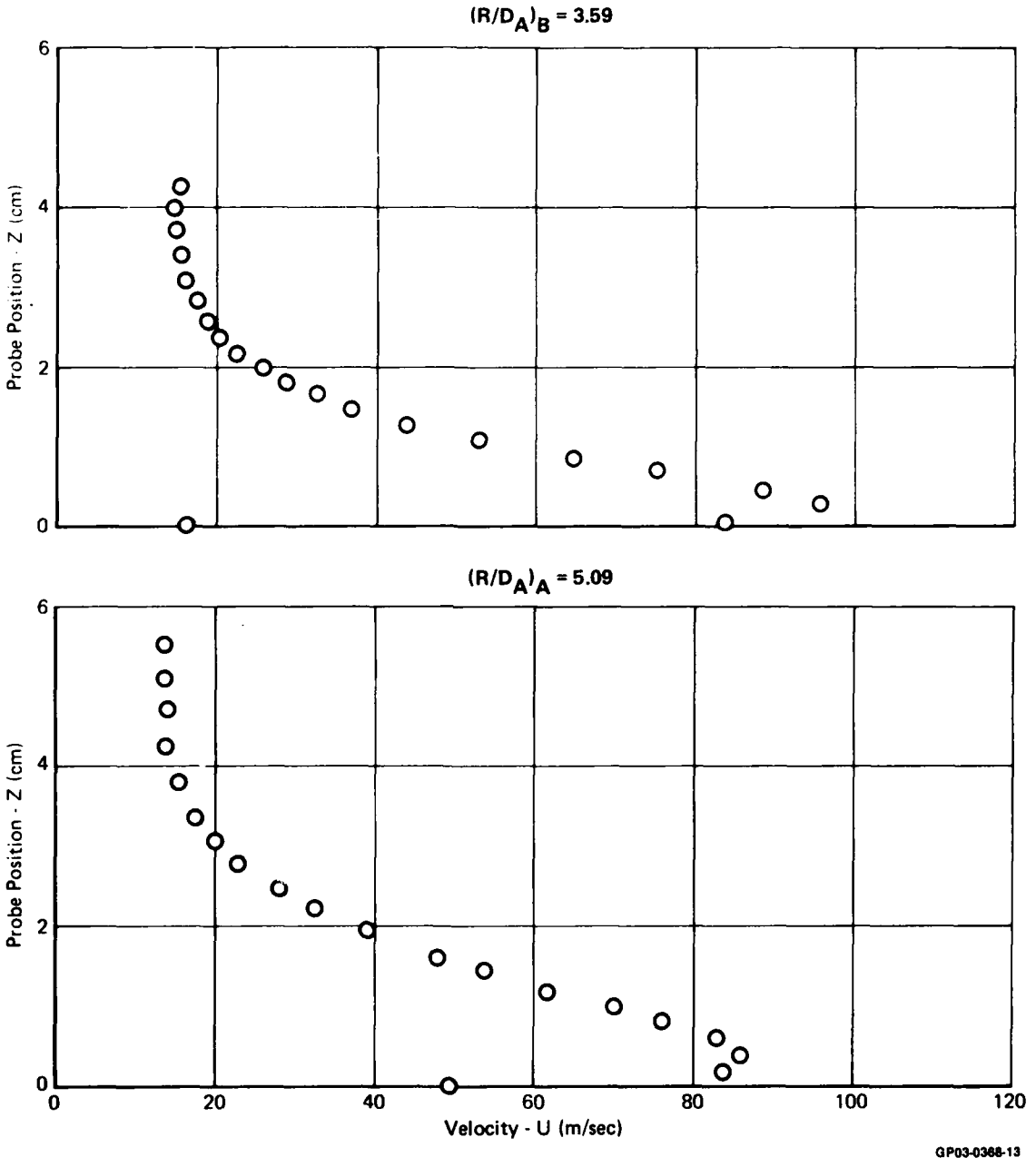

Figure 8. Wall Jet Velocity Profiles
Case 3c3
$NPR_B/NPR_A = 0.74$ $D_B/D_A = 1.00$ $AR_{Plate} = 3.0$

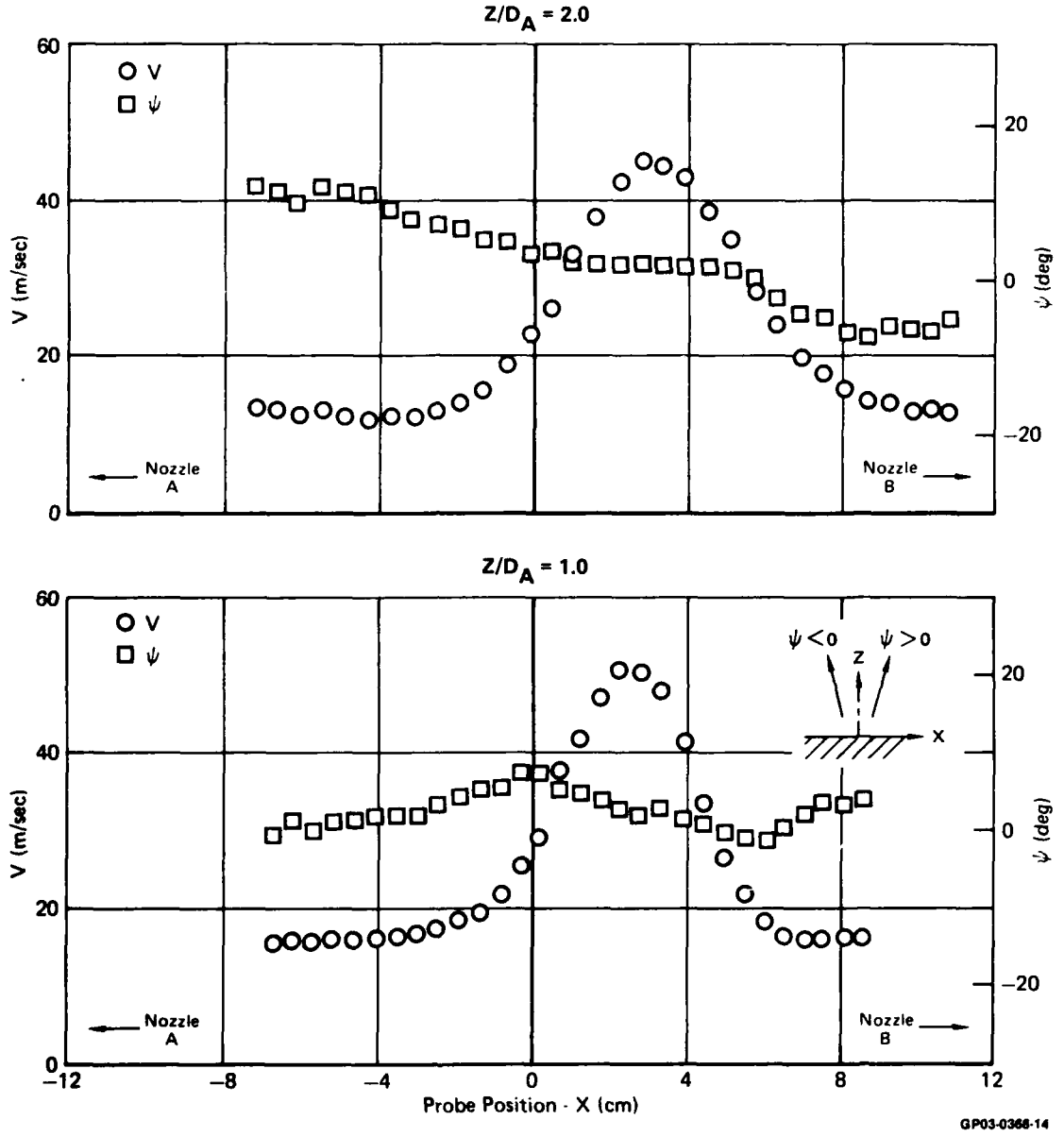

Figure 8. (Continued) Fountain Velocity Profiles
Case 3c3
NPR_B/NPR_A = 0.74 D_B/D_A = 1.00 AR_{Plate} = 3.0

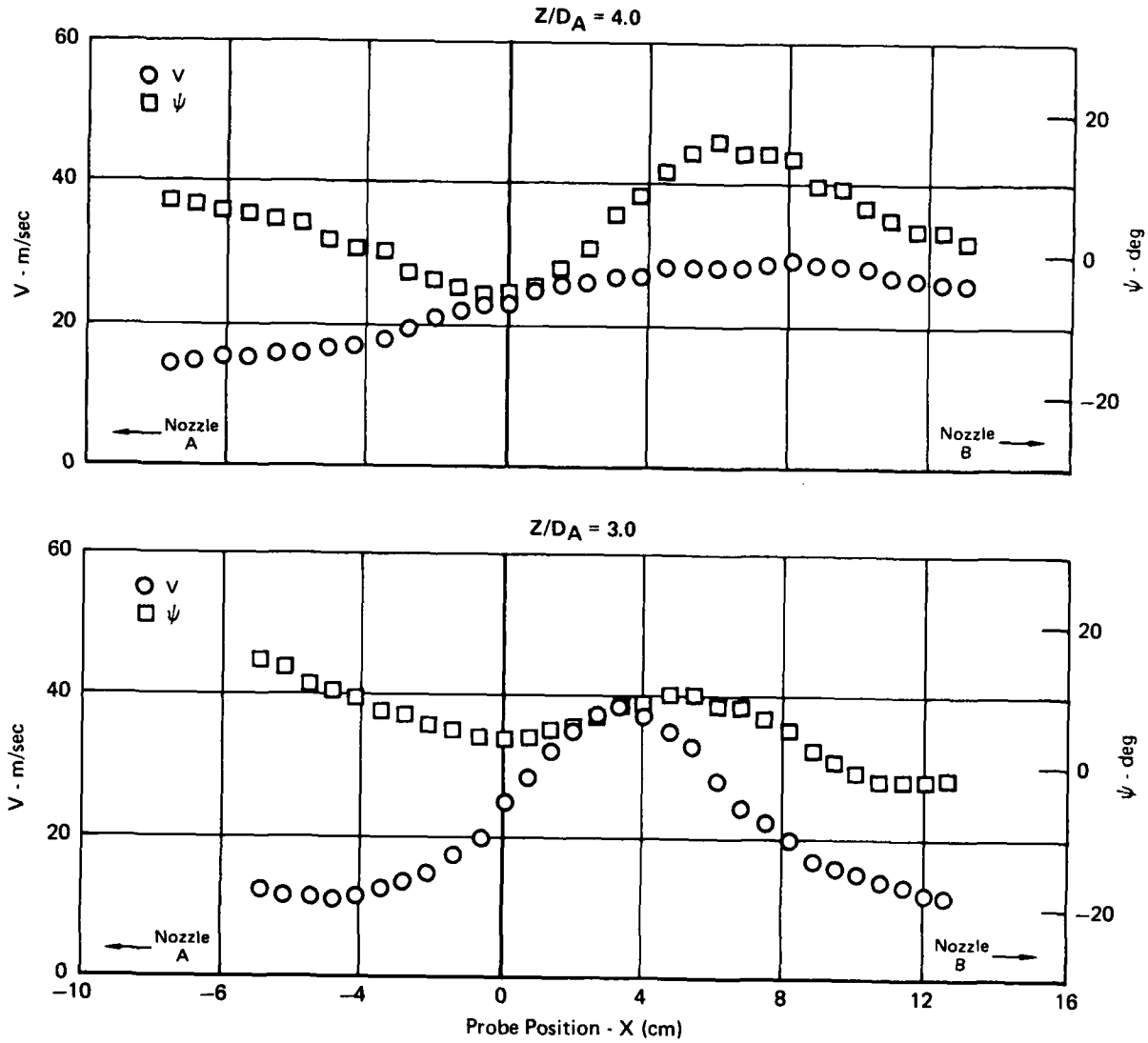

Figure 8. (Concluded) Fountain Velocity Profiles

Case 3c3

$NPR_B/NPR_A = 0.74$ $D_B/D_A = 1.00$ $AR_{Plate} = 3.0$

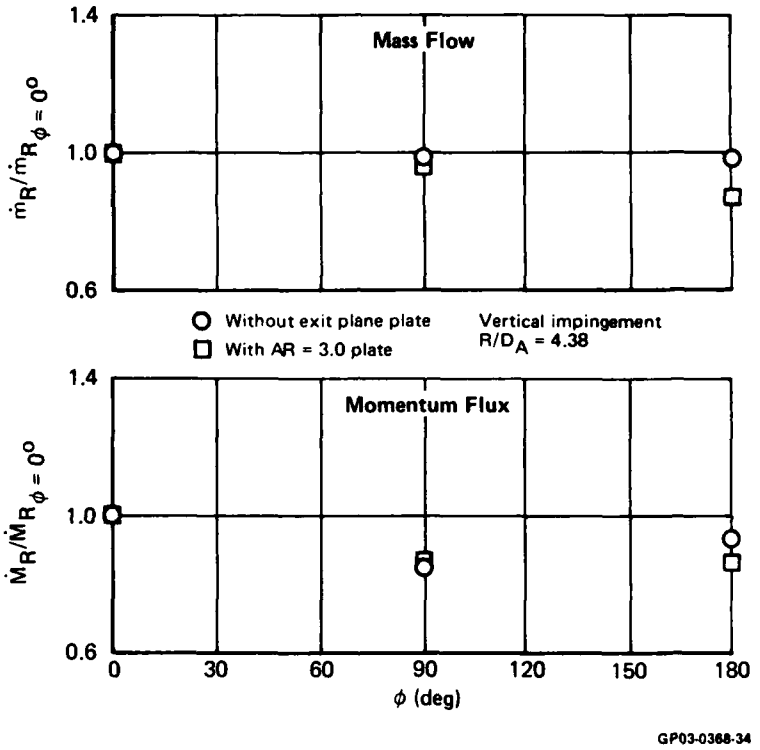

Figure 9. Azimuthal Distribution of Wall Jet Radial Mass Flow and Momentum Flux
Case 1

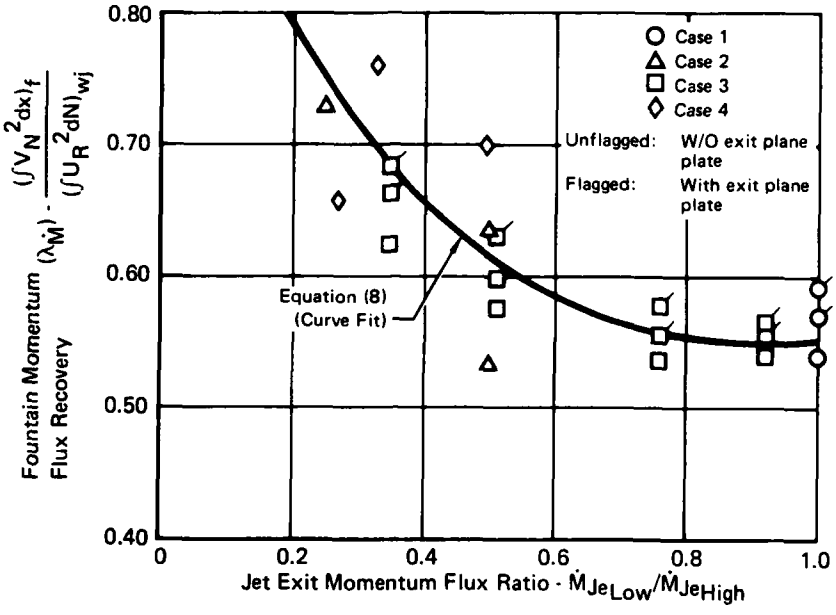

Figure 10. Fountain Momentum Flux Recovery
Based on Conservation of Mass Flux Through
the Fountain Formation Region
Cases 1-4

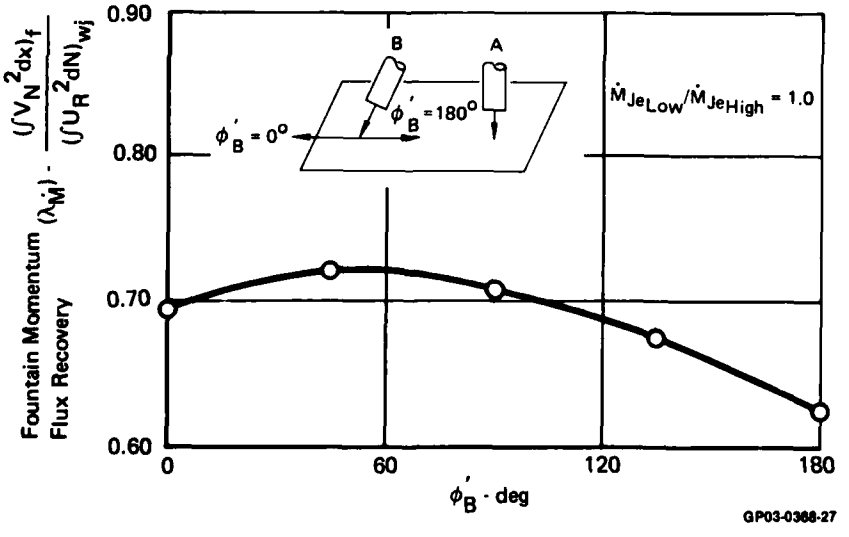

Figure 11. Fountain Momentum Flux Recovery
Based on Conservation of Mass Flux Through
the Fountain Formation Region
Case 5

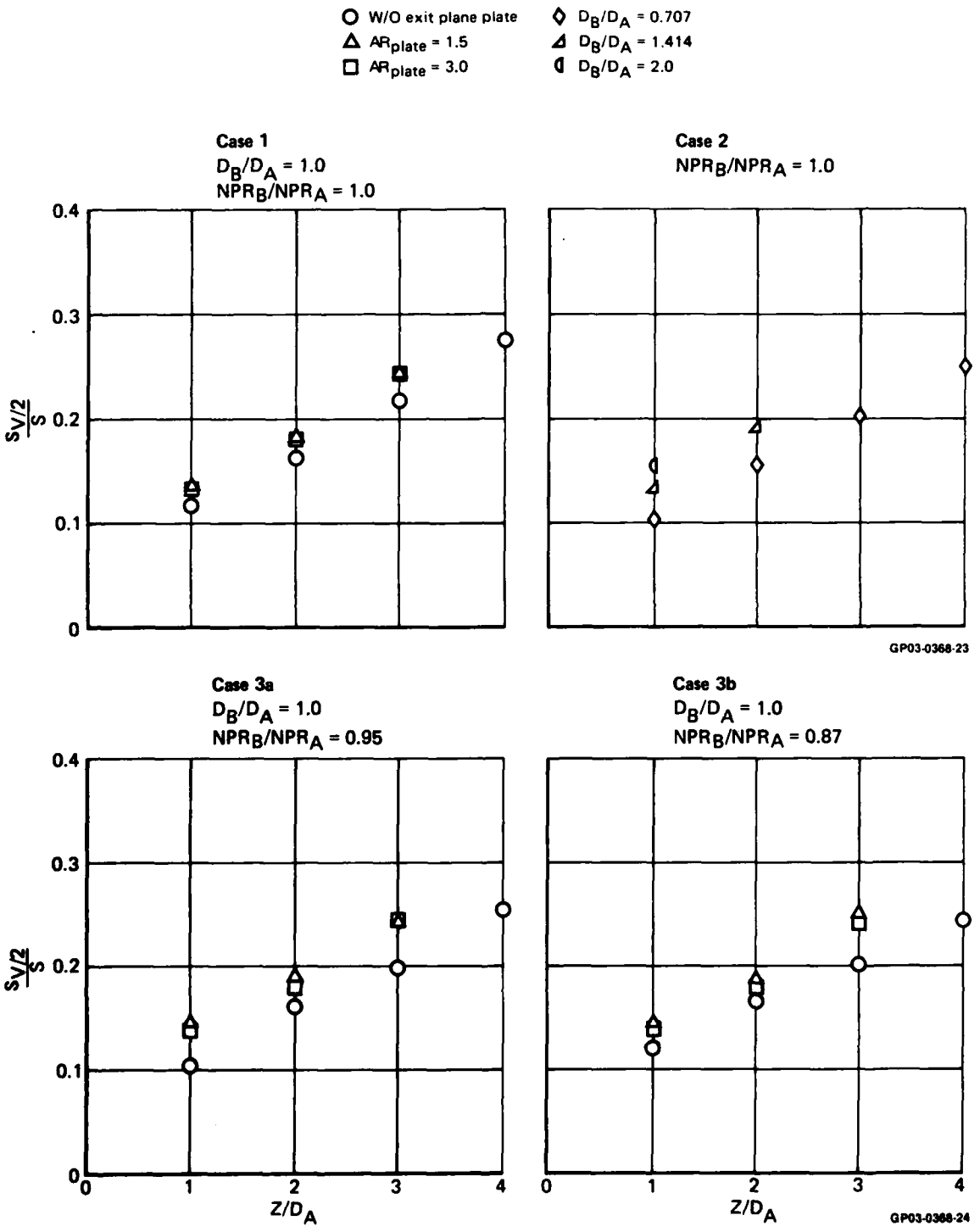

Figure 12. Fountain Spreading Characteristics

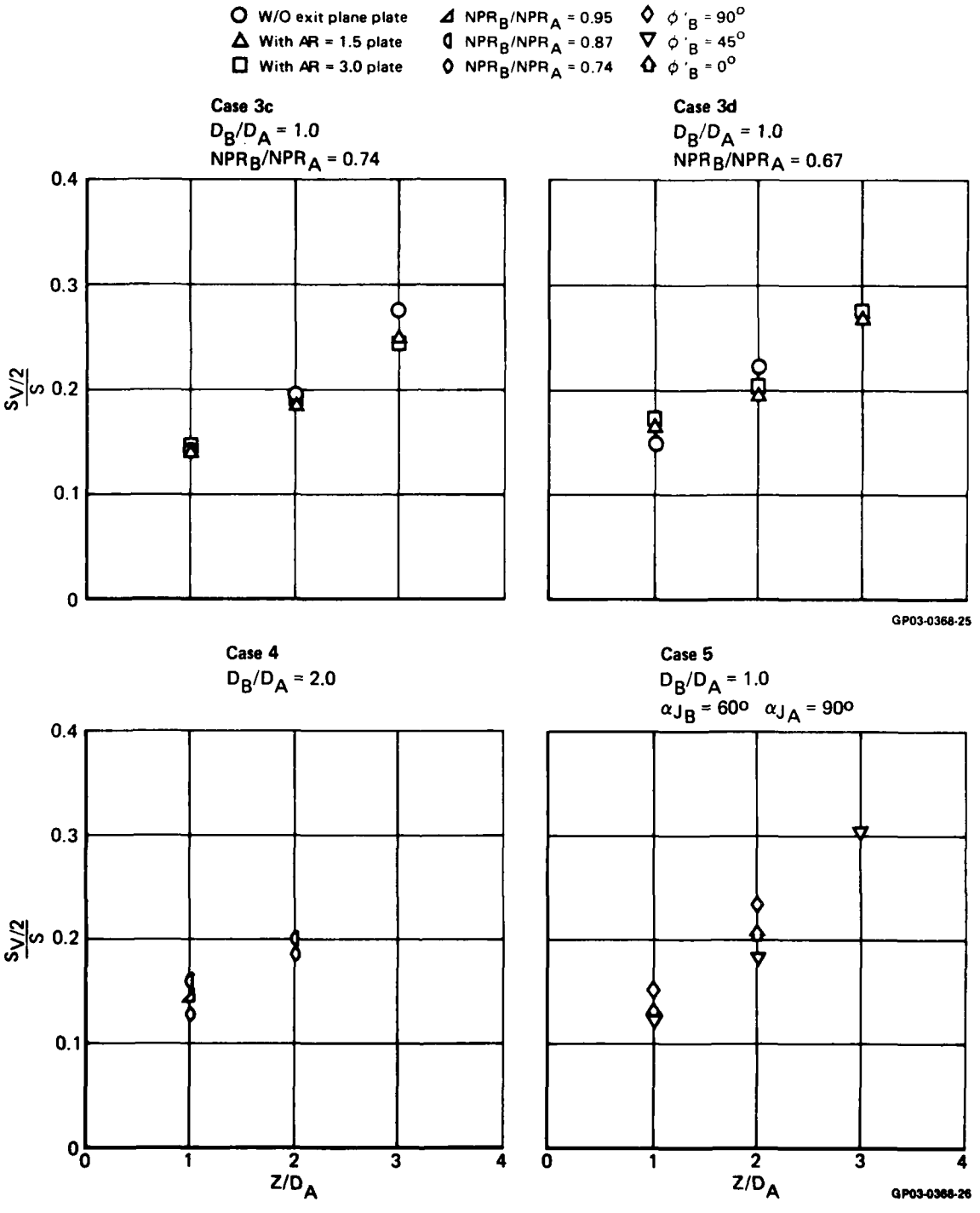

Figure 12. (Concluded) Fountain Spreading Characteristics

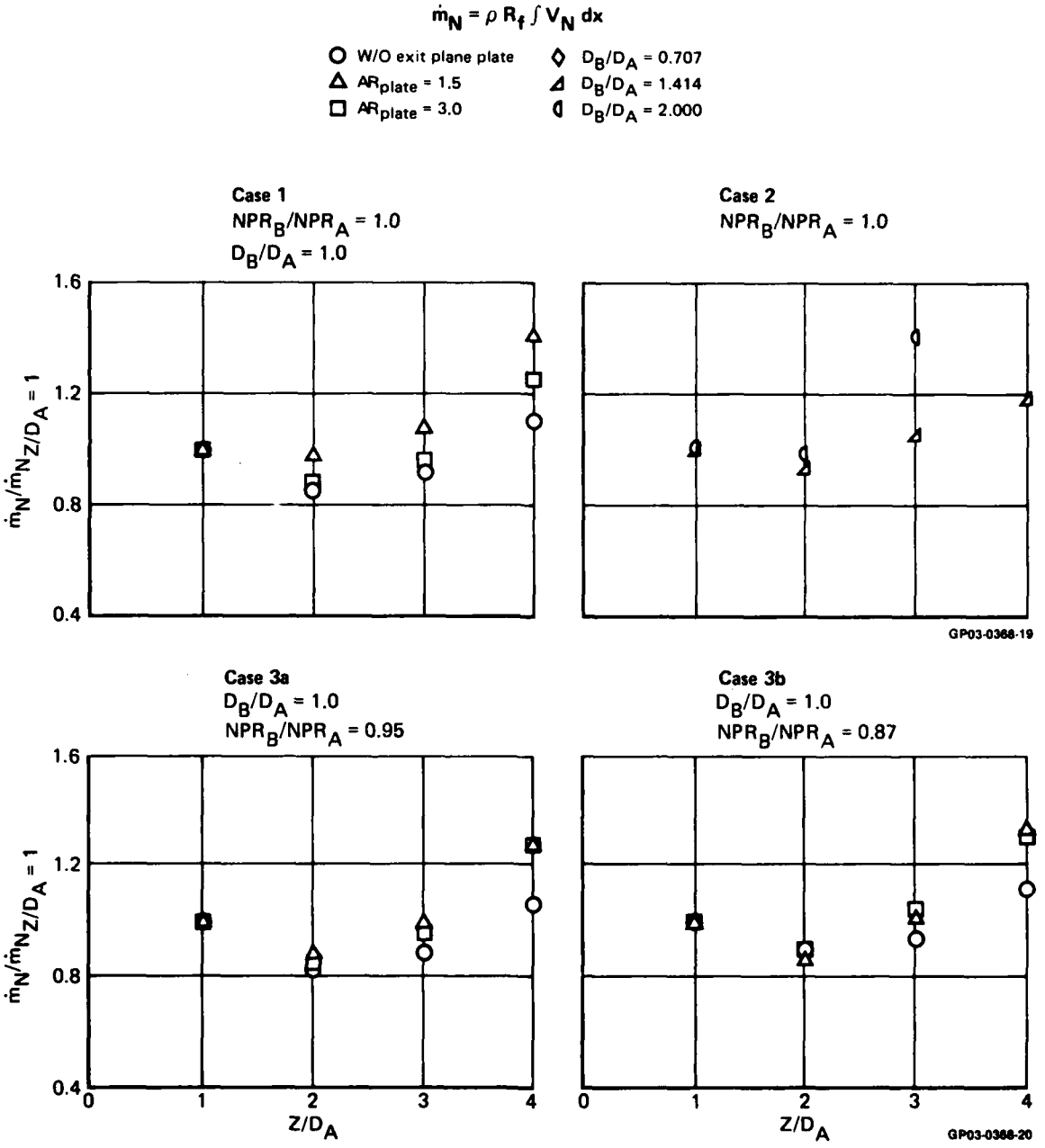

Figure 13. Fountain Mass Flow
Based on Conservation of Vertical Momentum Flux
(Method 1)

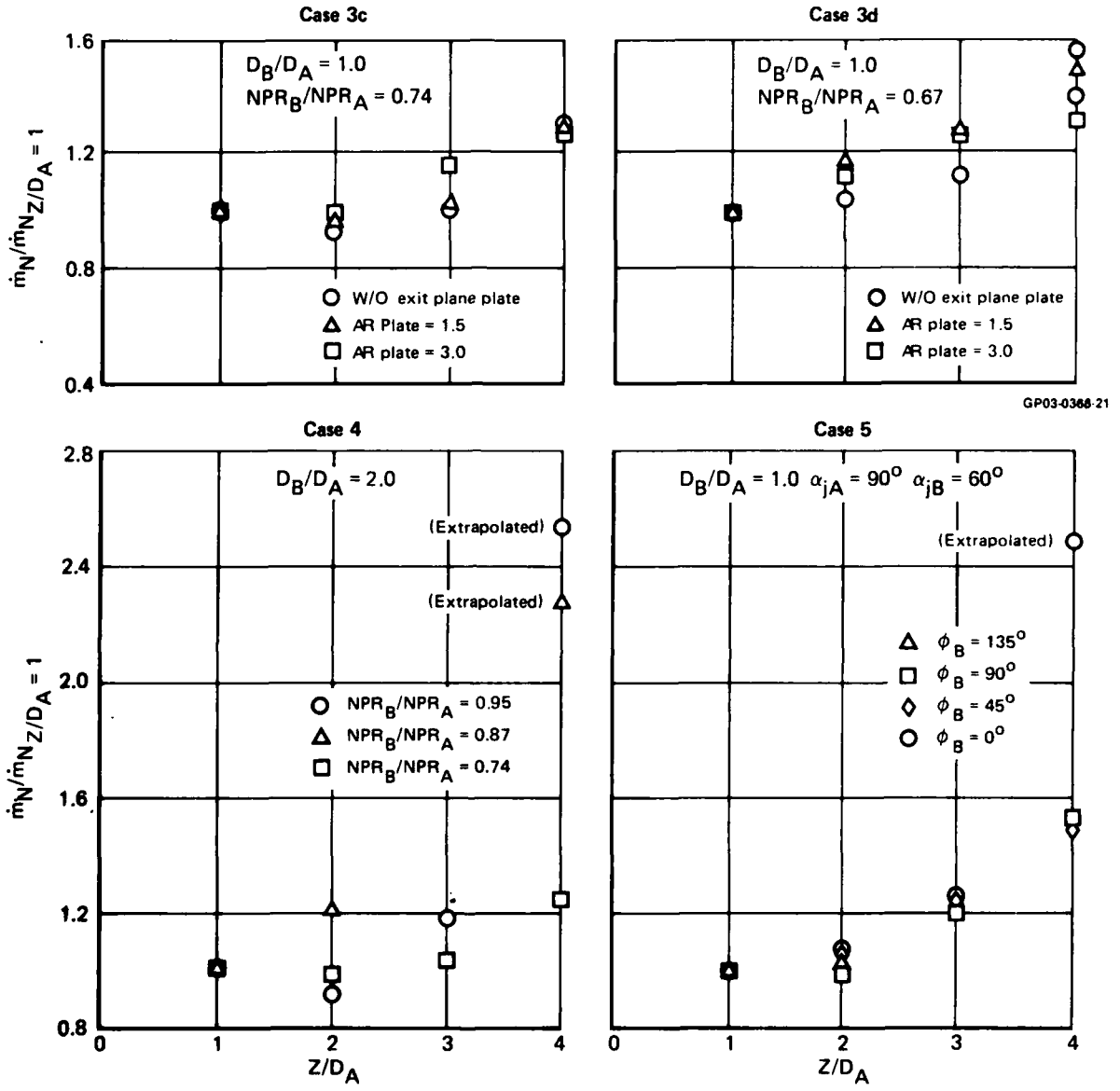

Figure 13. (Concluded) Fountain Mass Flow
Based on Conservation of Vertical Momentum Flux
(Method 1)

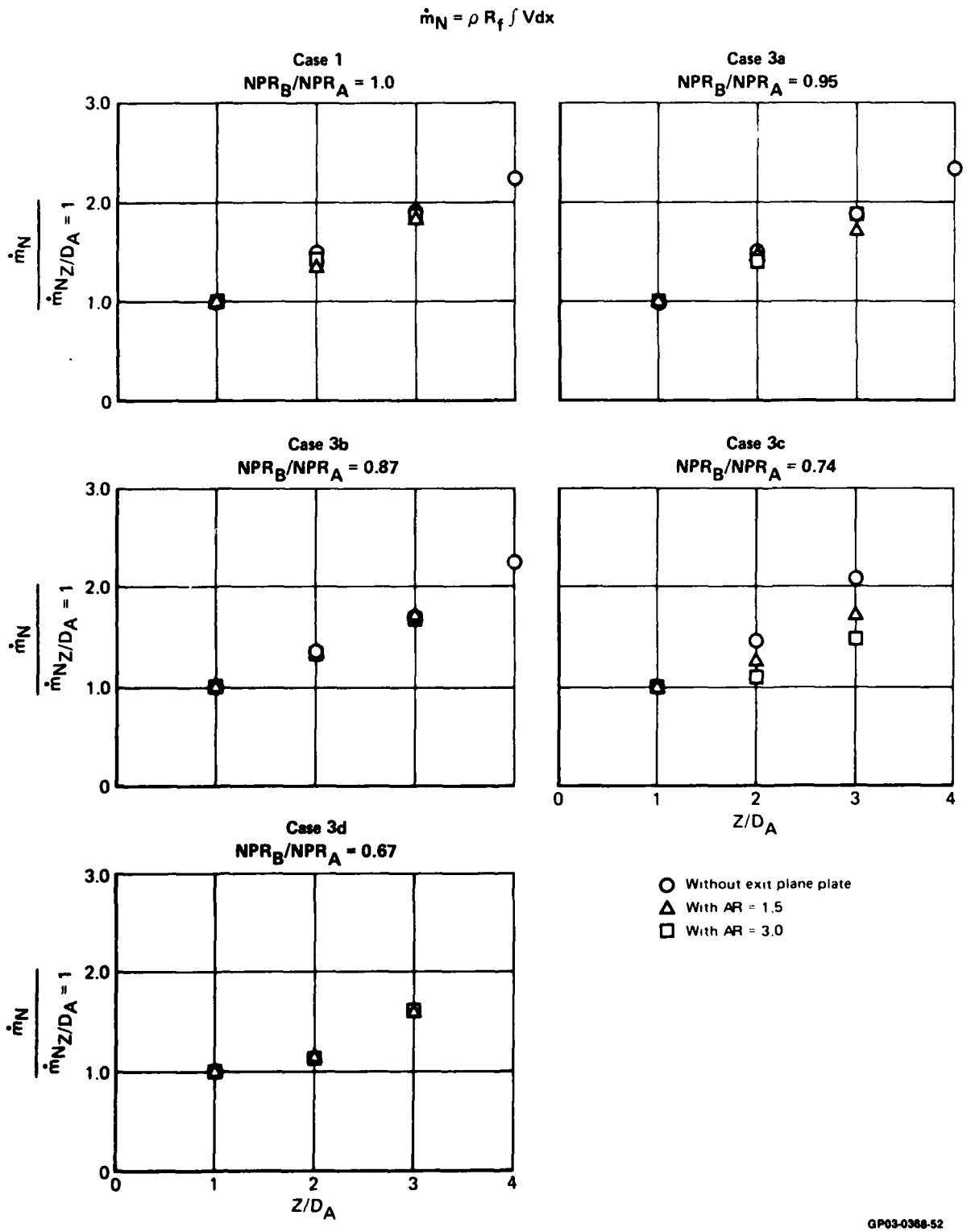

Figure 14. Fountain Mass Flow
(Method 2)

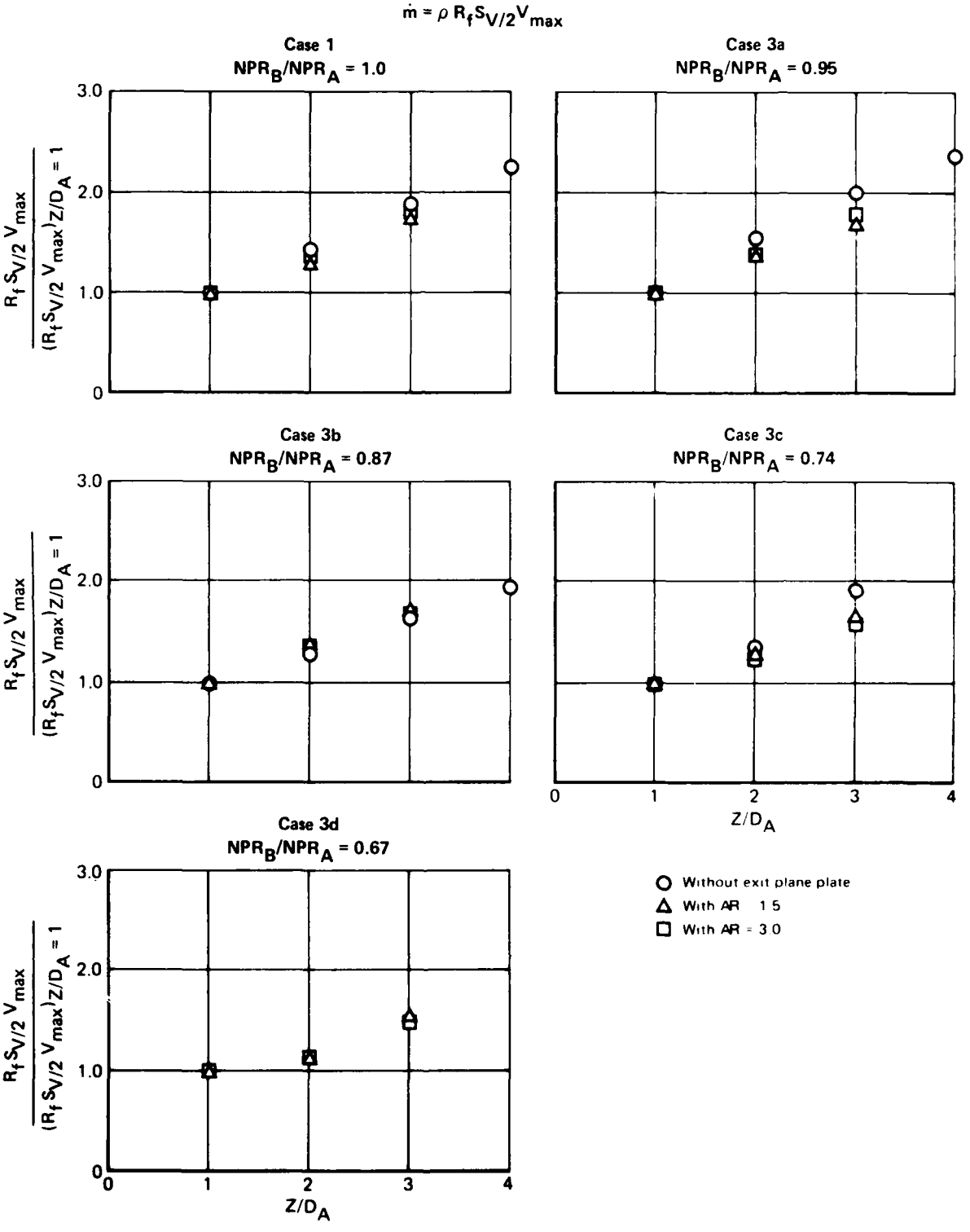

Figure 15. Fountain Mass Flow
(Method 3)

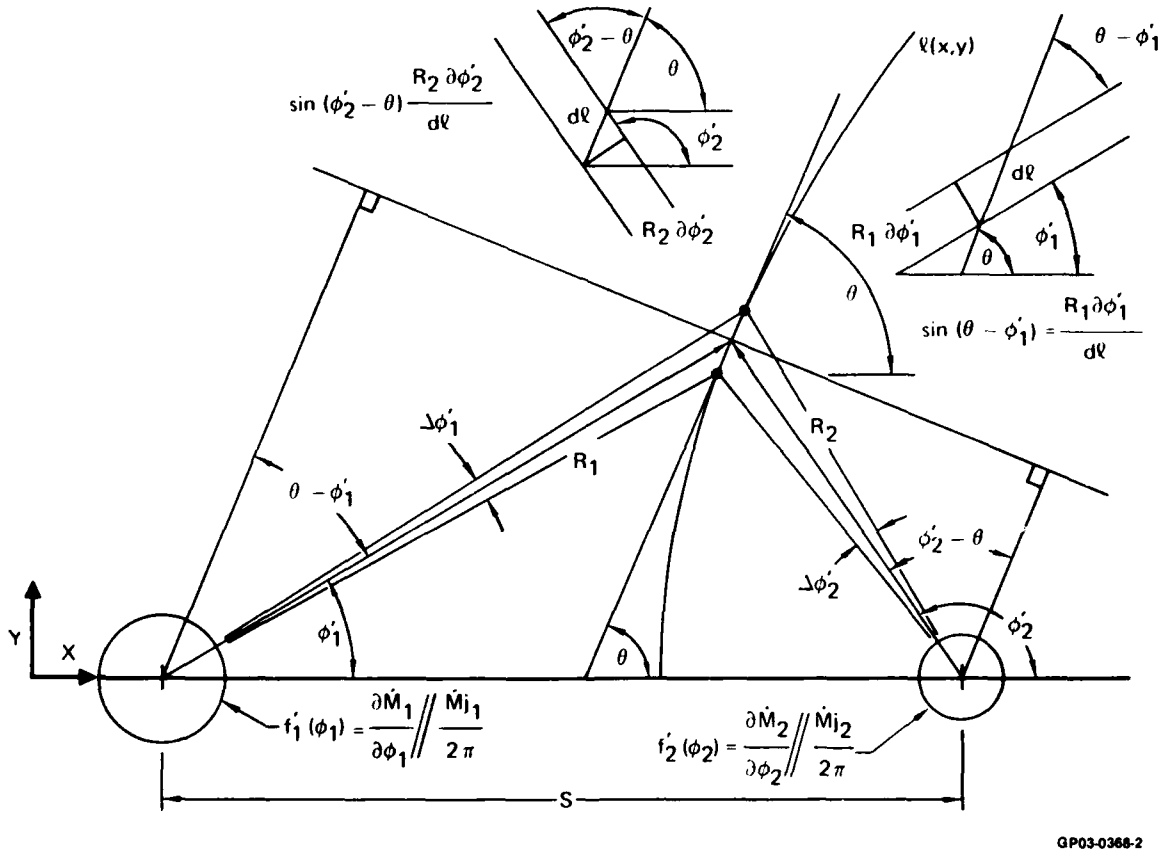

Figure 16. Wall Jet Interaction Geometry

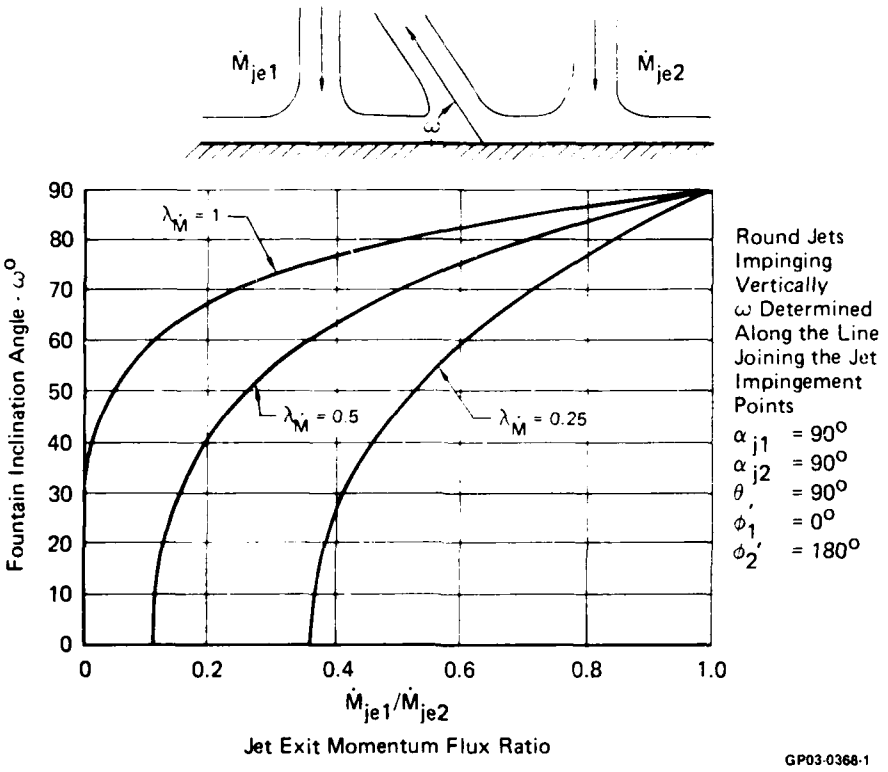

Figure 17. Fountain Inclination Angle

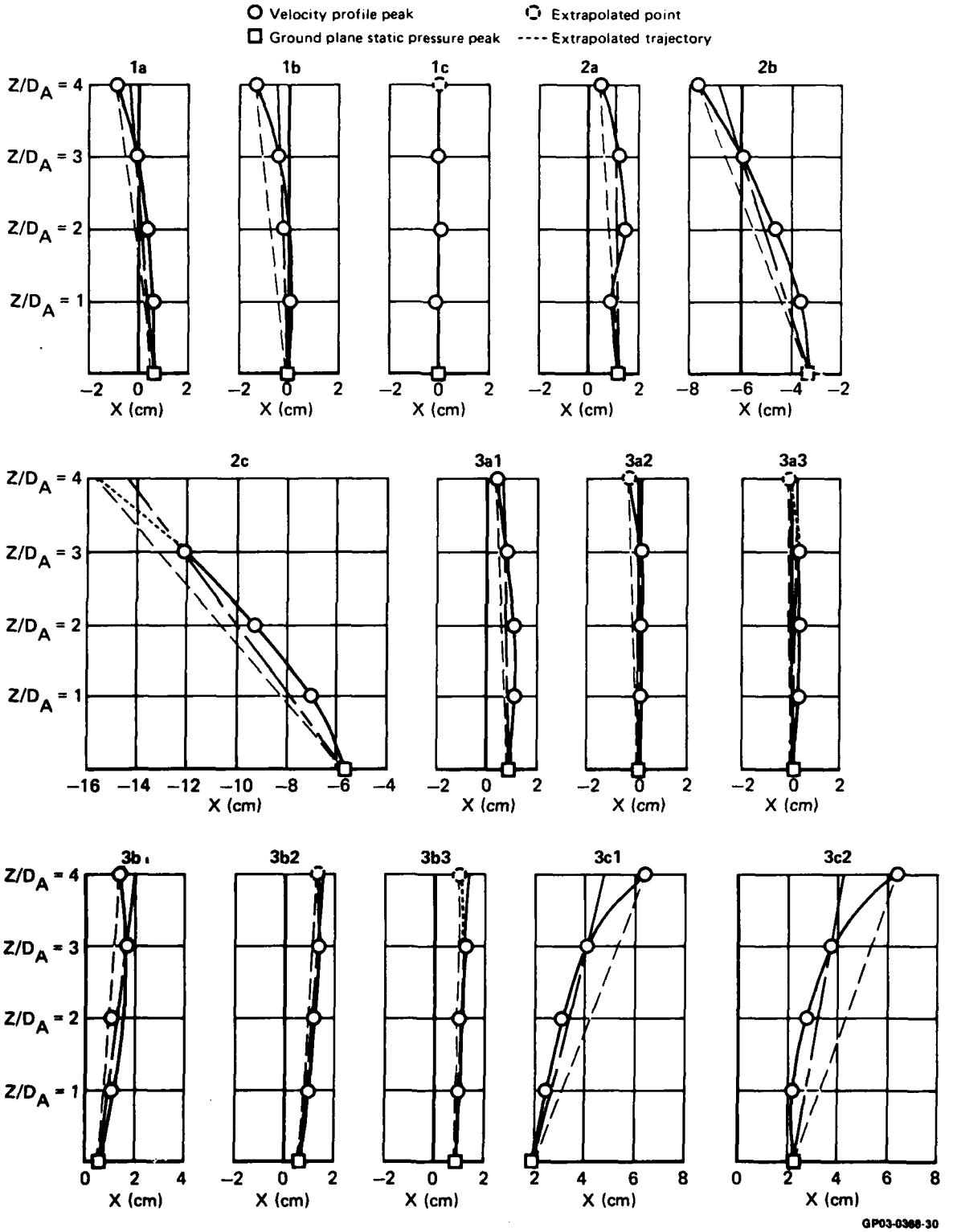

Figure 18. Fountain Trajectories

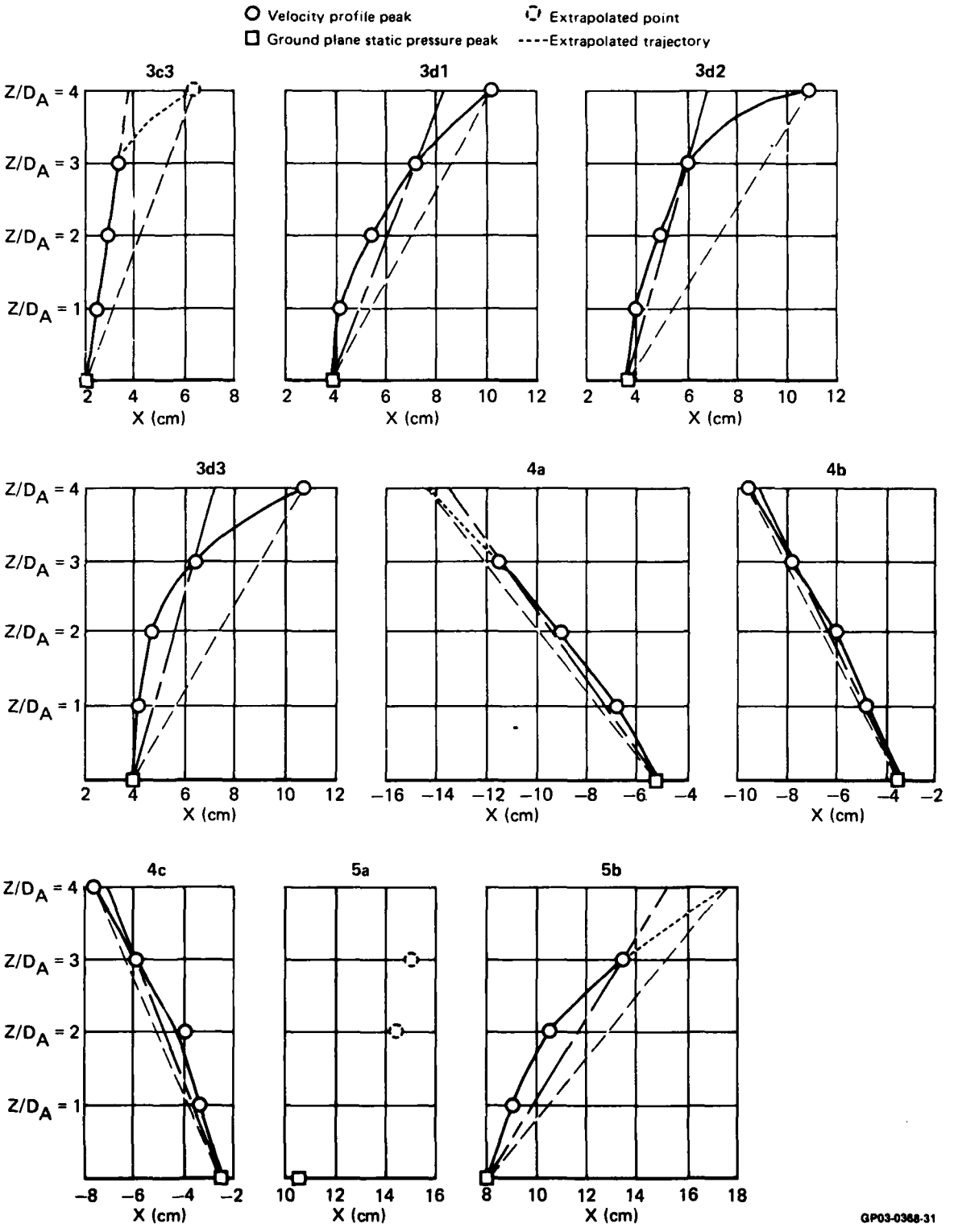

Figure 18. (Continued) Fountain Trajectories

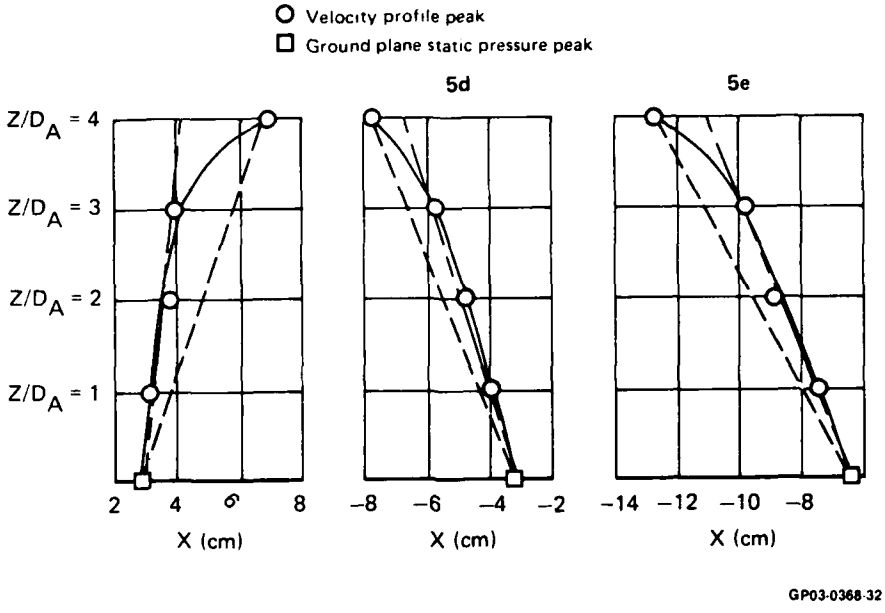

Figure 18. (Concluded) Fountain Trajectories

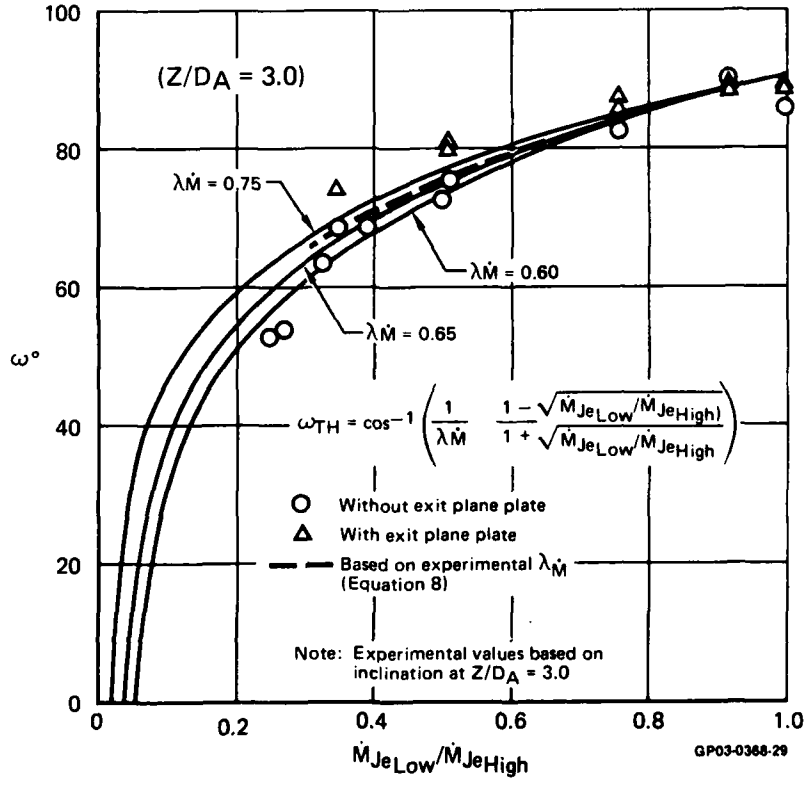

Figure 19. Two-Jet Fountain Inclination - Vertical Impingement

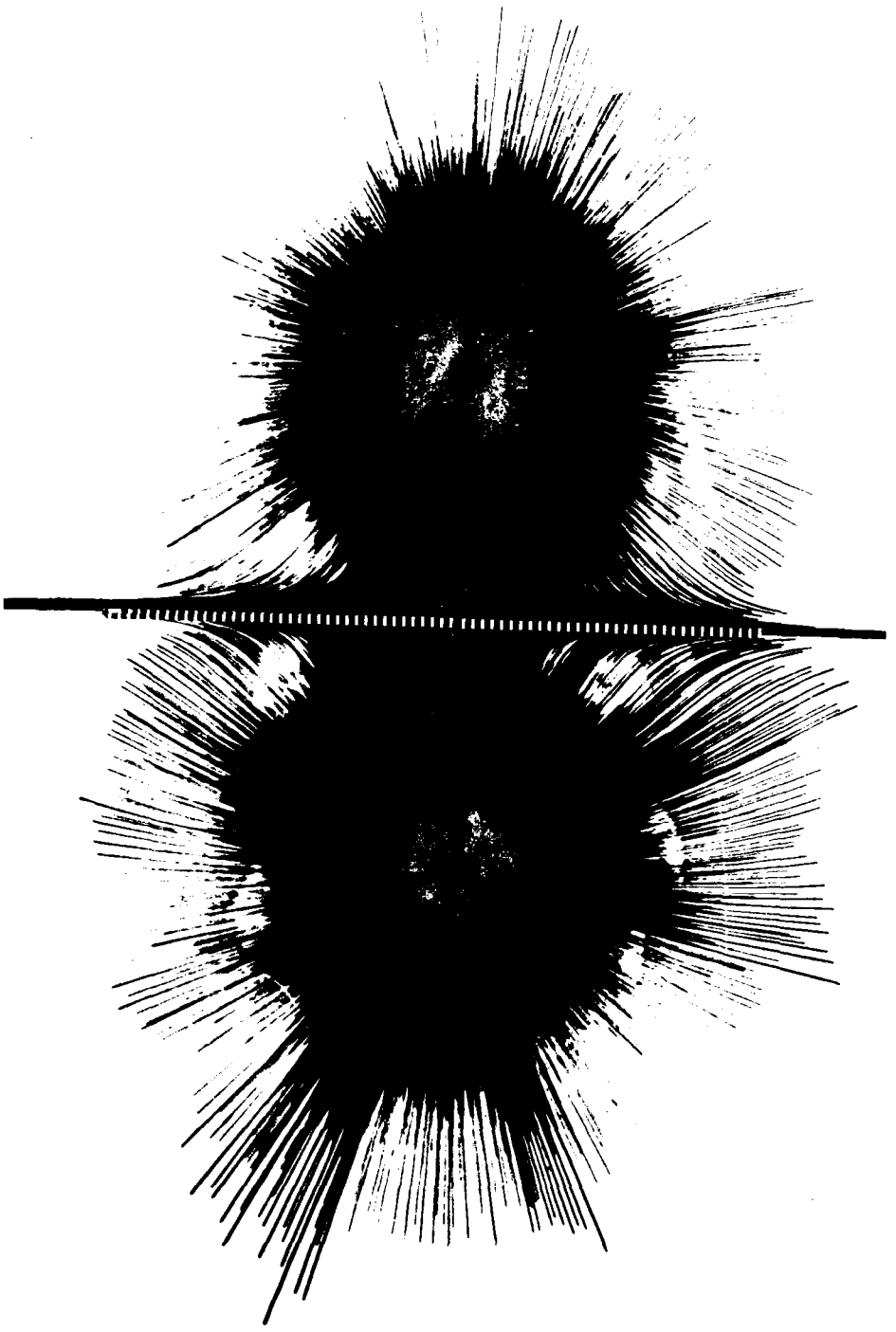

GP03-0368-35

Figure 20. Flow Visualization
Case 1a

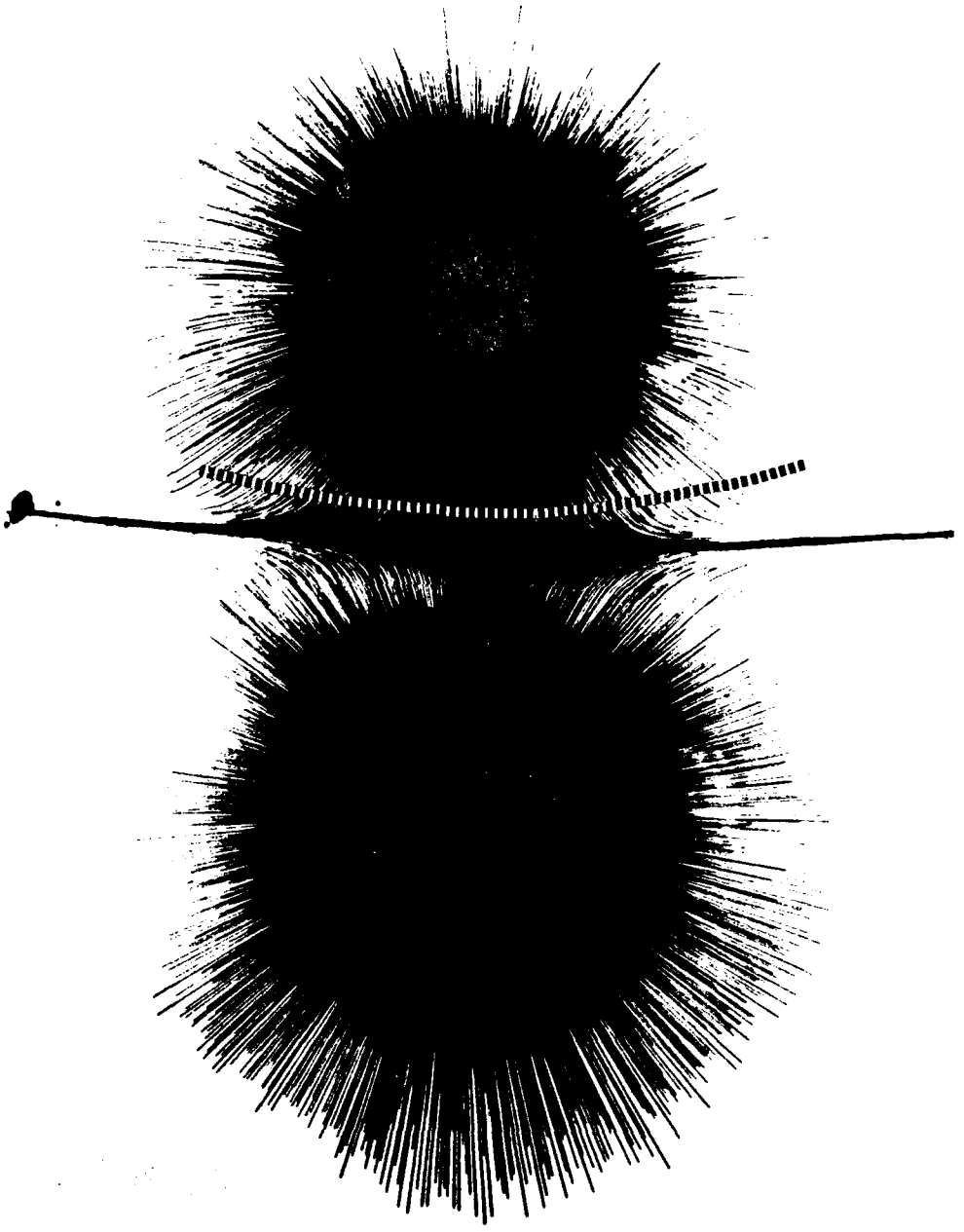

GP03-0368-36

Figure 21. Flow Visualization
Case 2a

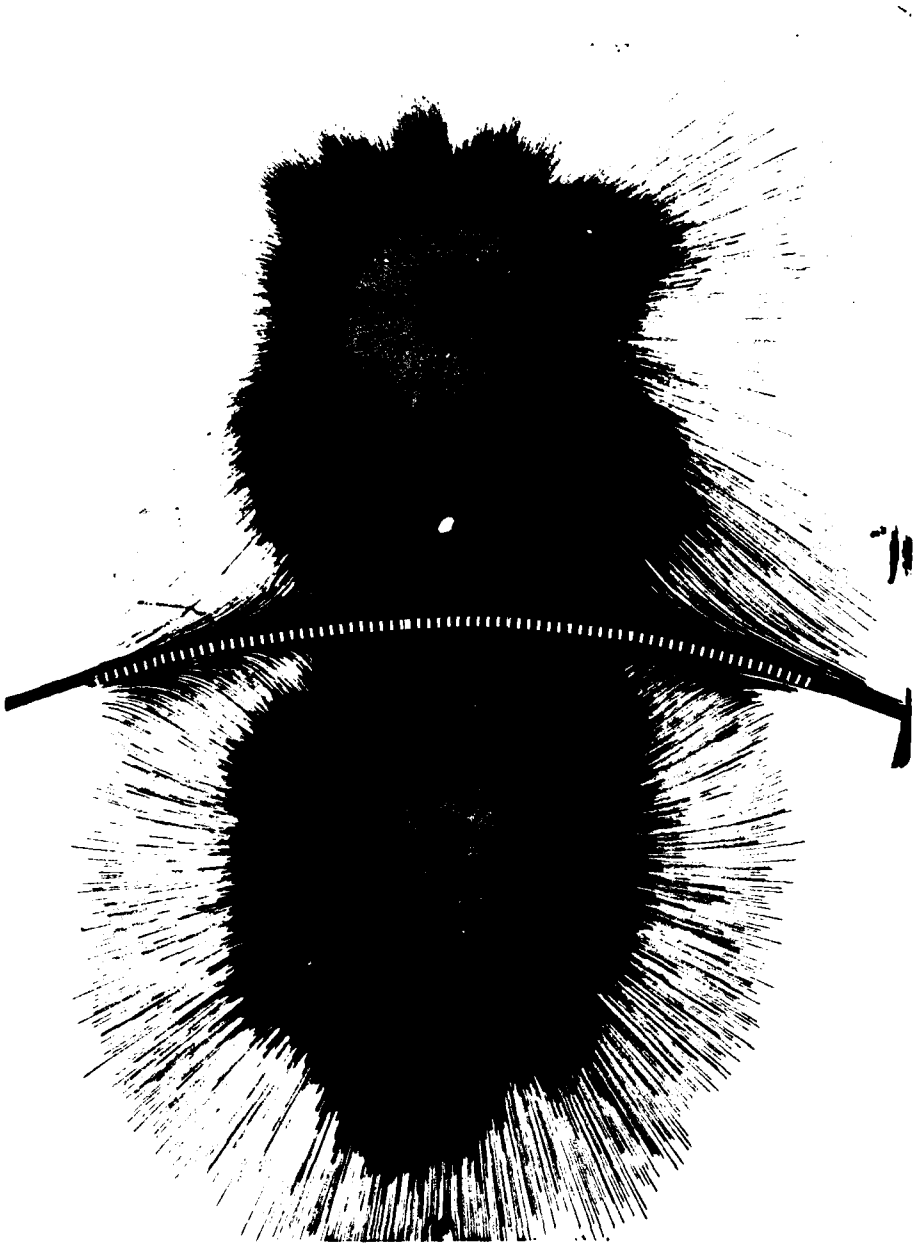

GP03-0368-37

Figure 22. Flow Visualization
Case 2b

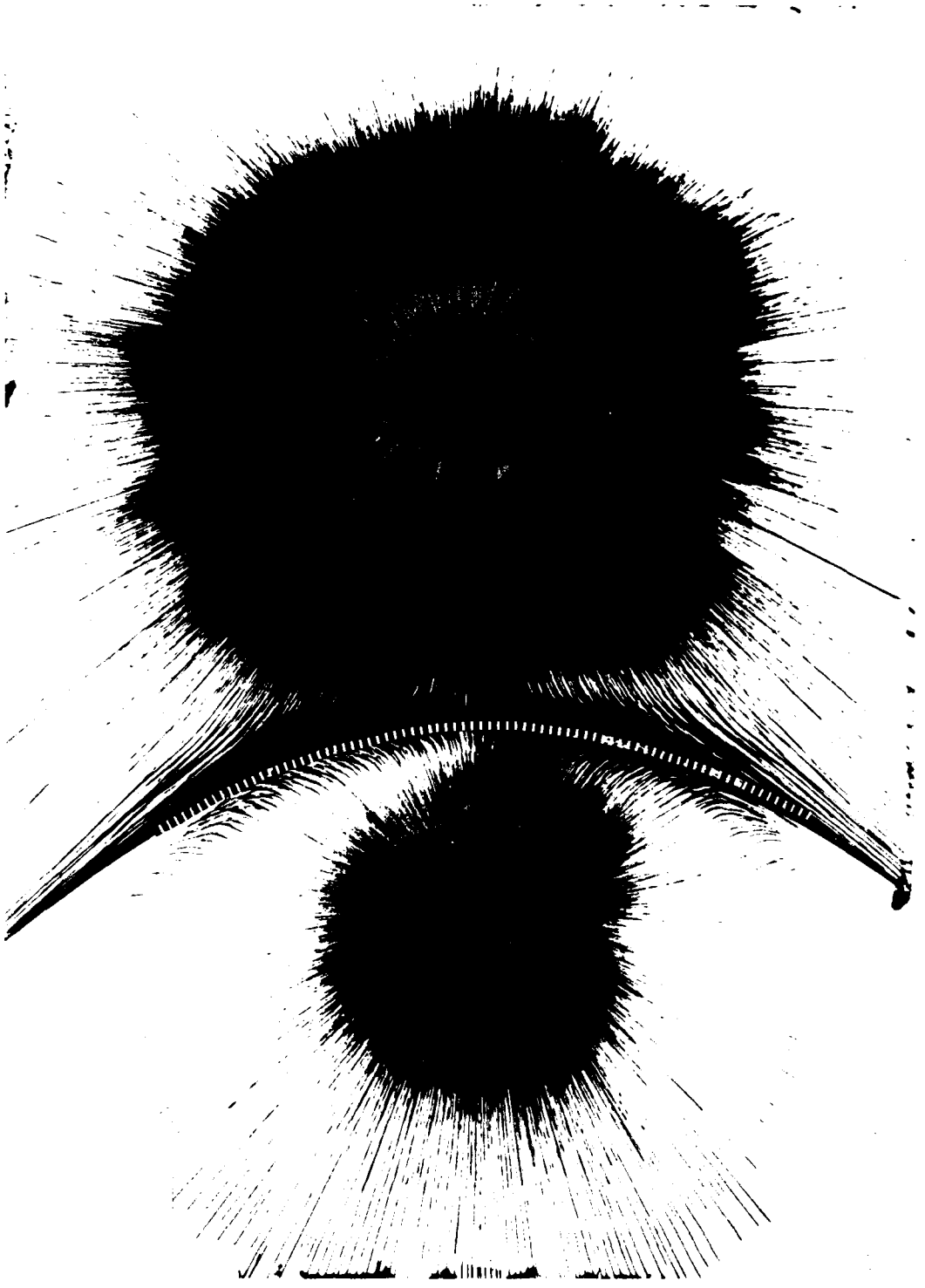

GP03-0368-39

Figure 23. Flow Visualization
Case 2c

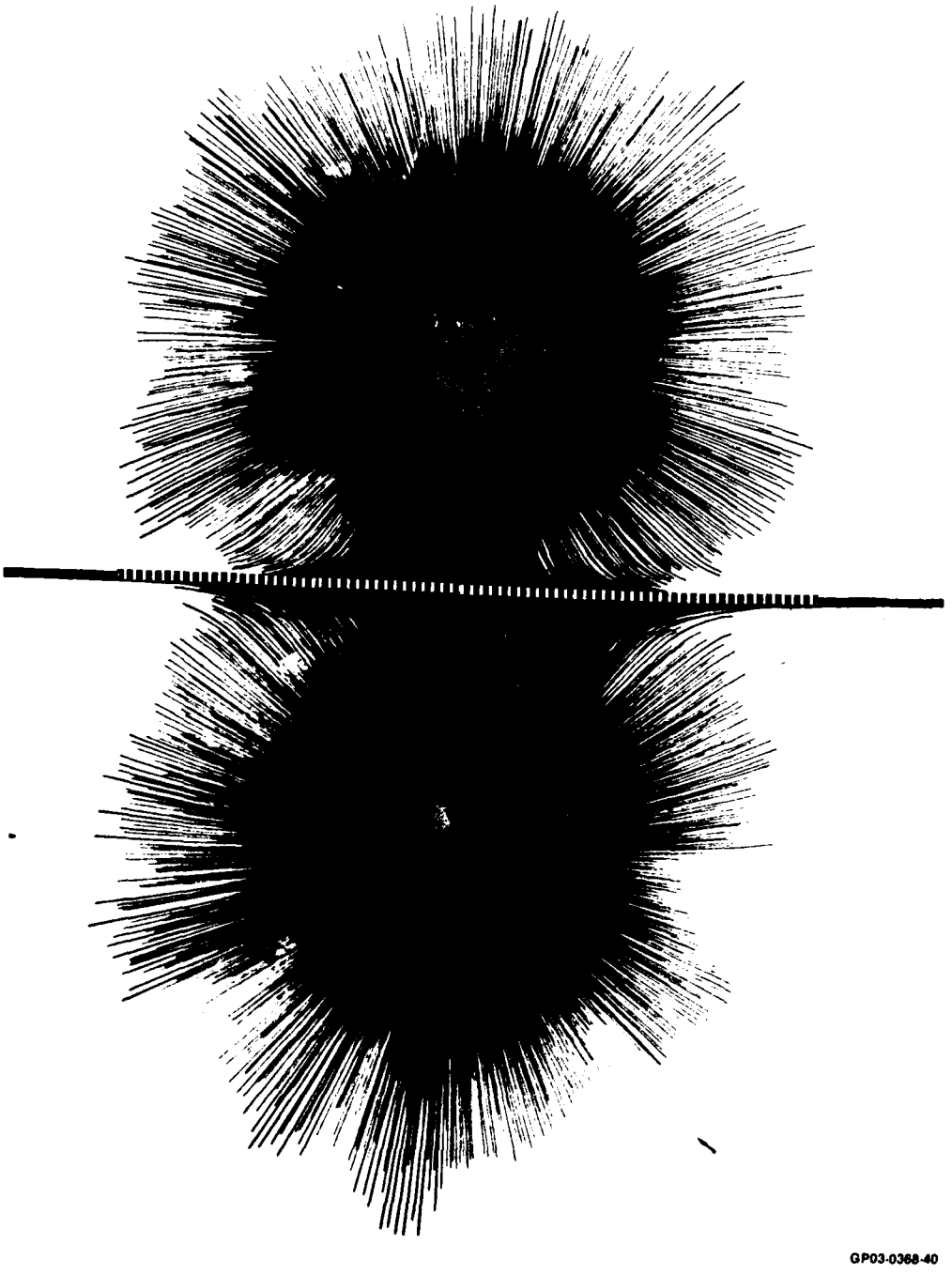

Figure 24. Flow Visualization
Case 3a1

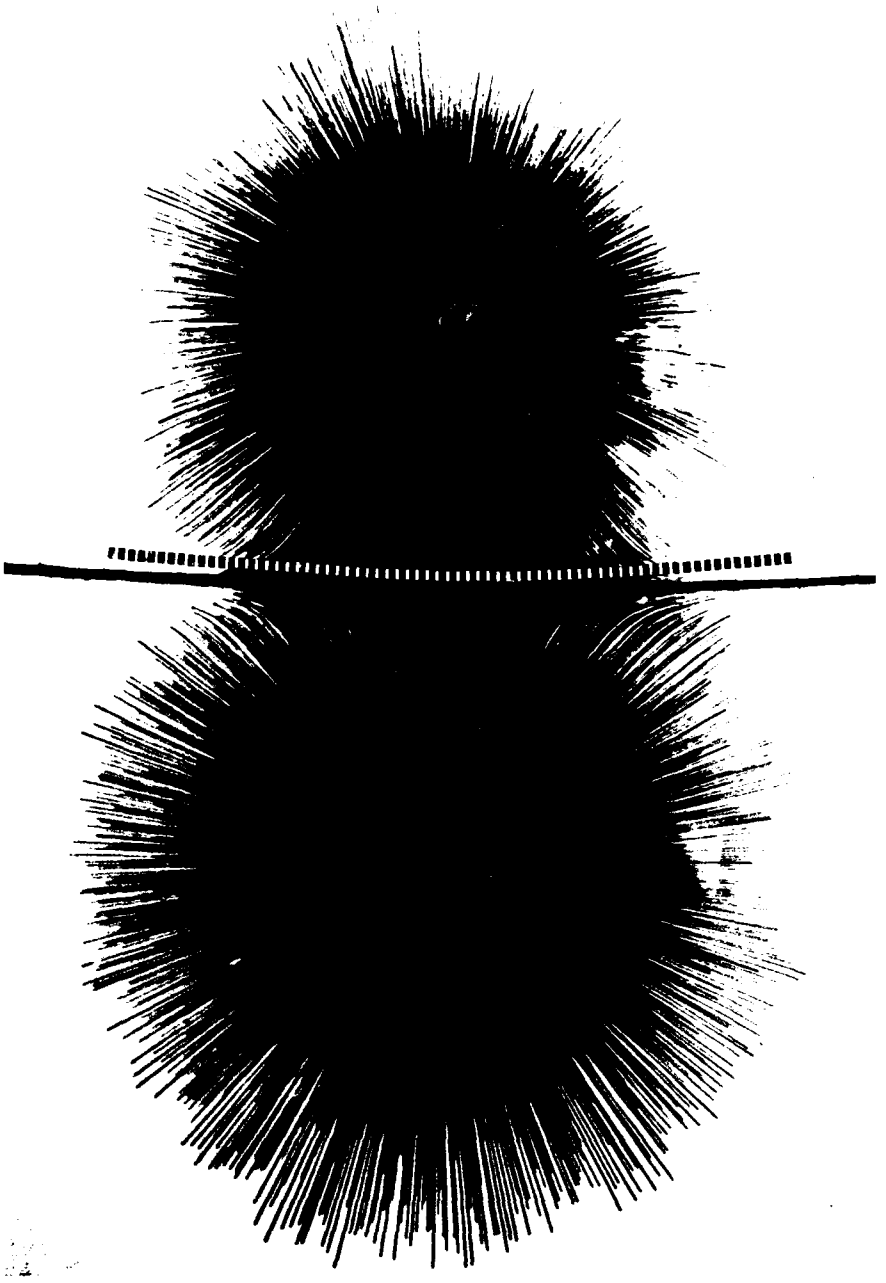

GP03-0388-38

Figure 25. Flow Visualization
Case 3b1

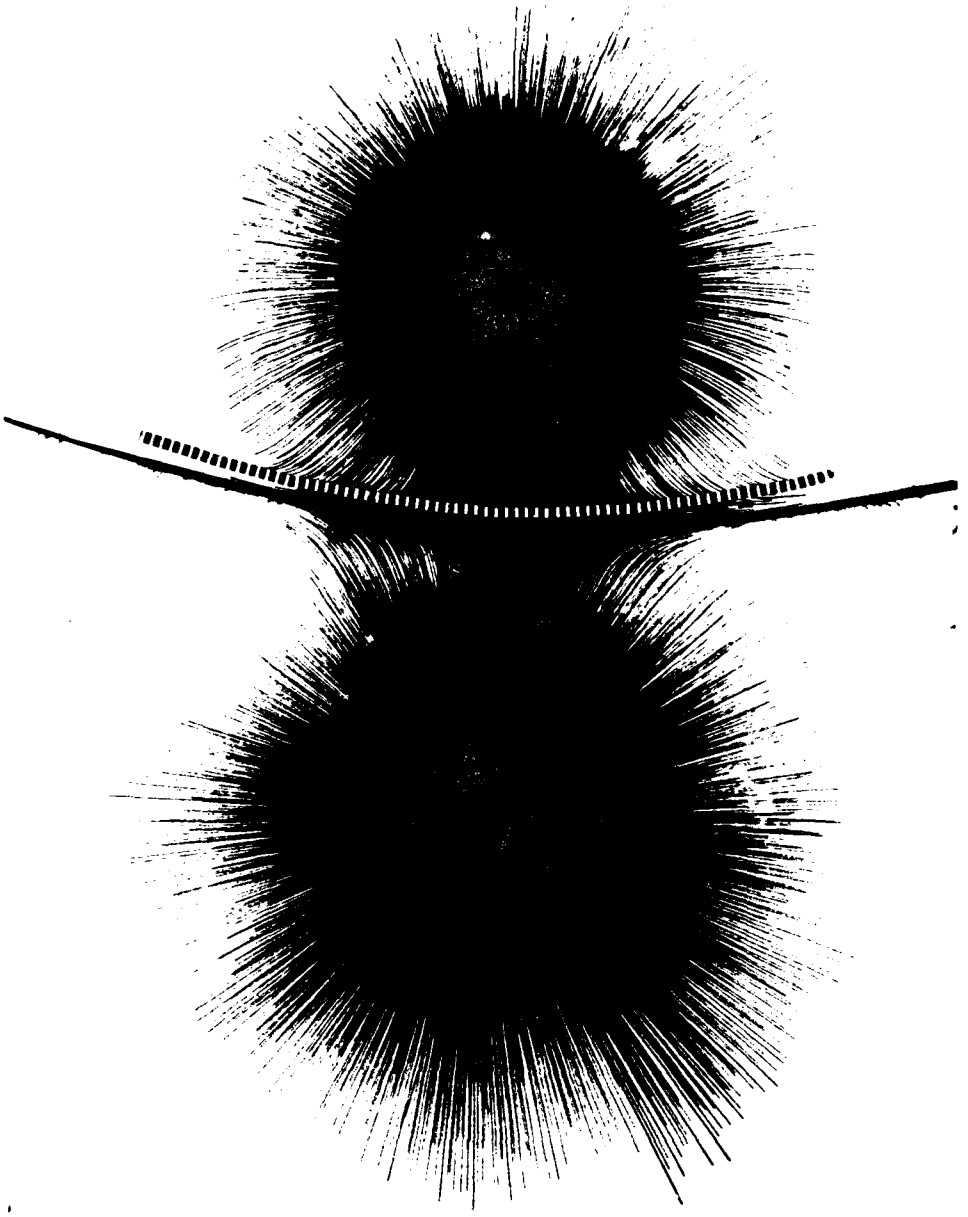

GP03-0368-41

Figure 26. Flow Visualization
Case 3c1

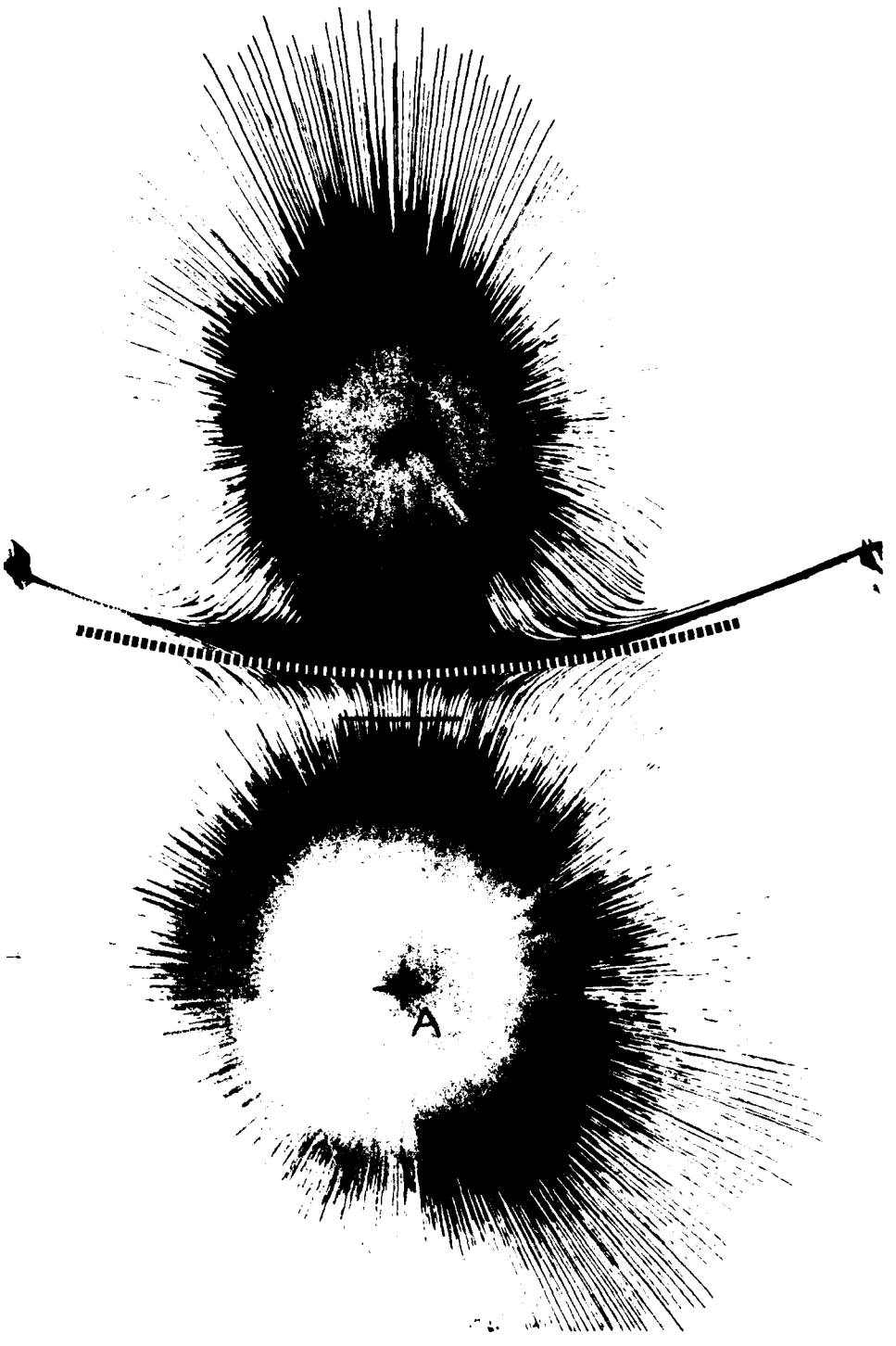

Figure 27. Flow Visualization
Case 3d1

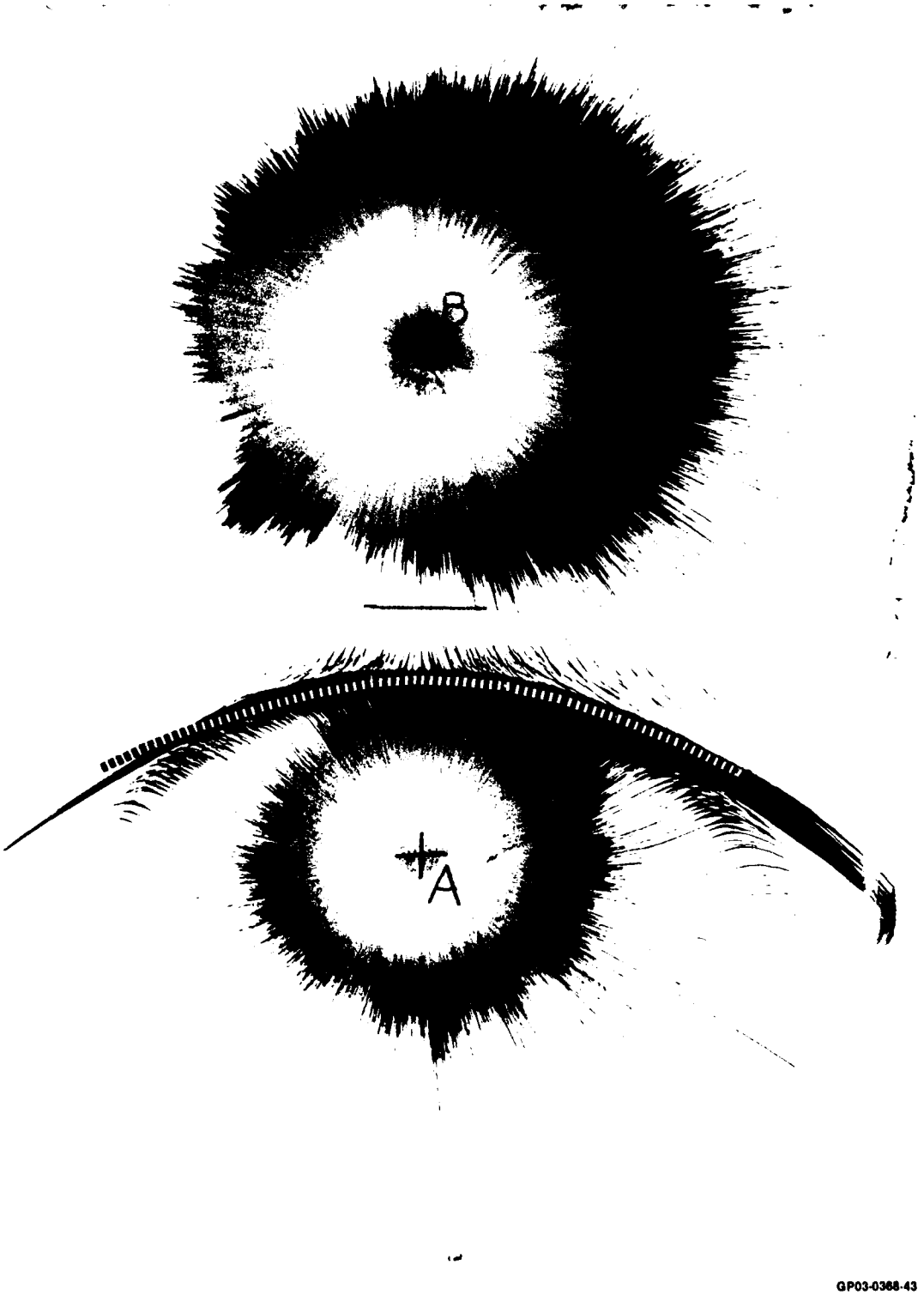

GP03-0368-43

Figure 28. Flow Visualization
Case 4a

GP03-0368-44

Figure 29. Flow Visualization
Case 4b

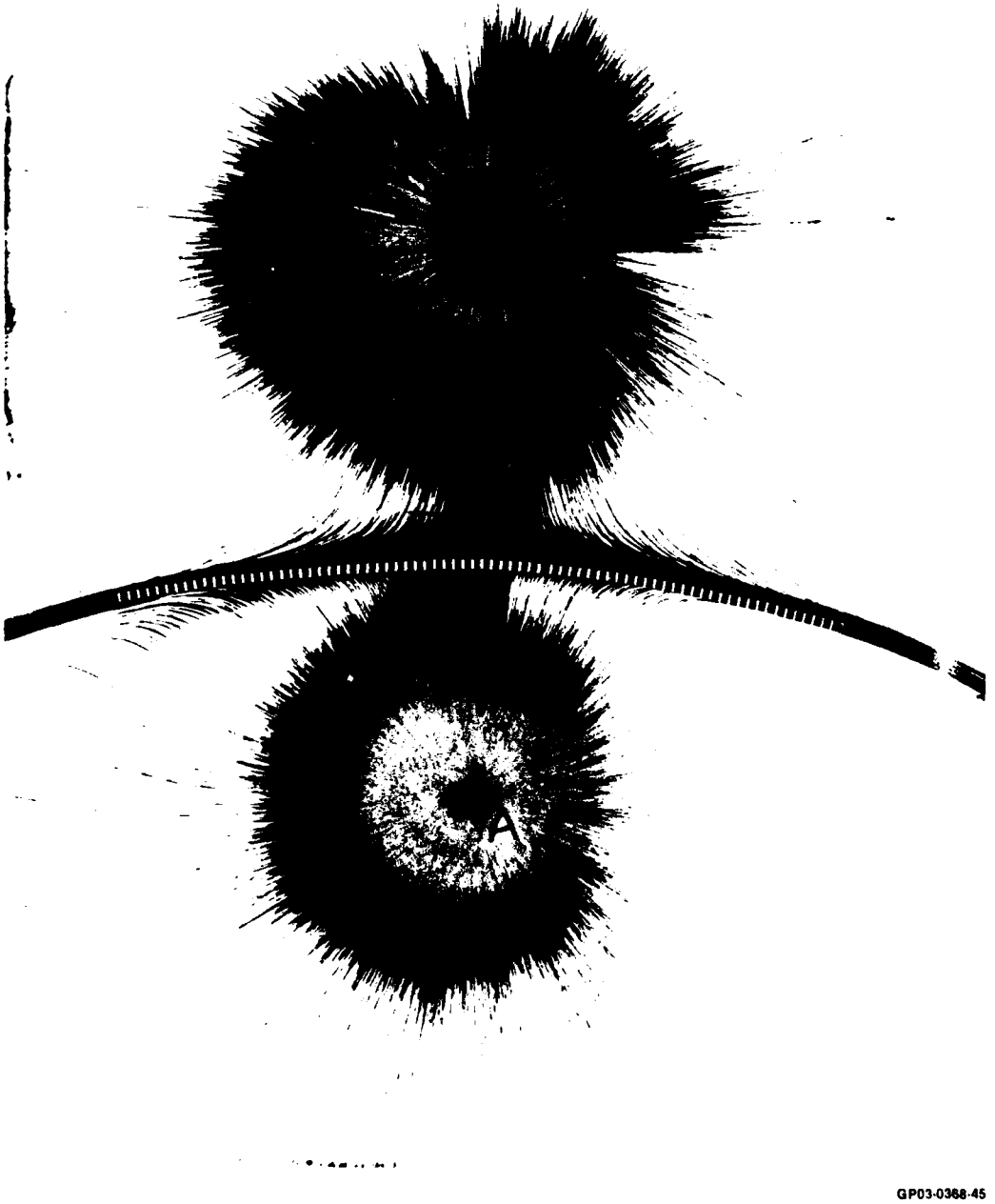

GP03-0368-45

Figure 30. Flow Visualization
Case 4c

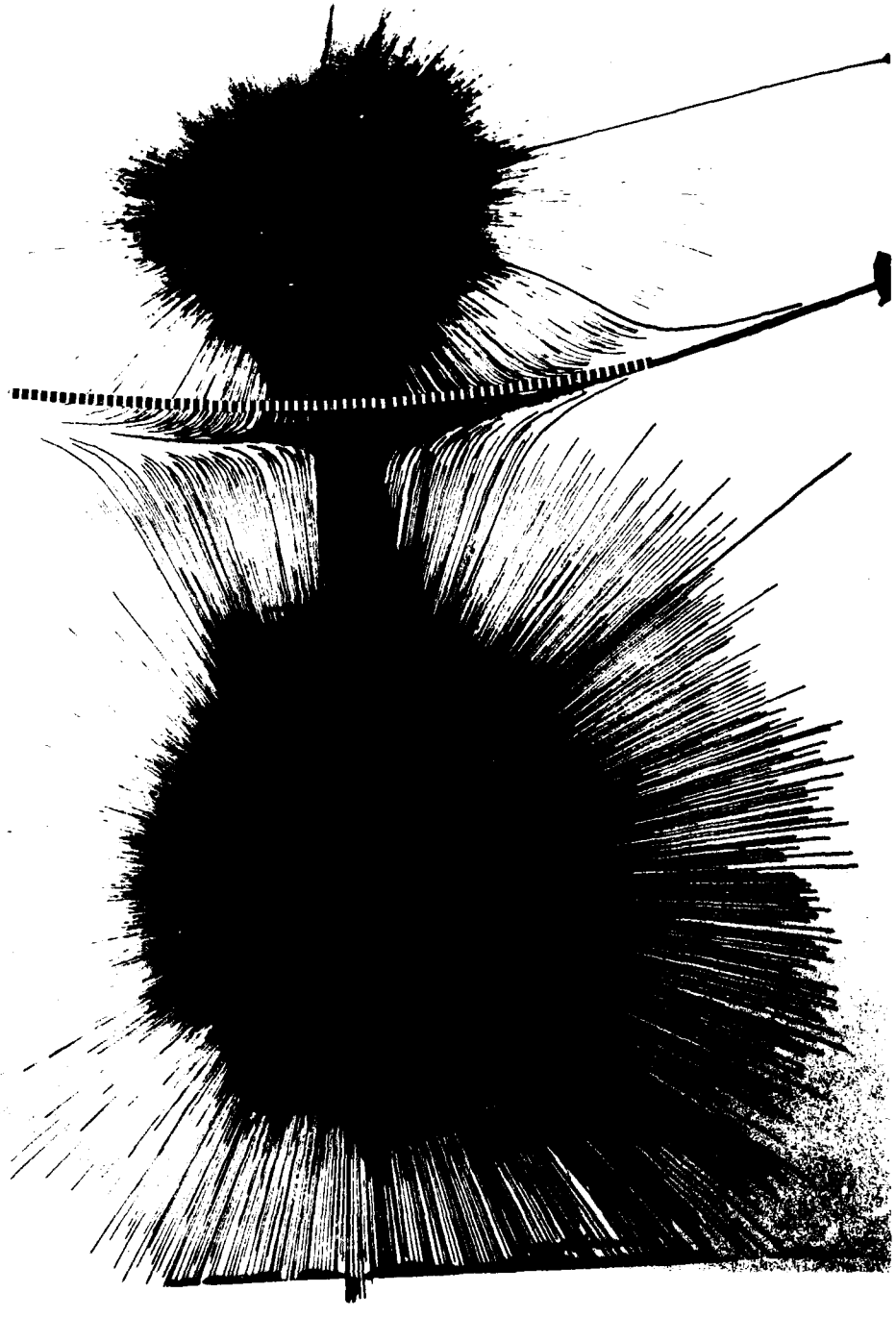

Figure 31. Flow Visualization
Case 5a

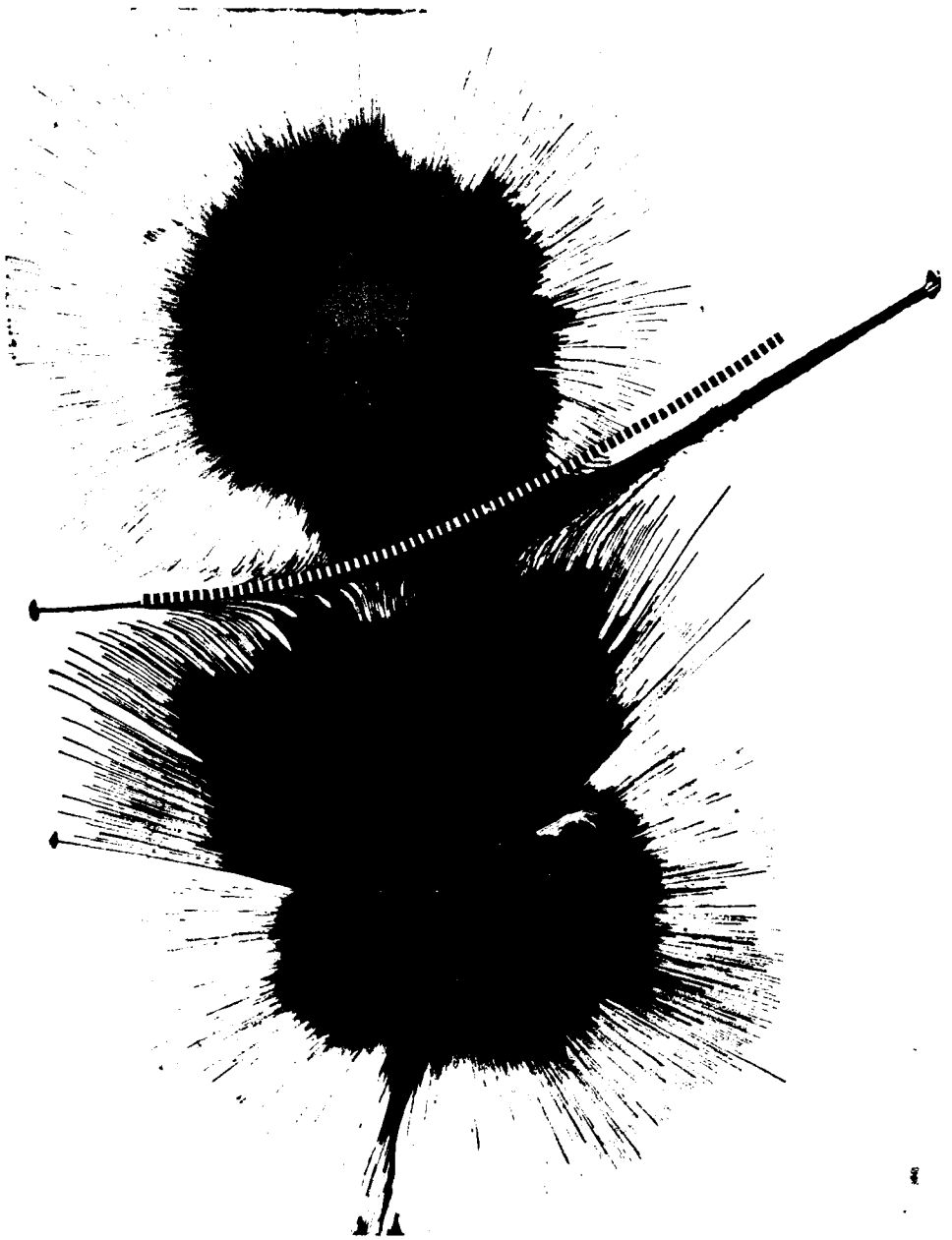

GP03-0368-47

Figure 32. Flow Visualization
Case 5b

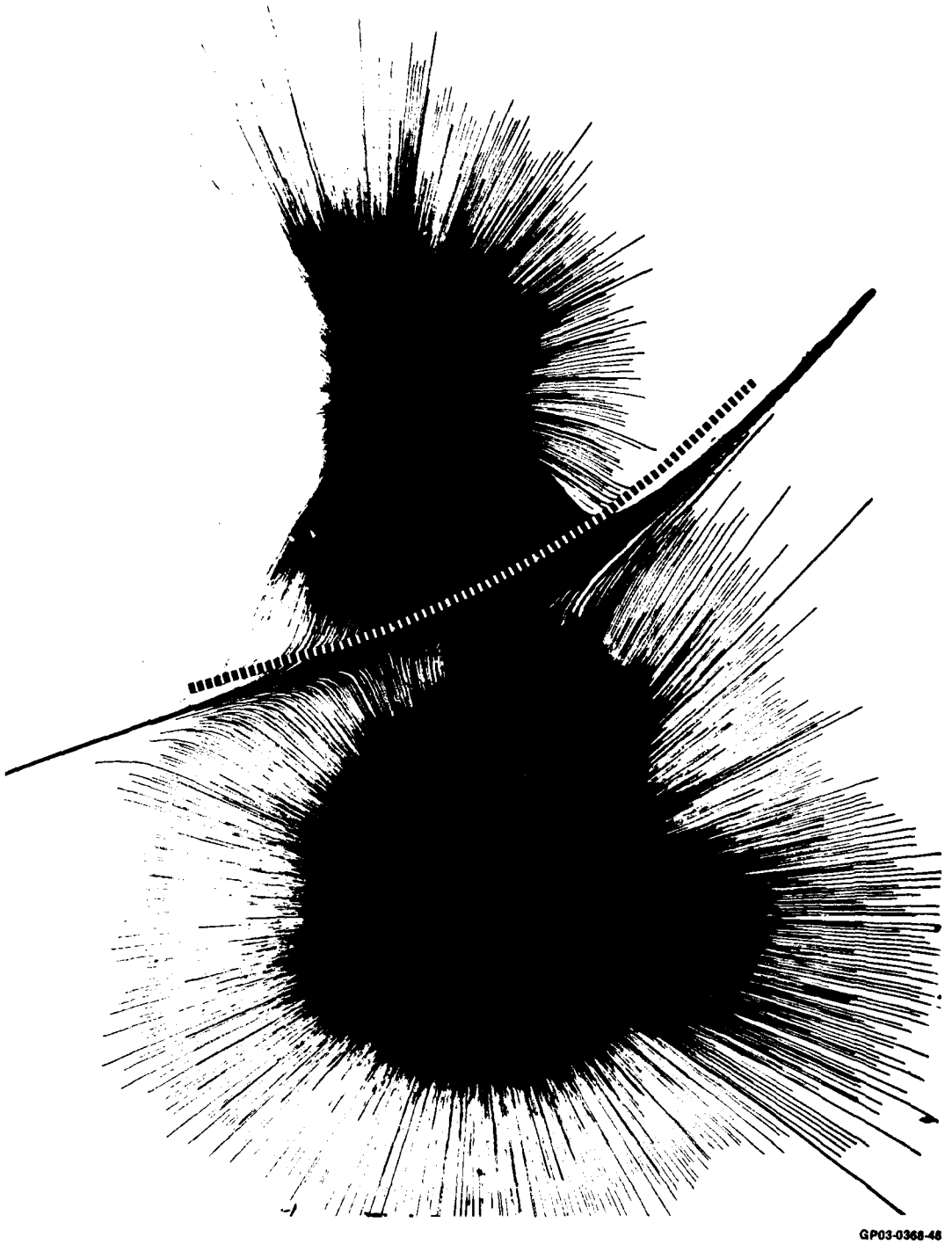

Figure 33. Flow Visualization
Case 5c

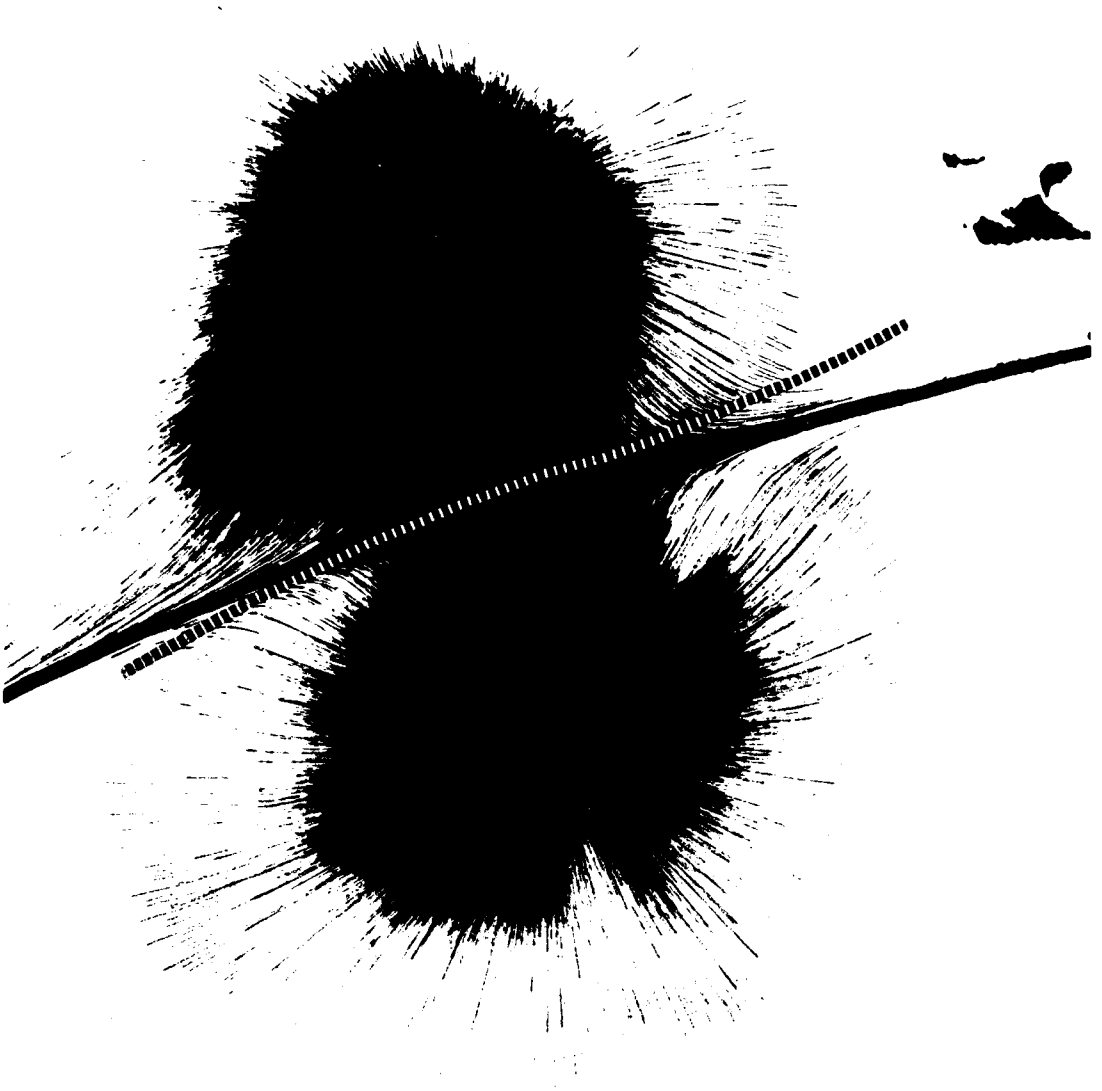

GP03-0368-49

Figure 34. Flow Visualization
Case 5d

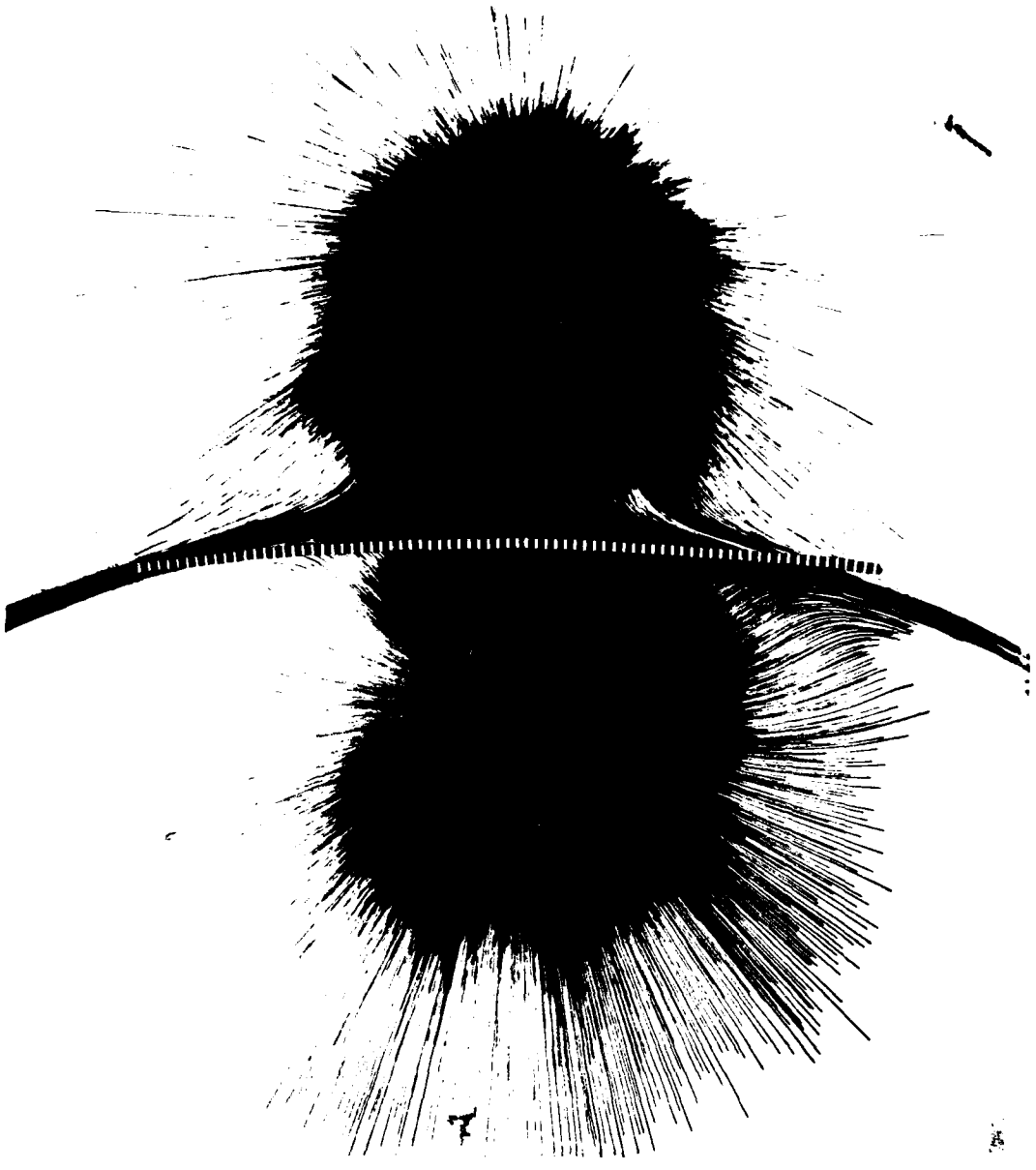

GP03-0368-50

Figure 35. Flow Visualization
Case 5e

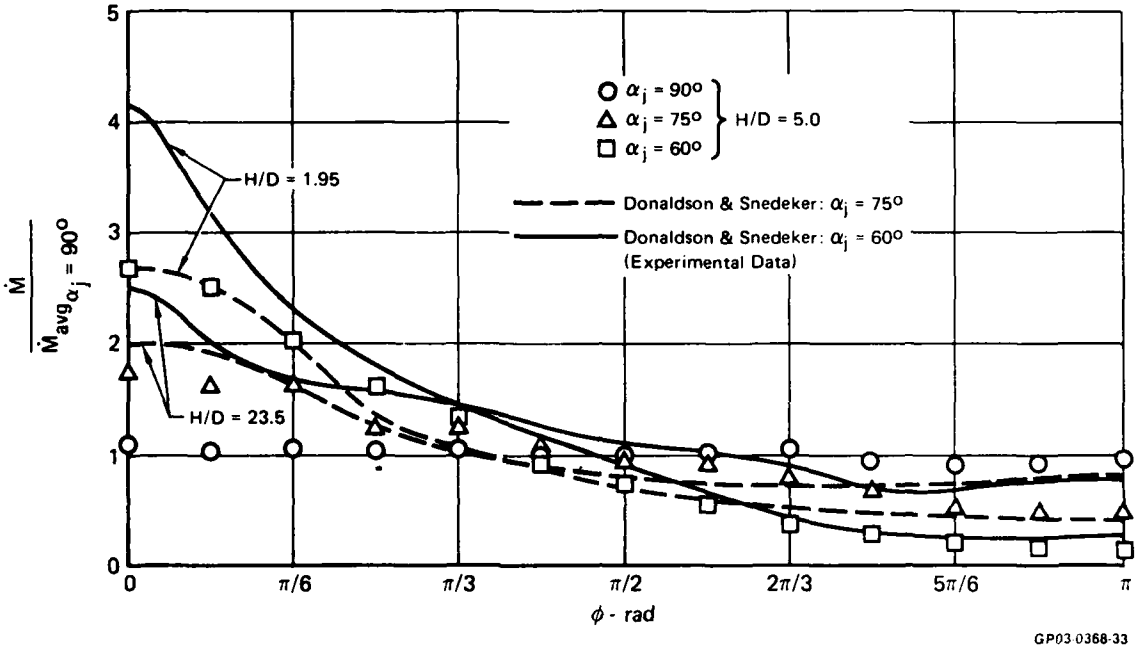

Figure 36. Azimuthal Distribution of Wall Jet Radial Momentum Flux
Axisymmetric Jet

SECTION VI

CONCLUSIONS

Based on an inspection of the experimental data, the following conclusions were reached:

1. There is no major effect on either stagnation line location or fountain upwash flow development due to the method of producing the free jet thrust bias; ie, increased nozzle exit area vs. increased nozzle pressure ratio.

2. The momentum flux (magnitude) loss in the fountain formation region varies from approximately 25%-45% depending on the jet exit momentum flux ratio, $\dot{M}_{je_{LOW}}/\dot{M}_{je_{HIGH}}$, with decreased losses occurring for a decrease in $\dot{M}_{je_{LOW}}/\dot{M}_{je_{HIGH}}$.

3. For the jet spacing ($S/D_A = 12.8$) and nozzle exit height ($H/D_A = 5.0$) investigated, the fountain upwash entrains mass.

4. The presence of a nozzle exit plane plate was found to produce: (a) an increase in the fountain upwash momentum flux recovery, $\lambda_{\dot{M}}$, (b) a decrease in the fountain upwash mass entrainment, (c) an increase in the overall strength ($\int U^2\, dN$) of the wall jets, and (d) an increase in the fountain upwash angle, ω (more vertical).

5. Change of the nozzle exit plane plate aspect ratio had negligible effect on the fountain momentum recovery, the fountain upwash mass entrainment, the wall jet strength or the fountain upwash inclination.

6. The fountain upwash inclination, ω, was found to be a function of the jet exit momentum flux ratio, $\dot{M}_{je_{LOW}}/\dot{M}_{je_{HIGH}}$, with ω decreasing (becoming less vertical) with decreasing $\dot{M}_{je_{LOW}}/\dot{M}_{je_{HIGH}}$. The fountain upwash inclination model gives good correlation with experimental data with the appropriate choice of the fountain formation momentum recovery coefficient, $\lambda_{\dot{M}}$.

7. The fountain upwash trajectories were generally found to be curved with the curvature increasing with increased height in the fountain.

8. Comparison of the stagnation line solutions calculated by the ground flow field prediction computer program using the "Momentum Flux Density Method" with those determined experimentally indicate good agreement with the experimental data.

9. A check of the wall jet radial momentum flux distributions determined by Donaldson and Snedeker (Reference 8) for the vertical and oblique impingement of axisymmetric jets suggests a reduction of the momentum flux peak in the region of azimuth near $\phi = 0°$.

REFERENCES

1. Kotansky, D.R., Durando, N.A., Bristow, D.R., and Saunders, P.W., "Multi-Jet Induced Forces and Moments on VTOL Aircraft Hovering in and Out of Ground Effect", Final Technical Report, Naval Air Development Center, NADC Report No. 77-229-30, June 1977.

2. Siclari, M.J., Barche, J., and Migdal, D., "V/STOL Aircraft Prediction Technique Development for Jet-Induced Effects", Vol. I, Grumman Aerospace Corp., PDR-623-18, Report Prepared Under NAPTC Contract N00140-74-C-0113, 15 April 1975.

3. Louisse, J., and Marshall, L., "Prediction of Ground Effects for VTOL Aircraft with Twin Lifting Jets", Journal of Aircraft, Vol. 13, No. 2, February 1976, pp. 123-127.

4. Pollard, D.J., and Bradbury, L.J.S., "Impingement of a Two-Dimensional Supersonic Jet Upon a Normal Ground Surface", AIAA Journal, Vol. 14, No. 8, August 1976, pp. 1095-1098.

5. Private Correspondence, K. A. Green, Naval Air Development Center to D.R. Kotansky, 24 August 1978.

6. Kotansky, D.R., and Glaze, L.W., "Investigation of the Interaction of Lift Jets and a Ground Plane", Report No. NASA CR 152343, Ames Research Center, April 1980.

7. Kotansky, D.R., and Glaze, L.W., "Investigation of Impingement Region and Wall Jets Formed by the Interaction of High Aspect Ratio Lift Jets and a Ground Plane", Report No. NASA CR 152174, Ames Research Center, 19 September 1978.

8. Donaldson, C. du P., and Snedeker, R.S., "A Study of Free Jet Impingement, Part I - Mean Properties of Free and Impinging Jets", Journal of Fluid Mechanics, Vol. 45, Part 2, 1971, pp. 281-319.

DISTRIBUTION LIST

Addessees	Copies
Office of Naval Research 800 N. Quincy St. Arlington, VA 22217	
ONR 210	1
ONR 438	4
Office of Naval Research Branch Office 1030 E. Green St. Pasadena, CA 91106	1
Office of Naval Research Branch Office Bldg. 114 Section D 666 Summer St. Boston, MA 02210	1
Office of Naval Research Branch Office 536 South Clark St. Chicago, IL 60605	1
Naval Research Laboratory Washington, DC 20375	
Code 2627	1
Code 2629	1
Defense Technical Information Center Bldg. 5 Cameron Station Alexandria, VA 22314	12
Naval Air Systems Command Washington, DC 20361	
AIR 320D (Mr. D. Kirkpatrick)	1
AIR 5301-33B (Mr. Lynn Trobaugh)	1
AIR 03PA (H. Andrews)	1
AIR ADPO-16 (CDR J. Farley)	1
Naval Air Development Center Warminster, PA 18974	
Code 6053 (Dr. K. Green)	1
Code 6053 (Dr. K. T. Yen)	1
David Taylor Naval Ship Research and Development Center Bethesda, MD 20084	
Code 16 (Dr. H. Chaplin)	1
Code 1660 (Mr. J. Nichols)	1
Code 522.3 Aero Library	1
Code 1606 (Dr. T. C. Tai)	1

DISTRIBUTION LIST (Continued)

Addressees	Copies
U. S. Naval Postgraduate School Monterey, CA 93940	
Dept. of Aeronautics (Code 57)	1
Library	1
Superintendent U. S. Naval Academy Annapolis, MD 21402	1
NASA Ames Research Center Moffett Field, CA 94035	
FAE Branch (Dr. T. Gregory)	1
Mr. D. Koenig	1
NASA Langley Research Center Hampton, VA 23665	
Mr. R. Margason	1
Wright Patterson Air Force Base Dayton, OH 45433	
Aero & Airframe Branch (Dr. T. Weeks)	1
Air Force Office of Scientific Research Bolling AFB, DC 20332	
Code NA (Dr. J. Wilson)	1
Nielsen Engineering & Research, Inc. 510 Clyde Avenue Mountain View, CA 94043	1
Vought Corporation Advanced Technology Center, Inc. P. O. Box 6144 Dallas, TX 75222	
Dr. C. S. Wells, Jr.	1
Grumman Aerospace Corporation Bethpage, NY 11714	
Research Dept. (Dr. R. Melnik)	1
Advanced Dev. Dept. (Mr. F. Berger)	1
University of Southern California Dept. of Aerospace Engineering University Park Los Angeles, CA 90007	
Prof. John Laufer	1

DISTRIBUTION LIST (Continued)

Addressees	Copies
Virginia Polytechnic Institute Dept. of Engr. Sciences & Mechanics Blacksburg, VA 24061	1
University of Maryland Dept. of Aerospace Engr. College Park, MD 20742 Dr. J. D. Anderson, Jr.	1
United Aircraft Corporation Research Laboratories Silver Lane East Hartford, CT 06108 Dr. M. Werle	1
Polytechnic Institute of New York Long Island Center Dept. of Aero Engr. and Applied Mechanics Route 110 Farmingdale, NY 11735	1
Scientific Research Associates, Inc. P.O. Box 498 Glastonbury, CT 06033 Dr. H. McDonald	1
General Dynamics/Fort Worth Division Aerospace Tech. Dept. Fort Worth, TX 76101 Dr. W. Foley	1
Aeronautical Research Associates of Princeton, Inc. 50 Washington Road Princeton, NJ 08540 Dr. J. E. Yates	1
Scientific Research Associates, Inc. P.O. Box 498 Glastonbury, CT 22060 Dr. H. McDonald	1
Douglas Aircraft Company 3855 Lakewood Blvd. Long Beach, CA 90803 Dr. T. Cebeci Doris K. Steckel	1 1

END

DATE
FILMED

8-80

DTIC